

# 1. INTRODUCTION

Tin is a technologist's metal, in the sense that whilst its manifold applications reach into all aspects of life, nevertheless, most people are usually unaware of its presence. Long before history came to be written, tin was associated with the technological advance of mankind and archaeological evidence confirms that tin was one of the earliest metals known to human society. From early Bronze Age to Space Age of today, tin has continued to play an important role out of proportion to the gross tonnage produced and used [1]. In 2007, the People's Republic of China was the largest producer of tin, where the tin deposit are concentrated in the southeast Yunnan tin belt, with 43% of the world's share, followed by Indonesia and Peru [2]. The main physical properties of tin are listed as **Table 1.1**[1]:

Properties	Values and Units
Atomic Number	50
Atomic mass	118.710 g. mol <sup>-1</sup>
Electron configuration	[Kr] 4 d <sup>10</sup> 5s <sup>2</sup> 5p <sup>2</sup>
Electron per shell	2, 8, 18, 18, 4
Appearance	Silvery lustrous gray
Density at 298K	7310 kg/m <sup>3</sup>
Melting Point	231.93 °C
Boiling Point	2602 °C
Specific heat capacity at 298K	27.112 J·mol <sup>-1</sup> ·K <sup>-1</sup>
Electrical resistivity at 273K	115 nΩ·m
Thermal conductivity at 300K	66.8 W·m <sup>-1</sup> ·K <sup>-1</sup>
Thermal expansion at 298K	22.0 μm·m <sup>-1</sup> ·K <sup>-1</sup>
Young's modulus	50 GPa
Shear modulus	18 Gpa

**Table 1.1:** Main physical properties of Tin

Tin has many industrial applications and is widely used in tin plating, solder manufacturing, chemical production, brass and bronze fabrication and variety of other application. The main objective of tin plating is to:

1. Increase resistance to wear,
2. Increase electrical conductivity,
3. Improve surface reflectivity especially for decorative purposes.

Tin and its alloys can be electrodeposited from various electrolytes including aqueous fluoroborate, sulfate and methane sulfonate solutions. The sulfate electrolyte is generally adopted as a first choice of plating electrolyte due to its low cost and long history. The fluoroborate bath is used when high current density is required. The methanesulfonate- based electrolyte is favored for its environmental benefits and it facilitates higher stannous ion saturation solubility with a low oxidation rate to stannic ions [3]. However, hydrogen evolution reaction often occurs in the aqueous based electrolyte electrodeposition resulting in profound effect on current efficiency and quality of the tin deposits. As a result, different additives may be needed to suppress such difficulties [4].

In contrast, a fundamental advantage of using ionic liquid electrolytes in electroplating is that, since these are non-aqueous solutions, there is negligible hydrogen evolution during electroplating and the coatings possess the much superior mechanical properties of the pure metal. Hence essentially crack-free, more corrosion-resistant deposits are possible. This may allow thinner deposits to be used, thus reducing overall material and power consumption [5]. Electrodeposition in ionic liquids was rarely studied in the past. In 1992, Wilkes and Zaworotko reported the first air and moisture stable imidazolium based ionic liquid with either tetrafluoroborate or

hexafluorophosphate as anions. Then, several, liquids consisting of 1-ethyl-3-methylimidazolium, 1,2-dimethyl-3-propylimidazolium, or 1-butyl-1-methylpyrrolidinium cations with various anions, such as tetrafluoroborate ( $\text{BF}_4^-$ ), tri-fluoromethanesulfonate ( $\text{CF}_3\text{SO}_3^-$ ), bis(trifluoromethanesulfonyl)imide [ $(\text{CF}_3\text{SO}_2)_2\text{N}^-$ ] & tris(trifluoromethanesulfonyl)methide [ $(\text{CF}_3\text{SO}_2)_3\text{C}^-$ ], were found and received much attention because of low reactivity against moisture [6].

Few studies were reported on the electrodeposition of Tin(II) in ionic liquids. The first was done by Hussey and Xu [7] in an  $\text{AlCl}_3$  mixed in 1-methyl-3-ethylimidazolium chloride melt. W. Yang *et al.* [8] has done Tin and Antimony electrodeposition in 1-ethyl-3-methylimidazolium tetrafluoroborate, and N. Tachikawa *et al.* [9] has done electrodeposition of Tin(II) in a hydrophobic ionic liquid, 1-*n*-butyl-1-methylpyrrolidinium bis(trifluoromethylsulfonyl)imide.

In view of the advantages of the air and water stable ionic liquids, the aim of this study is to investigate the electrochemical behavior of the Tin electrodeposition from a mixture of an ionic liquid, 1-butyl-1-methyl-pyrrolidinium trifluoro-methanesulfonate, (BMPOTF) with Tin(II) Methane Sulfonate in Methane Sulfonic Acid (MSA).

# 2. LITERATURE REVIEW

## 2.1 Electrodeposition

Electrodeposition or electroplating is a form of metal finishing. It is often regarded as both an art and a science because its theory and practices are derived from many branches of science and technology. Electroplating is a branch of electrochemistry which uses electrical energy to deposit a metal coating onto a conducting substrate in order to impart much improved physical properties such as:

1. Resistance to wear
2. Increased electrical conductivity, for example in printed circuit boards,
3. Increased magnetic susceptibility, for example on printed circuit boards,
4. Increased surface reflectivity, for example for decorative purposes.

Electrodeposition occurs during electrolysis in a solution known as “electrolyte”. The current enters and leaves the electrolyte via two conducting electrodes which are called the “anode” and “cathode”. The overall (conventional) current flow and the principle components of an electroplating process are shown schematically in **Figure 2.1** [10].

1. An electroplating bath containing a conducting salt and the metal to be plated in a soluble form. , as well as perhaps additives.
2. The electronically conducting cathode, i.e. the work piece to be plated.
3. The anode (also electronically conducting) preferably insoluble.
4. An inert vessel to contain (1)-(3), typically, e.g. polypropylene, polyvinylchloride.

5. A d.c. electrical power source, usually a regulated transformer/ rectifier. (**Figure 2.2)**)

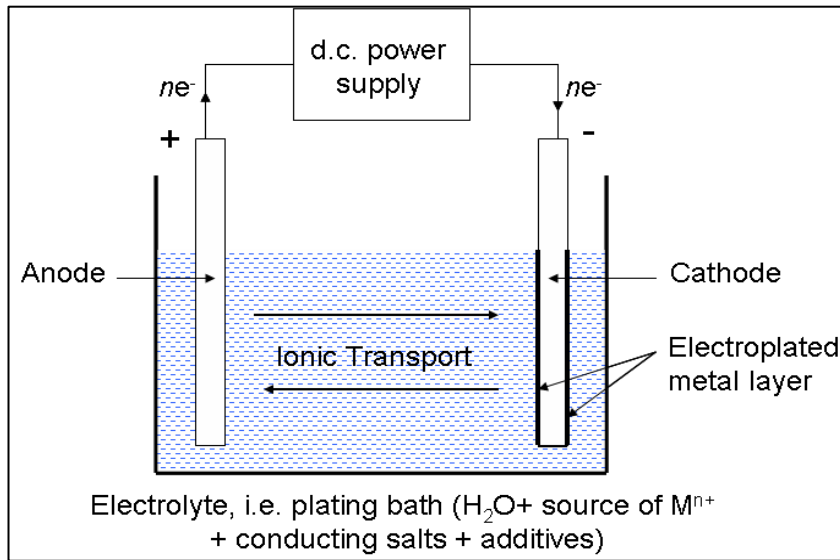
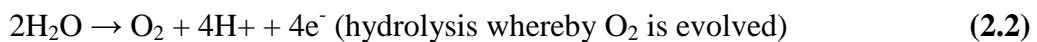
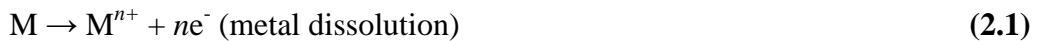


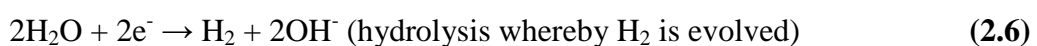
**Figure 2.1:** Schematic diagram showing an electroplating process

During electrolysis, all the ions in solution carry current and the current capacity depends on its concentration and mobility at the electrodes. Eventually this leads to a build-up (i.e. an excess) of positive ions or cations at the cathode, and those with most positive discharge potentials are first reduced. The anions with most negative discharge potential are oxidized at the anode. At each electrode, there are more than one reactions occurring.

At the anode:



At the cathode:





If the metal deposition process is the major process, it is said to have good current efficiency [11].



**Figure 2.2:** A d.c. rectifier used in electroplating industry

## 2.2 Electroplating mechanism

If a voltage is applied across the two electrodes in an electrolysis cell, a current consisting of electron flow, will be set up, with these moving from the anode, through the external circuit and back to the cathode. The anode will thereby dissolve anodically, and the cations so formed will migrate to the cathode. Anions present in solution will move in the opposite direction towards the anode. Current will thus flow through the solution by virtue of the movement of these charged ions and this is known as ionic current, or electrolytic conductance. Of critical importance in electrodeposition, is the mechanism by which metal cations are delivered to the cathode, and the means for their replenishment as they are lost to solution by deposition at the cathode. The rate at which fresh ions (and also uncharged species required for reaction) are delivered to the cathode surface from the bulk of solution, depends on the prevailing hydrodynamic

conditions at and near the cathode surface. There are three main mechanisms involved in delivery of ions to the electrode surface, these being [12]:

1. Migration (under a potential gradient),
2. Diffusion (under a concentration gradient)
3. Convection (movement of the electrolyte liquid itself).

### **2.2.1 Migration**

Voltage applied across the electrodes of an electrolysis cell sets up an electrical field between anode and cathode. Assuming that the electrolytic conductivity of the electrolyte is the same at all points in solution, the potential gradient is given by the voltage across the solution (excluding overvoltage at the electrodes) divided by the distance between the electrodes. The magnitude of this potential gradient determines the rate at which ions move through solution. The term 'migration' is understood here as the movement of charged species in solution under a potential gradient. The effect operates throughout the solution, anions being electrostatically attracted to the anode, cations to the cathode. The progress of such ions through solution is impeded by collisions with solvent molecules and viscous drag as the ions, with their hydration sheaths, move through the liquid. The ions thereby acquire a given velocity, depending on the nature of the ion, the potential gradient, solution viscosity, etc. These velocities are very low, of the order of micrometers per second. It follows that the overall contribution to the supply of ions resulting from the migration process is very small, and can generally be neglected [12,13].

### **2.2.2 Convection**

In contrast to the preceding and following transport mechanisms which involve the movement of species through an electrolyte, convection can be said to be the movement of reactants, etc. with the electrolyte. The so-called 'convective mass transport' results from movement of the bulk solution, whether by stirring, movement of the work through the solution (deliberate measures to enhance convection, known as 'forced convection') or by the natural circulation of a liquid caused by adventitious differences in solution density caused by thermal effects. Such movement of solution ceases to be significant in the region immediately adjacent to the electrode surface, where a liquid layer sometimes known as the 'stagnant layer' or more usually as the 'diffuse layer' is formed. Movement of ions etc across this diffuse layer takes place by diffusion. Convection is important not only because it moves the solution (with dissolved species) up to the diffuse layer, but also because the thickness of the diffuse layer is determined by convective action. The stronger the agitation (pumping, stirring, air-purging) the thinner is the diffuse layer [12,14].

### **2.2.3 Diffusion**

The penultimate step, before charge transfer takes place at the electrode surface, is the migration of species, both charged and uncharged, across the diffuse layer. The driving force here is the concentration gradient, more formally expressed as chemical potential. The concentration of species at the electrode surface will, under open circuit conditions, be much the same as that in bulk solution. However, once current flows, species will, by their reaction, be removed at the electrode surface and a concentration gradient will be established. The tendency of species to move from regions of high concentration to

those of lower concentration, are what drive the diffusion process, and this is enshrined in Fick's laws of diffusion. The thickness of the 'diffuse layer', also known as the Nernst or Nernstian layer, is denoted by  $\delta$ . Without forced convection, in a static solution,  $\delta$  would be approximately 0.2 mm. Under conditions of forced convection, this value will decrease, and can reach values as low as 0.001 mm. It is generally assumed that diffusion is the only significant transport mechanism operating within the Nernstian layer. **Figure 2.3** shows what might be described as a concentration-depth profile. It shows the electrode surface as a vertical line on the left of the diagram. The vertical dashed line indicates the outer edge of the Nernst layer. The solid line shows the concentration profile predicted by the Nernst equation, the curved dashed line shows typical experimental results.

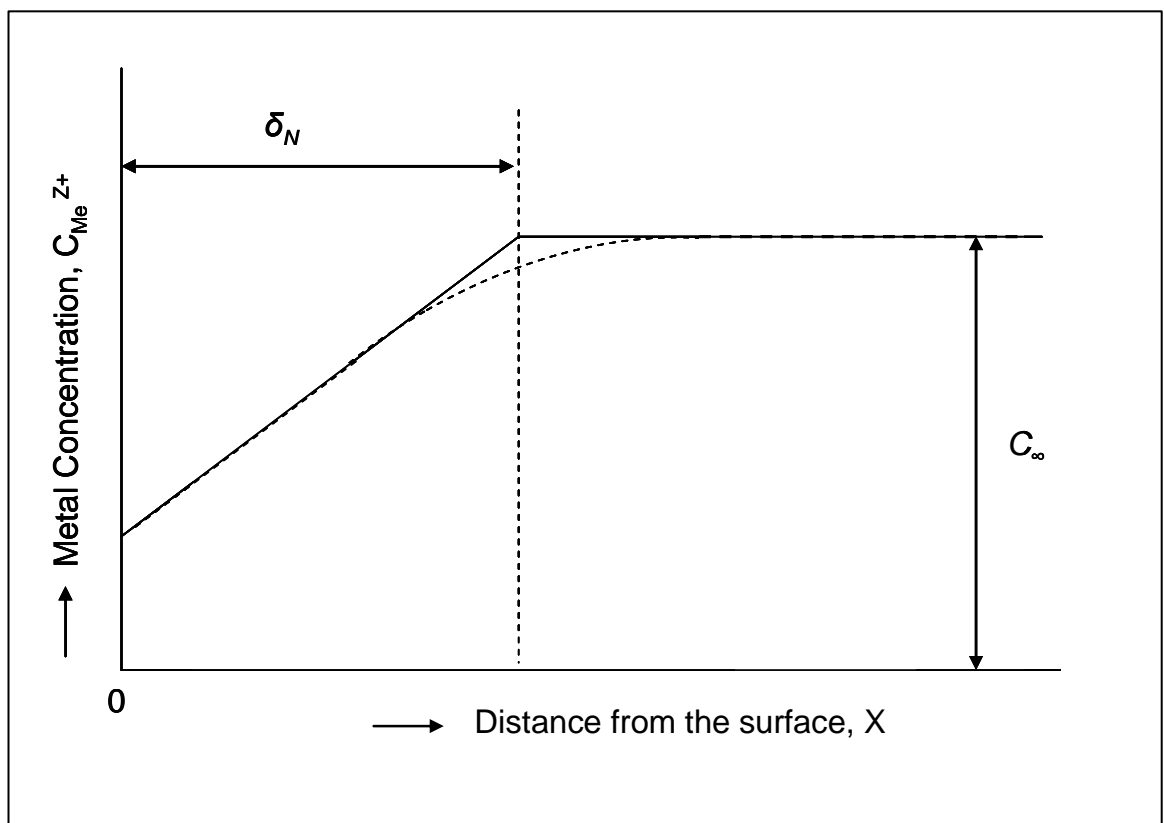


**Figure 2.3:** Metal ion concentration profile as a function of distance from the surface

**Figure 2.3** depicts the situation in a typical electrolysis and shows how the concentration of reactants is depleted at the electrode surface. In the extreme case, the

concentration of reactants at the electrode surface is zero. Otherwise expressed, the species arriving at the electrode surface react instantly. The flux of cations through the diffuse layer, expressed as mol/s/cm<sup>2</sup> is known as the diffusion current density  $n^*$ . It is a function, as Fick's law indicates, of the concentration gradient across the Nernst layer, as expressed in **Equation 2.8**, where  $D$  is the diffusion coefficient,  $C_\infty$  is the metal ion concentration in bulk solution,  $C_c$  is the concentration at the electrode surface [12]:

$$n^* = D \frac{dc}{dx} = D \frac{(C_\infty - C_c)}{\delta_N} \quad (2.8)$$

At 100% cathode efficiency, the cathode current density  $i_c$  (A/cm<sup>2</sup>) is given by the following expression:

$$i_c = z * F * D \frac{(C_\infty - C_c)}{\delta_N} \quad (2.9)$$

where  $z$  is the number of electrons per ion being transferred,  $F$  the Faraday constant (96,485 C/equivalent). The cathodic current density is proportional to the value of  $(C_\infty - C_c)/\delta_N$ , the Nernstian concentration gradient. The metal ion concentration decreases from outside to inside of the Nernstian layer. If the current density is further increased, there comes a point where  $C_c = 0$ . The current is then said to have reached the diffusion-limited current density, or mass-transport-limited current density. Increasing the voltage, at this point, will then (on this simplified theory) bring no further increase in current. We can then rewrite **Equation 2.9** in a simplified form as below, **Equation 2.10** [15]:

$$i_D = z * F * D \frac{C_\infty}{\delta_N} \quad (2.10)$$

The rate of metal deposition is then limited to this value, mass-transport being the rate-determining step. The diffusion-limiting current density  $i_D$  represents the maximum

current density at which the metal can be deposited under the given hydrodynamic conditions. In practice, metals deposited under these conditions tend to be powdery or friable and of no practical use except where there is a deliberate intention to produce metal powders. Having crossed the Nernst diffusion layer, the metal ions face a further barrier separating them from the electrode surface, namely the electrode double layer or interfacial layer. This is formed, as indicated earlier, by the aggregation of electrons on one side of the interface, and metal ions on the other. As a first approximation, as shown in **Figure 2.4**, this can be modeled as an electrolytic capacitor. In this scheme,  $\Delta\phi$  is the difference between the potential of the metal electrode,  $\phi_{Me}$  and that of the solution,  $\phi_L$  [12].

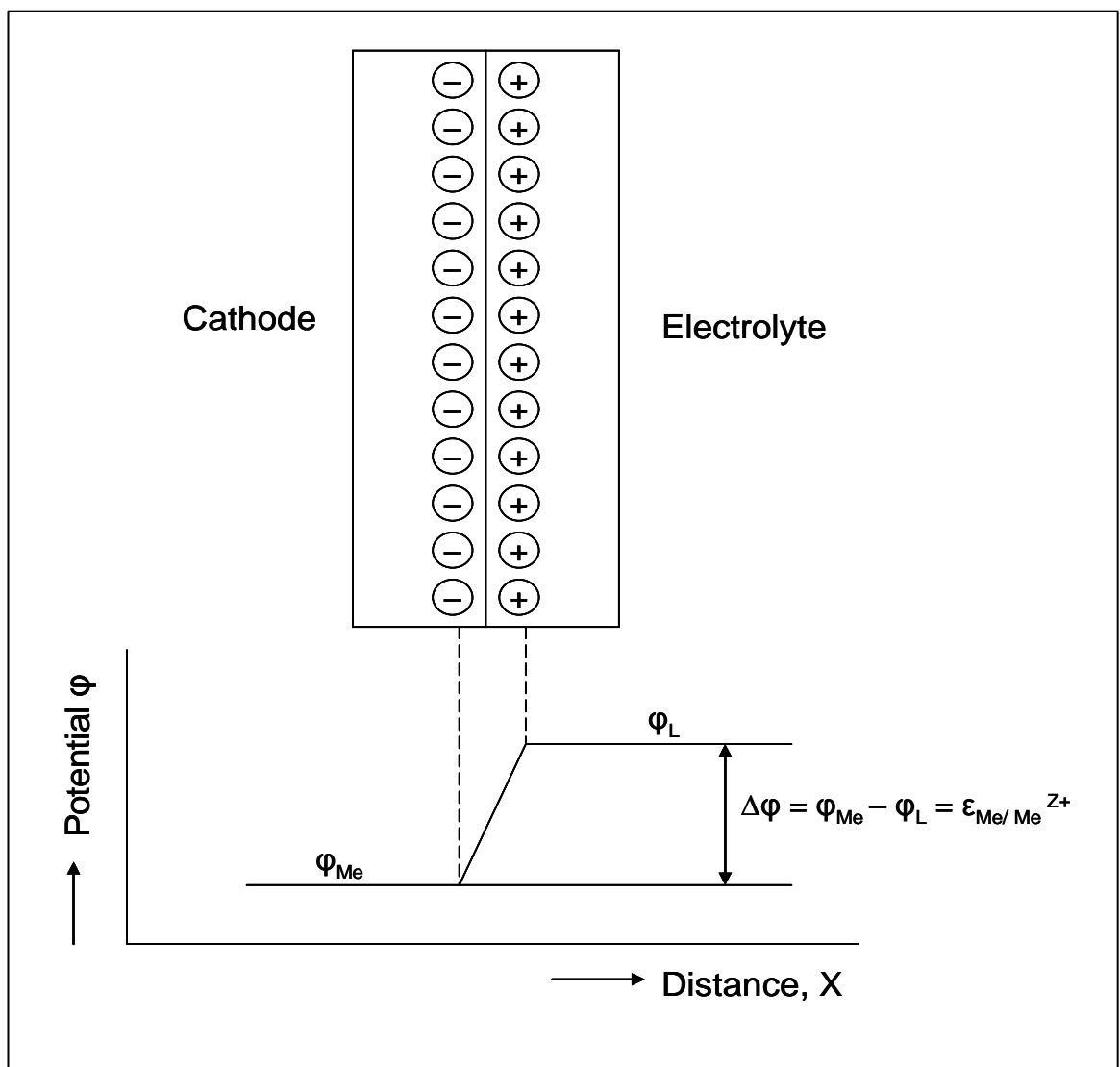


**Figure 2.4:** Structure of the electrical double layer at a metal-solution interface

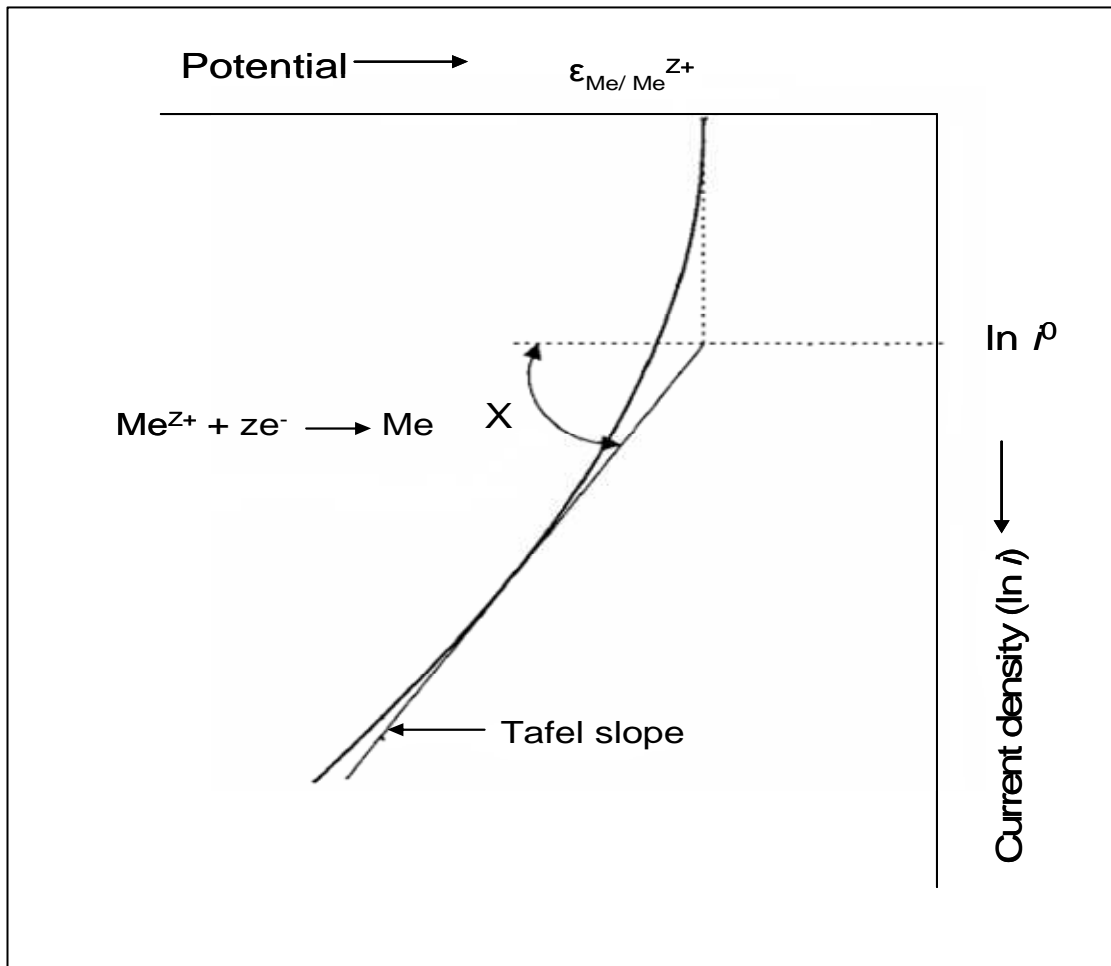


**Figure 2.5:** Dependence of cathodic current density on potential. Graphical determination of  $\epsilon_{\text{Me/Me}^{Z+}}$ ,  $i^0$ , and  $\alpha$  by drawing a tangent to the curve

In **Figure 2.5**, the natural logarithm of the cathodic current density is plotted versus potential. As this representation shows, the value of the equilibrium potential can be derived from the asymptotic value of the log function. The corresponding exchange current density is derived by drawing a tangent and is given by the intersection of the tangent with the asymptotic value of the current-potential plot. This value, which is proportional to the transfer coefficient, is known as the Tafel slope, named after the German scientist who first derived an empirical relationship linking current density and overpotential. Cathodic deposition of metals is initiated by discharge of metal ions which are already in close proximity to the electrode. Thus, at the onset of the process, the rate determining step is the movement of the charged species through the electrical double layer to the electrode surface. This leads to a depletion of the dischargeable

metal ions in the near-electrode region, and metal electrodeposition can only continue if these are replenished from bulk solution. It follows that, in most cases (except at very low current densities and high metal ion concentrations), the deposition process is increasingly mass-transport controlled. In the limiting case, where mass transport becomes the rate controlling stage, the current-potential plot assumes the form seen in **Figure 2.6**. In practice, it must be recognized that only certain metals can be electrodeposited from aqueous solution and these are shown in **Figure 2.7** enclosed within the frame [12,16,17].

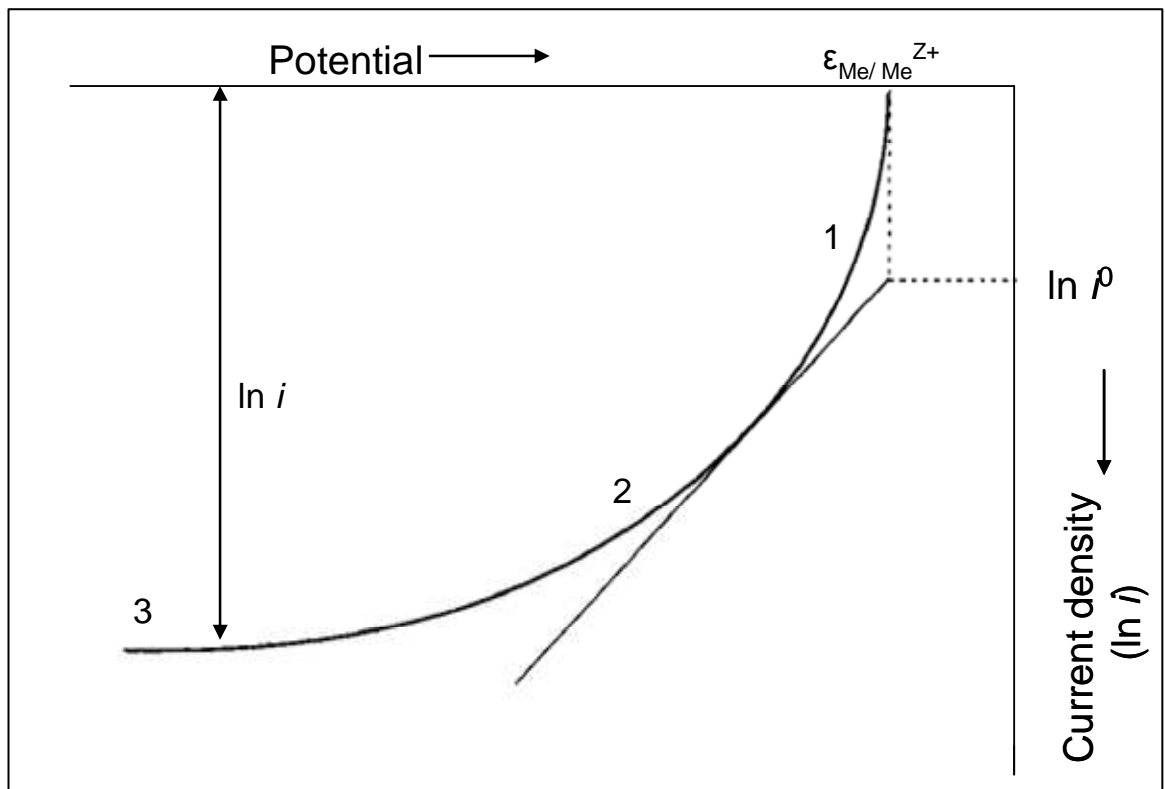


**Figure 2.6:** Shape of the current-voltage plot: (1) under activation control, (2) intermediate region with both mechanisms rate-determining and (3) under diffusion control

IA	IIA	IIIB	IVB	VB	VIB	VII B	VIII B				IB	IIB	IIIA	IVA	VA	VIA	VIIA	VIIIA
1 H																		2 He
3 Li	4 Be											5 B	6 C	7 N	8 O	9 F	10 Ne	
11 Na	12 Mg											13 Al	14 Si	15 P	16 S	17 Cl	18 Ar	
19 K	20 Ca	21 Sc	22 Ti	23 V	24 Cr	25 Mn	26 Fe	27 Co	28 Ni	29 Cu	30 Zn	31 Ga	32 Ge	33 As	34 Se	35 Br	36 Kr	
37 Rb	38 Sr	39 Y	40 Zr	41 Nb	42 Mo	43 Tc	44 Ru	45 Rh	46 Pd	47 Ag	48 Cd	49 In	50 Sn	51 Sb	52 Te	53 I	54 Xe	
55 Cs	56 Ba	57 La	72 Hf	73 Ta	74 W	75 Re	76 Os	77 Ir	78 Pt	79 Au	80 Hg	81 Tl	82 Pb	83 Bi	84 Po	85 At	86 Rn	
87 Fr	88 Ra	89 Ac	104 Ku															

**Figure 2.7:** Periodic table showing those metals (inside frame and shaded) which can be deposited from aqueous solution

## 2.3 Components of plating bath

Hydrogen evolution reaction (HER) often occurs in the aqueous based electrolyte electrodeposition resulting in profound effect on current efficiency and quality of the metal deposited. As a result, different additives may be needed to suppress such difficulties [5]. A wide range of organic molecules such as polyethylene glycol (PEG), polypropylene glycol (PPG), thiourea, gelatin, hydroquinone and etc. are added in relatively low concentration to the electroplating bath to modify the structure, morphology and properties of the deposit. Their involvement has been almost totally empirical and details of their mode of operation are seldom known. Indeed, it is not always clear whether their effect is due to the additive itself or to decomposition products formed in electrode reactions. Several generalizations concerning their operation are, however, possible. Certainly, additives are usually capable of adsorption on the cathode surface, and in some cases organic matter is occluded into the deposit, especially when the plated metal has a high surface energy (high melting point). Many additives also increase the deposition overpotential and change the Tafel slope. This may be due to the need for electron transfer to occur through the adsorbed layer or due

to complex formation at the electrode surface. While the additives may affect more than one property of the deposit and there is clear evidence that when several additives are present in the electrolyte their effect is synergistic, they are often classified in the following [11]:

1. Brighteners- For a deposit to be bright, the microscopic roughness of the deposit must be low compared with the wavelength of the incident light so that is reflected rather than scattered. Brighteners are commonly used in relatively high concentration (several  $\text{g dm}^{-3}$ ) and may result in substantial organic matter in deposit. They usually cause the deposit formed as an even and fine-grained, hence, may act as modifier to the nucleation process.
2. Levelers- These produce a level deposit on a more macroscopic scale and act by adsorption at points where otherwise there would be rapid deposition of metal. Thus, adsorption of additives occurs preferentially at dislocations because of a higher free energy of adsorption and at peaks. The phenomenon happened due to the rate of their diffusion to such points is enhanced, the adsorbed additive will reduce the rate of electron transfer. In practice, additive act as both brighteners and levellers.
3. Structure modifiers- These additives change the structure of the deposit and maybe even the preferred orientation or the type of lattice. Some are used to optimize particular deposit properties, and others to adjust the stress in the deposit (stress is due to lattice misfit). The latter are often called “stress relievers”.

4. Wetting agents- These are added to accelerate the release of hydrogen gas bubbles from the surface. In their absence, the hydrogen which is often evolved in a parallel reaction to metal deposition can become occluded in the deposit causing, for example, hydrogen embrittlement.

## 2.4 Ionic Liquid

The recognized definition of an ionic liquid is “an ionic material that is liquid below 100 °C” but leaves the significant question as to what constitutes an ionic material. The whole electroplating sector is based on aqueous solutions. Clearly, the key advantages of using aqueous solution are [5]:

1. Cost
2. Non-flammable
3. High solubility of electrolytes
4. High conductivities resulting in low ohmic losses
5. High solubility of metal salts
6. High rate of mass transfer

For these reason, water will remain the mainstay of the metal plating industry. However, there are also limitations of aqueous solutions including [5]:

1. Limited potential windows
2. Gas evolution processes can be technically difficult to handle and result in hydrogen embrittlement.
3. Passivations of metals cause difficulties with both anodic and cathodic materials.
4. Necessity for organic additives.

5. All water must eventually be returned to the water source.

### 2.4.1 Deposition with Ionic Liquid

In contrast, a fundamental advantage of using ionic liquid electrolytes in electroplating is that, since these are non-aqueous solutions, there is negligible hydrogen evolution during electroplating and the coatings possess the much superior mechanical properties of the pure metal. Hence essentially crack-free, more corrosion-resistant deposits are possible. This may allow thinner deposits to be obtained, thus reducing overall material and power consumption. Between year 1980 and 2000 most of the studies on the electrodeposition in ionic liquids were performed in the first generation of ionic liquids, formerly called “room-temperature molten salts” or “ambient temperature molten salts”. The recognized definition of an ionic liquid is an ionic material that is liquid below 100 °C. A series of transition and main-group metal containing ionic liquids have been formulated and the feasibility of achieving electrodeposition has been demonstrated for the majority of these metals, **Figure 2.8** shows the elements in the periodic table that have been deposited using ionic liquids. It must be stressed that while the deposition of a wide range of metals has been demonstrated from a number of ionic liquids the practical aspects of controlling deposit morphology have not been significantly addressed due to the complex nature of the process parameters that still need to be understood. Despite the lack of reliable models to describe mass transport and material growth in ionic liquids, there are tantalizing advantages that ionic liquid solvents have over aqueous baths that make the understanding of their properties vitally important. Some of these advantages include [5]:

1. Electroplating of a range of metals impossible to deposit in water due to hydrolysis e.g. Al, Ti, Ta, Nb, Mo, W. As an example, the deposition of Al by

electrolysis in a low-temperature process has long been a highly desirable goal, with many potential applications in aerospace for anti-friction properties, as well as replacing Cr in decorative coatings. The deposition of Ti, Ta, Nb, Mo, will open important opportunities in various industries, because of their specific properties (heat, corrosion, abrasion resistance, low or high density etc.).

2. Direct electroplating of metals on water-sensitive substrate materials such as Al, Mg and light alloys with good adherence should be possible using ionic liquids.
3. There is potential for quality coatings to be obtained with ionic liquids rather than with water. Currently available metallic coatings suffer from hydrogen embrittlement; a major problem caused by gaseous hydrogen produced during water electrolysis. During electroplating with ionic liquids, negligible hydrogen is produced, and coatings will have the better mechanical properties.
4. Metal ion electrodeposition potentials are much closer together in ionic liquids compared with water, enabling easier preparation of alloys and the possibility of a much wider range of possible electroplated alloys, which are difficult or impossible in water.
5. Ionic liquids complex metals offer the possibility to develop novel electroless plating baths for coating polymers (e.g. in electronics) without the need for the toxic and problematic organic complexants used in water.
6. Although the cost of ionic liquids will be greater than aqueous electrolytes, high conductivity and better efficiency will provide significant energy savings

compared with water, and capital costs will be much lower than the alternative techniques such as PVD and CVD.

7. When used in electropolishing and electropickling processes, strongly acidic aqueous electrolytes create large quantities of metal-laden, corrosive effluent solution, whereas in ionic liquid electrolytes the metals will precipitate and be readily separated and recycled.
8. The replacement of many hazardous and toxic materials currently used in water, e.g. toxic form of chromium (VI), cyanide, highly corrosive and caustic electrolytes, would save about 10% of the current treatment costs.
9. Nano composite coatings – nano particles giving improved properties compared to micro particles e.g. thermal and electrical conductivity, transparency, uniformity, low friction.
10. An increased range of metal coatings on polymers is accessible by electroless plating using ionic liquids containing reducing agents.

1																	18																												
H	2											13	14	15	16	17	He																												
Li	Be											B	C	N	O	F	Ne																												
Na	Mg	3	4	5	6	7	8	9	10	11	12	Al	Si	P	S	Cl	Ar																												
K	Ca	Sc	Ti	V	Cr	Mn	Fe	Co	Ni	Cu	Zn	Ga	Ge	As	Se	Br	Kr																												
Rb	Sr	Y	Zr	Nb	Mo	Tc	Ru	Rh	Pd	Ag	Cd	In	Sn	Sb	Te	I	Xe																												
Cs	Ba	La	Hf	Ta	W	Re	Os	Ir	Pt	Au	Hg	Tl	Pb	Bi	Po	At	Rn																												
Fr	Ra	Ac																																											
<table border="1" style="margin-left: auto; margin-right: auto;"> <tr> <td>Ce</td> <td>Pr</td> <td>Nd</td> <td>Pm</td> <td>Sm</td> <td>Eu</td> <td>Gd</td> <td>Tb</td> <td>Dy</td> <td>Ho</td> <td>Er</td> <td>Tm</td> <td>Yb</td> <td>Lu</td> </tr> <tr> <td>Th</td> <td>Pa</td> <td>U</td> <td>Np</td> <td>Pu</td> <td>Am</td> <td>Cm</td> <td>Bk</td> <td>Cf</td> <td>Es</td> <td>Fm</td> <td>Md</td> <td>No</td> <td>Lr</td> </tr> </table>																		Ce	Pr	Nd	Pm	Sm	Eu	Gd	Tb	Dy	Ho	Er	Tm	Yb	Lu	Th	Pa	U	Np	Pu	Am	Cm	Bk	Cf	Es	Fm	Md	No	Lr
Ce	Pr	Nd	Pm	Sm	Eu	Gd	Tb	Dy	Ho	Er	Tm	Yb	Lu																																
Th	Pa	U	Np	Pu	Am	Cm	Bk	Cf	Es	Fm	Md	No	Lr																																
<table style="margin-left: auto; margin-right: auto;"> <tr> <td style="background-color: yellow; width: 20px; height: 15px; display: inline-block;"></td> <td>As metal</td> </tr> <tr> <td style="background: repeating-linear-gradient(45deg, transparent, transparent 2px, red 2px, red 4px); width: 20px; height: 15px; display: inline-block;"></td> <td>As alloy</td> </tr> <tr> <td style="background: repeating-linear-gradient(45deg, transparent, transparent 2px, black 2px, black 4px); width: 20px; height: 15px; display: inline-block;"></td> <td>As Metal and Alloy</td> </tr> </table>																			As metal		As alloy		As Metal and Alloy																						
	As metal																																												
	As alloy																																												
	As Metal and Alloy																																												

**Figure 2.8:** Summary of the elements deposited as single metal or alloys

## 2.4.2 Electrodeposition of Tin with Ionic Liquid

Electrodeposition of Sn in ionic liquids was rarely studied in the past. Few studies were reported on the electrodeposition of Tin(II) in ionic liquids. The first was done by Hussey and Xu [7] in an AlCl<sub>3</sub> mixed in 1-methyl-3-ethyl imidazolium chloride melt. W. Yang *et al.* [8] has done Tin and Antimony electrodeposition in 1-ethyl-3-methylimidazolium tetrafluoroborate, and N. Tachikawa *et al.* [9] has done electrodeposition of Tin(II) in a hydrophobic ionic liquid, 1-*n*-butyl-1-methylpyrrolidinium bis(trifluoromethylsulfonyl)imide.

In the work that carried out by Hussey and Xu, the ionic liquid 1-ethyl-3-methylimidazolium chloride [EMIm]<sup>+</sup>Cl<sup>-</sup> that they deployed is also called room temperature molten salts. This is a mixture of aluminum chloride and an organic halide (RX). It shows adjustable Lewis acidity depending on AlCl<sub>3</sub>/RX molar ratios [7].

Hussey and Xu showed that the electrodeposition of Sn on platinum in  $\text{AlCl}_3\text{-EMIC}$  is a quasi-reversible process [7].

W. Yang *et al.* [8] has done tin and antimony electrodeposition in 1-ethyl-3-methylimidazolium tetrafluoroborate,  $[\text{EMIm}]\text{BF}_4$ . In W. Yang *et al.* work, the  $\text{Sn(II)}$  was introduced into the  $[\text{EMIm}]\text{BF}_4$  along with  $\text{SnCl}_2$ . In the linear sweep voltammetry (LSV) experiments, the cathodic peak potentials of  $\text{Sn(II)}$  shifted negatively as the potential scan rate increased. This had indicated that the  $\text{Sn(II)}$  reductions on Pt electrode exhibit electrochemically irreversible behaviors (**Figure 2.9**). The surface morphologies were examined by SEM (**Figure 2.10**). The tin deposit produced was just needle-type islands, not a continuous plating film on Pt surface [8].

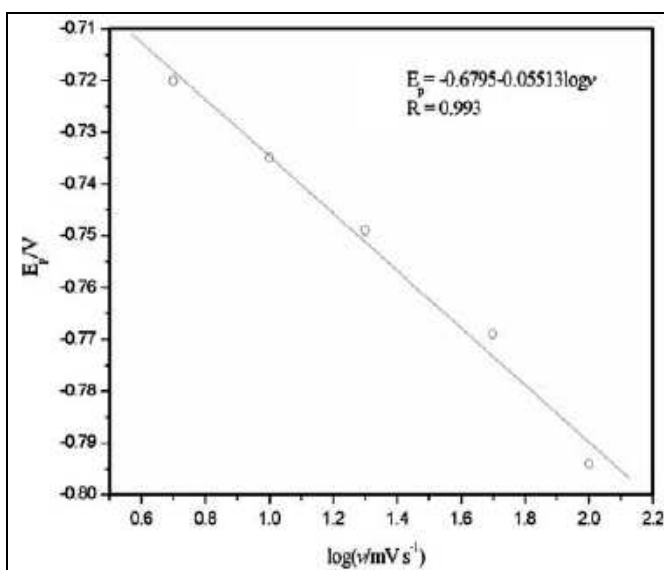


**Figure 2.9:** Linear relationship between the cathodic peak potential of  $\text{Sn(II)}$  reduction & the logarithm of potential scan rate in the  $[\text{EMIm}]\text{BF}_4$  containing 25 mM  $\text{Sn(II)}$  [8].

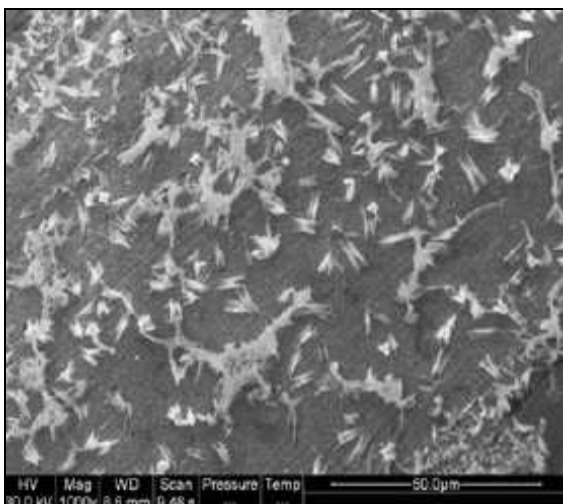


**Figure 2.10:** SEM micrographs of metal electrodeposits from the [EMIm]BF<sub>4</sub> ionic liquid containing 25 mM Sn(II) [8].

N. Tachikawa *et al.* [9] has done electrodeposition of Tin(II) in a hydrophobic ionic liquid, 1-*n*-butyl-1-methylpyrrolidinium bis(trifluoromethylsulfonyl)imide (BMPTFSI). N. Tachikawa *et al.* has reported that tin was introduced into the ionic liquid through potentiostatic anodic dissolution. The oxidation of Sn(II) to Sn(IV) was not possible within the electrochemical potential window of BMPTFSI [9]. In AlCl<sub>3</sub>-EMIC ionic liquids, the oxidation of Sn(II) to Sn(IV) is possible in a basic solution but not in an acidic one, probably because tetravalent species is stabilized by the complex formation with chloride ions in the basic ionic liquid [9]. In cyclic voltammetry experiments that carried out by N. Tachikawa *et al.*, a cathodic current was observed below -0.6 V as shown in **Figure 2.11**. The current loop of the cathodic current during the cathodic and anodic scan is characteristic of a nucleation process, indicating the cathodic current can be attributed to the deposition of Sn. The anodic current peak can be assigned to the stripping of Sn deposited during the preceding cathodic scan [9].

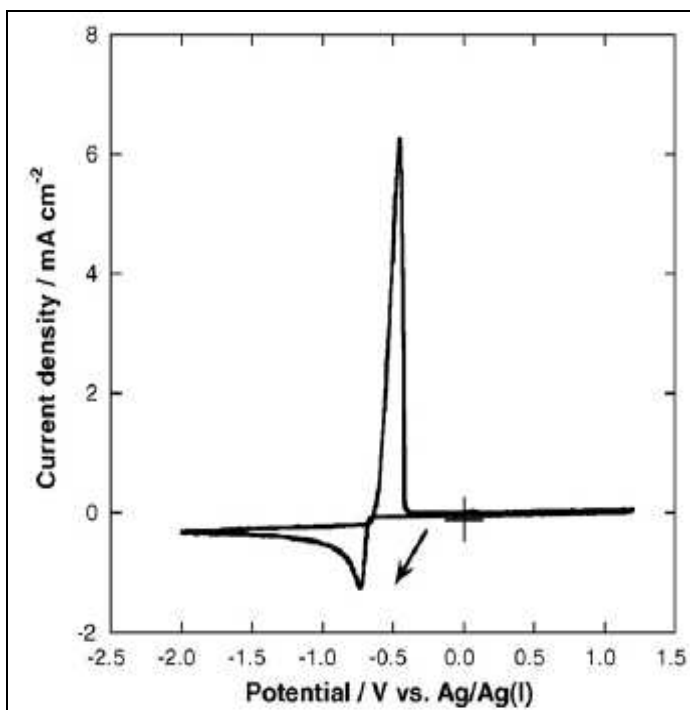


**Figure 2.11:** Cyclic voltammogram of a Pt electrode in BMPTFSI containing  $0.05 \text{ mol dm}^{-3} \text{ Sn(II)}$  at  $25 \text{ }^\circ\text{C}$ ; scan rate:  $20 \text{ mVs}^{-1}$  [9].

Tachikawa *et al.* has performed the electrodeposition of Sn on a Cu substrate in BMPTFSI containing  $0.05 \text{ mol dm}^{-3} \text{ Sn(II)}$  by galvanostatic electrolysis with the current density of  $-0.05 \text{ mA cm}^{-2}$ . A smooth and adhesive electrodeposit with slight brightness was obtained as shown in **Figure 2.12**.

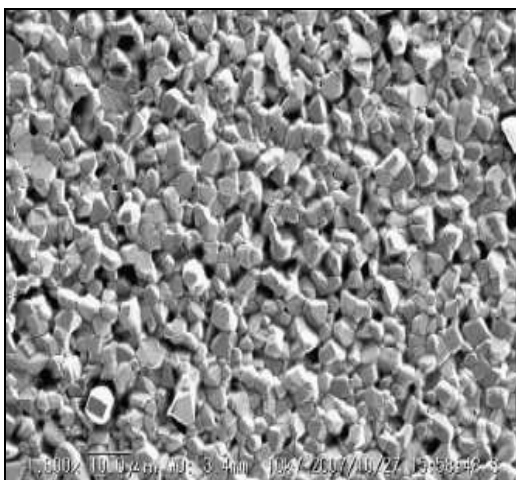


**Figure 2.12:** SEM image of the deposit on the Cu substrate in BMPTFSI containing  $0.05 \text{ mol dm}^{-3} \text{ Sn(II)}$ . The current density was  $-0.05 \text{ mA cm}^{-2}$  [9].

In 1992, Wilkes and Zaworotko reported the first air and moisture stable imidazolium based ionic liquid with either tetrafluoroborate or hexafluorophosphate as anions. Then, several, liquids consisting of 1-ethyl-3-methylimidazolium, 1,2-dimethyl-3-propylimidazolium, or 1-butyl-1-methyl-pyrrolidinium cations with various anions, such as tetrafluoroborate ( $BF_4^-$ ), tri-fluoro-methanesulfonate ( $CF_3SO_3^-$ ), bis(trifluoromethanesulfonyl)imide  $[(CF_3SO_2)_2N]$  & tris(tri fluoro methanesulfonyl) methide  $[(CF_3SO_2)_3C]$ , were found and received much attention because of low reactivity against moisture [6]. In view of the advantages of the air and water stable ionic liquids, we report here the first results on the tin electrodeposition via the mixture of ionic liquid and Methane Sulfonic Acid (MSA) based tin methane sulfonate salts.

### 2.4.3 Electrodeposition of Copper with Ionic Liquid

A study on the electrodeposition of copper in mixture of ionic liquid and acidic electrolyte was reported by Q. B. Zhang *et al.* [18]. Q. B. Zhang *et al.* has carried out copper electrodeposition in an electrolyte which contains mixture of ionic liquid 1-butyl-3-methylimidazolium hydrogen sulfate-[BMIM]HSO<sub>4</sub>, sulfuric acid, hydrated copper sulfate and distilled water. [BMIM]HSO<sub>4</sub> is found to be an efficient leveling additive in copper electrodeposition, leading to more leveled and fine grained cathodic deposits. **Figure 2.13** shows the scanning electron micrographs (SEM) of the copper deposition in the absence and in presence of ionic liquid [BMIM]HSO<sub>4</sub> [18].

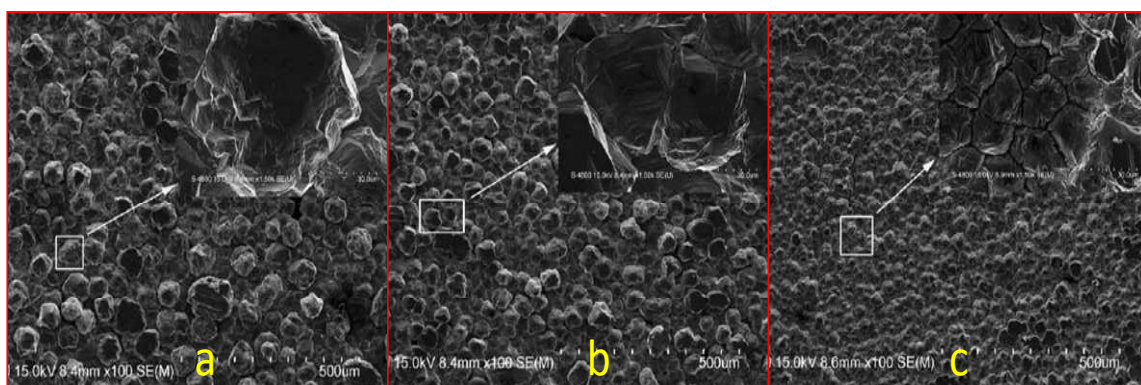


**Figure 2.13:** SEM of copper deposits in the absence and in presence of [BMIM]HSO<sub>4</sub>.

(a) Blank, (b) [BMIM]HSO<sub>4</sub>: 10 mg dm<sup>-3</sup>, (c) [BMIM]HSO<sub>4</sub>: 50 mg dm<sup>-3</sup> [18].

The polarization curves obtained from solution without and with different amounts of [BMIM]HSO<sub>4</sub> are shown in **Figure 2.14** [18]. It is clear that the addition of [BMIM]HSO<sub>4</sub> markedly increases the electro-reduction potential of Cu<sup>2+</sup> ion, along with the reduction of the cathodic current density, denoting an inhibition effect of the electro-crystallization process. [BMIM]HSO<sub>4</sub> increase the cathodic polarization of copper through their adsorption on the cathodic surface and inhibit the kinetics of the Cu<sup>2+</sup> reduction process [18].

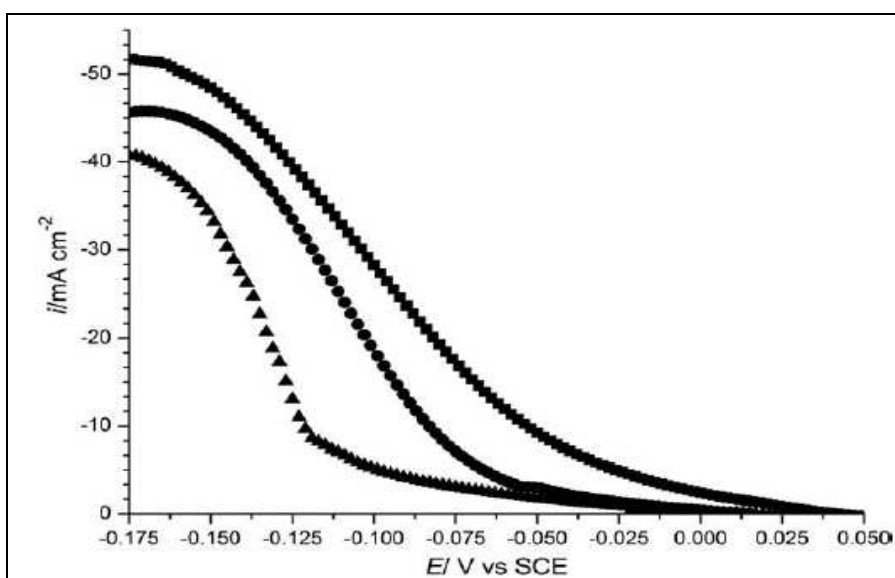


**Figure 2.14:** Effect of [BMIM]HSO<sub>4</sub> on the cathodic polarization for copper electro-deposition with different concentrations: (■) blank, (●) 10 mg dm<sup>-3</sup>, (▲) 50 mg dm<sup>-3</sup> [18].

#### 2.4.4 Electrodeposition of Nickel with Ionic Liquid

The electrodeposition behavior of nickel was investigated at glassy carbon and polycrystalline copper electrodes in the 1-ethyl-3-methylimidazolium dicyanamide (EMI-DCA) room-temperature ionic liquid by M. J. Deng *et al.* [4]. Metallic nickel coatings were prepared on copper substrates by potentiostatic reduction of Ni(II). The current efficiency for electrodeposition of Ni from this ionic liquid is higher than 98%. SEM results (**Figure 2.15**) indicated that the morphology of the Ni electrodeposits is dependent on the deposition potential. AFM results (**Figure 2.16**) also showed that the roughness of the nickel-deposited surface increased as the deposition potential decreased [4].

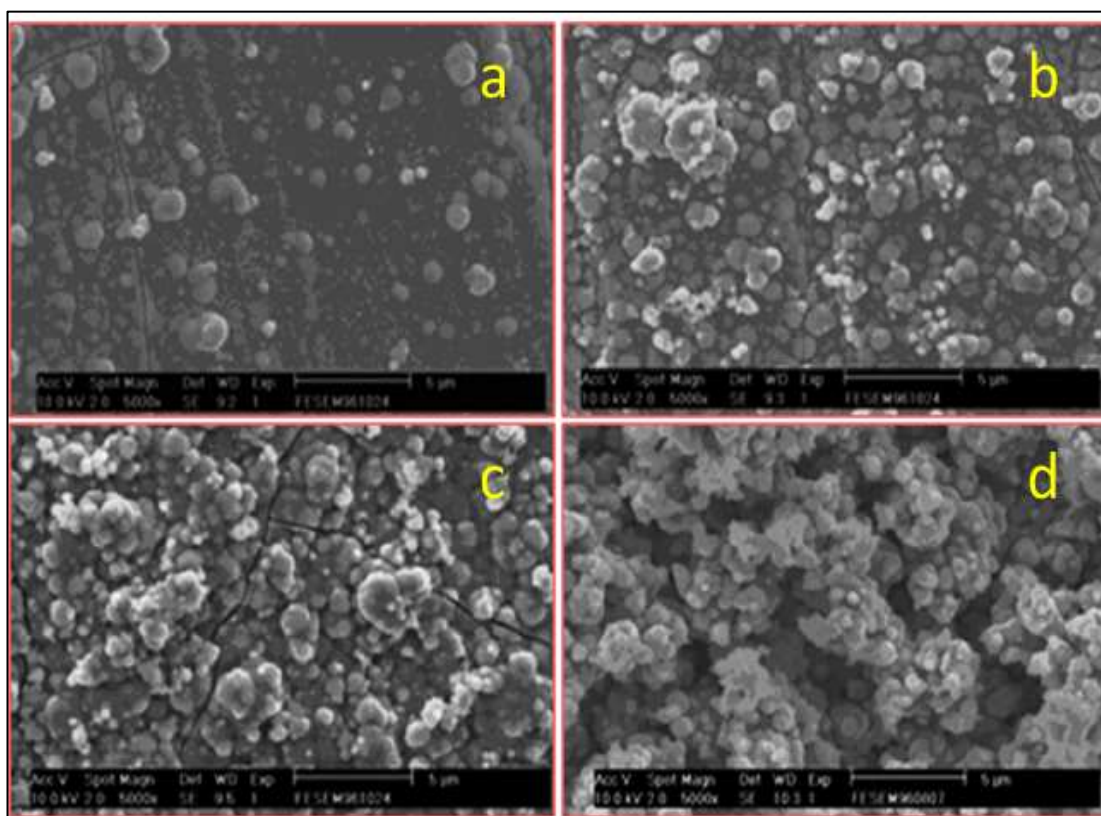


**Figure 2.15:** SEM micrographs of the nickel electrodeposits in the 0.1 M NiCl<sub>2</sub> EMI-DCA solutions at 301 K. a: -1.4V, b: -1.45V, c: -1.5V, d:-1.6V [4].

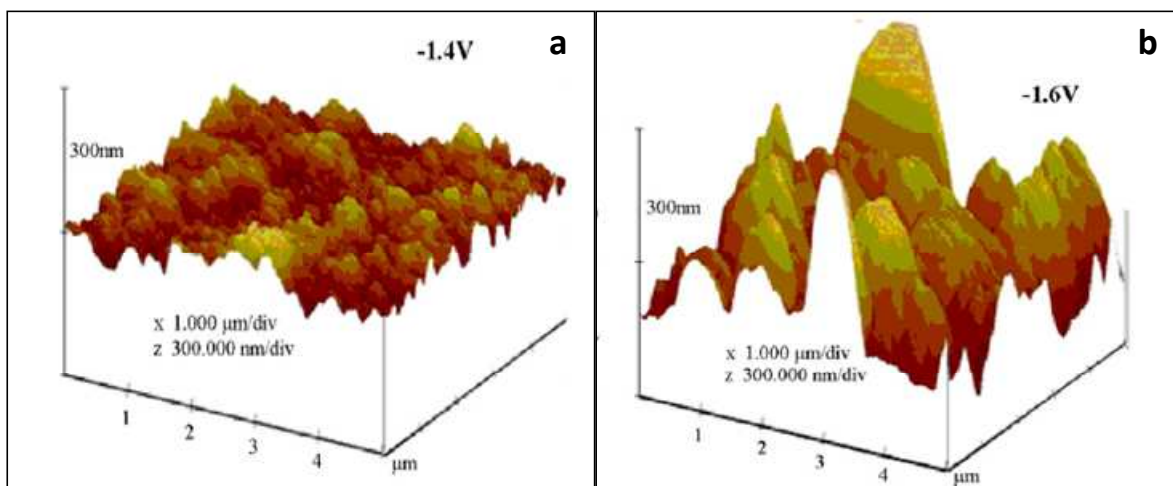


**Figure 2.16:** AFM micrographs of nickel electrodeposits in the 0.1 M NiCl<sub>2</sub> EMI-DCA solutions at 301 K. a: -1.4 V, b: -1.6 V [4].

### 2.4.5 Electrodeposition of Cobalt with Ionic Liquid

The electrodeposition of metallic cobalt from a 1-butyl-3-methylimidazolium tetrafluoroborate (BMIMBF<sub>4</sub>) ionic liquid was investigated by C. Su *et al.* [19]. The cyclic voltammograms of Co(II) in BMIMBF<sub>4</sub> ionic liquid on a Pt working electrode at different scan rates was recorded. The results showed that the reduction of Co(II) to cobalt on a Pt electrode was an irreversible process and controlled by the diffusion of Co(II). The diffusion coefficient for the reduction of Co(II) was calculated to be  $1.76 \times 10^{-8} \text{ cm}^2/\text{s}$  at 60 °C. The cobalt plating was uniform, dense, shining in appearance with good adhesion to the platinum substrate at 60 °C as shown in **Figure 2.17** [19].

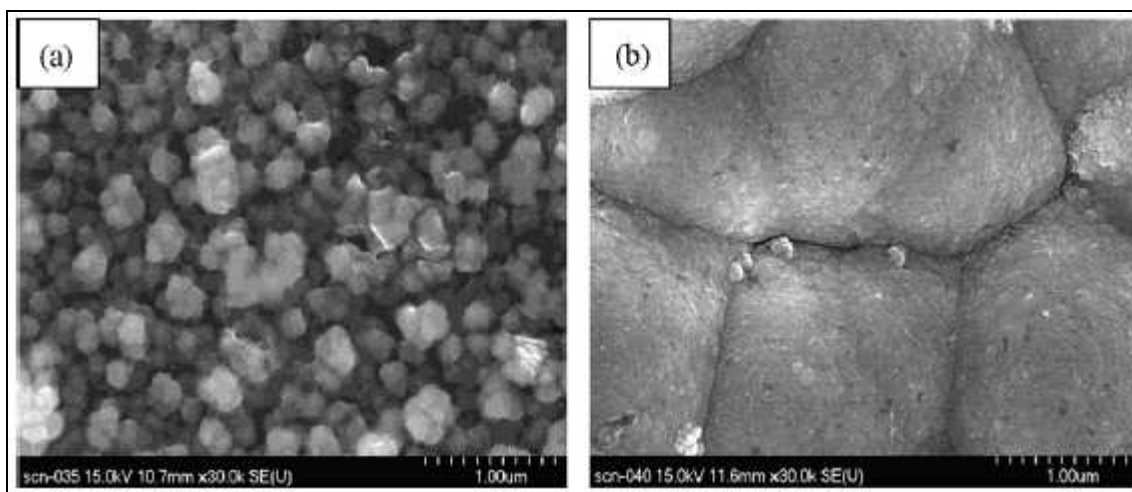


**Figure 2.17:** SEM of cobalt deposits on platinum wires obtained from a solution of 0.5M Co(II) in BMIMBF<sub>4</sub> ionic liquid at different bath temperatures: (a) 40 °C and (b) 60 °C [19].

#### 2.4.6 Electrodeposition of Aluminum with Ionic Liquid

Few studies were reported on the electrodeposition of aluminum in ionic liquids. In S. Z. E. Abedin *et al.* study [6], it has reported that aluminum is highly reactive ( $E^0 = -1.67$  V vs. NHE), the electrodeposition of aluminum in aqueous solutions is impossible owing to a massive hydrogen evolution at the cathode. Therefore, the electrolytes must be aprotic, such as molten salts or organic solvents. The electrodeposition of aluminum in organic solutions had limited success due to a low electrochemical window, low electrical conductivity, volatility, and flammability [6]. Electrodeposition of aluminum and its alloys in ionic liquids based on AlCl<sub>3</sub> was studied intensively in the past. These ionic liquids, formally called room temperature molten salts, are mixtures of aluminum chloride and an organic halide (RX), such as 1-ethyl-3-methylimidazolium chloride [EMIm]<sup>+</sup>Cl<sup>-</sup>. They show adjustable Lewis acidity depending on AlCl<sub>3</sub>/RX molar ratios. Liquids with more than 50 mol% AlCl<sub>3</sub> are Lewis acidic; less than 50 mol%, Lewis basic and neutral if the molar ratio AlCl<sub>3</sub>/RX is 1 [6].

According to S. Z. E. Abedin *et al.*, a major disadvantage of  $\text{AlCl}_3/\text{RX}$  is that the organic halide and  $\text{AlCl}_3$  as educts for the liquid are hygroscopic and extremely hygroscopic, respectively. Therefore, both the educts and the final ionic liquid must strictly be handled under an inert atmosphere or at least under dry air. Furthermore, it is not a standard procedure in the laboratory to make the organic halides water free. Thus, the synthesis of the rather novel air and water stable ionic liquids stimulated further interest in the use of ionic liquids in electrodeposition [6].

S. Z. E. Abedin *et al.* [6] have evaluated ionic liquid 1-butyl-1-methyl pyrrolidinium bis(trifluoromethylsulfonyl)imide saturated with  $\text{AlCl}_3$  in their study.  $\text{AlCl}_3$  dissolves well and homogeneously in the ionic liquid up to a concentration of about 1.5 mol/L giving a clear solution, from which aluminum cannot be deposited. By further increasing of the concentration of  $\text{AlCl}_3$  a biphasic mixture is obtained. By adding more  $\text{AlCl}_3$  the volume of the lower phase decreases till reaching a concentration of 2.7 mol/L, then only one solid phase is obtained at room temperature. The biphasic mixture  $\text{AlCl}_3/\text{IL}$  becomes monophasic by heating up to a temperature of 80 °C as shown in **Figure 2.18**.

S. Z. E. Abedin *et al.* have examined the electrodeposition of aluminum from both phases and they have found that at room temperature aluminum can only be deposited from the upper phase. This is believed that the lower phase is formed by neutral, mixed chloro-[bis(trifluoromethansulfonyl)imide]-aluminium species. In contrast, the upper phase contains the organic cation and a mixture of chloro-[bis(trifluoromethansulfonyl)imide]-aluminate ions. This means that reducible aluminum containing species only exist in the upper phase of the  $\text{AlCl}_3/\text{IL}$  mixture and hence the electrodeposition of aluminum occurs only from the upper phase [6].

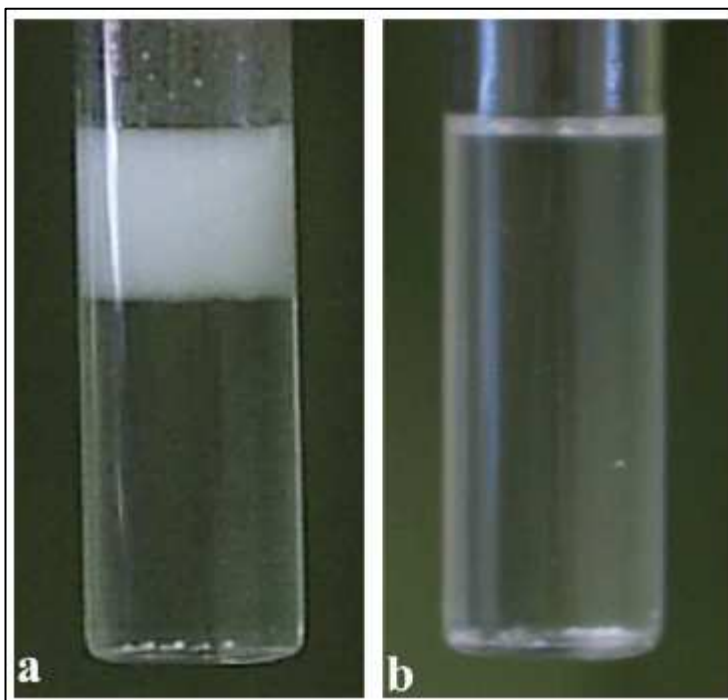


**Figure 2.18:** (a) A biphasic mixture of the ionic liquid 1-butyl-1-methyl pyrrolidinium bis(trifluoromethylsulfonyl)imide containing 1.6 M  $\text{AlCl}_3$  at room temperature. (b) The biphasic mixture becomes monophasic at 80 °C [6].

S. Z. E. Abedin *et al.* have carried out the cyclic voltammetry under two different conditions. One was under room temperature and another one was at 100 °C. A clear nucleation loop is observed in the forward scan for cyclic voltammetry at room temperature as shown in **Figure 2.19**. It indicates that the bulk deposition of aluminum in this complicated system seems to require certain overpotential. However, when the cyclic voltammetry study carried out at 100 °C, in the reverse scan, the anodic scan does not intersect the cathodic one indicating that the deposition of aluminum onto gold substrate at 100 °C does not require an overpotential to initiate nucleation and growth of the bulk deposit (**Figure 2.20**).

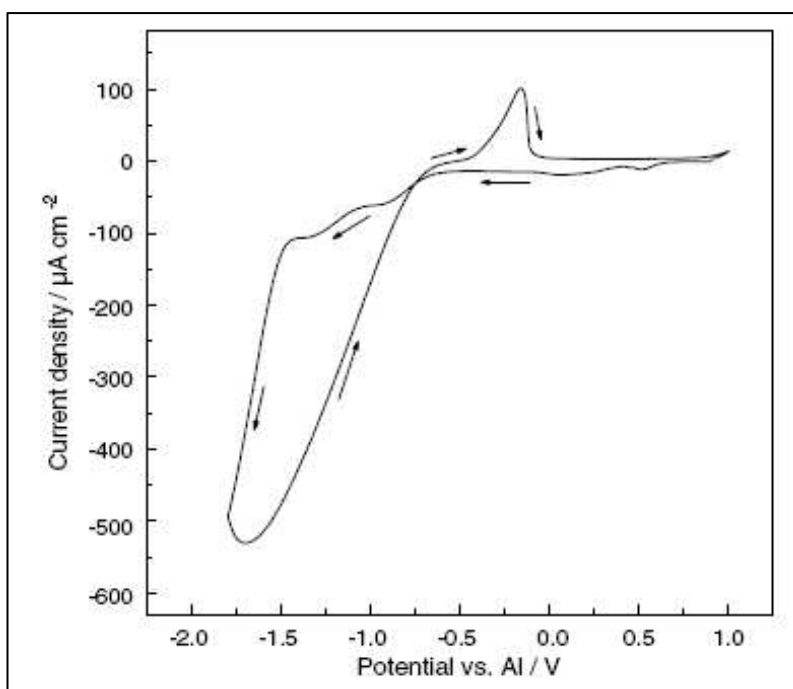


**Figure 2.19:** Cyclic voltammogram in the ionic liquid ([BMP]-Tf<sub>2</sub>N) containing 1.6M AlCl<sub>3</sub> at room temperature [6].

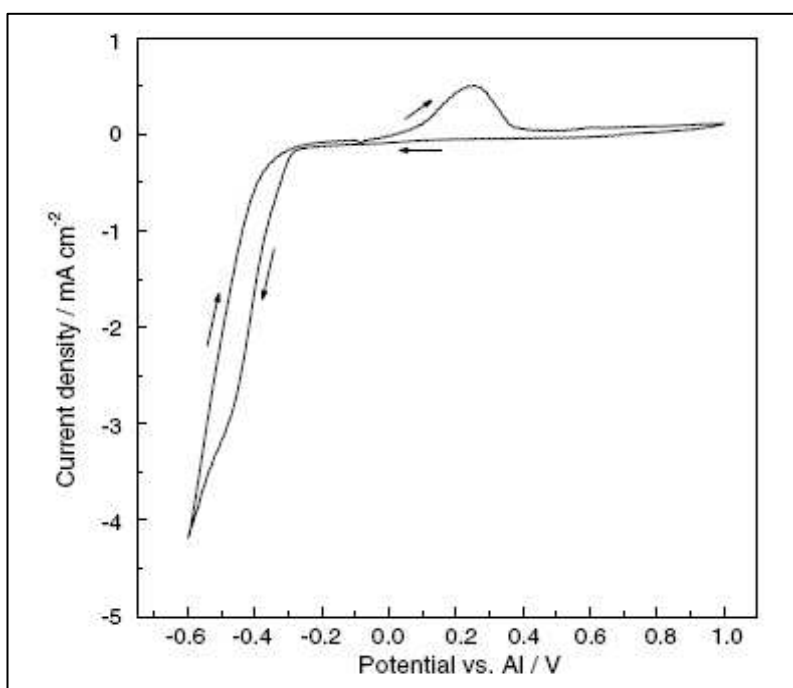


**Figure 2.20:** Cyclic voltammogram in the ionic liquid ([BMP]-Tf<sub>2</sub>N) containing 1.6M AlCl<sub>3</sub> at 100 °C [6].

The aluminum electrodeposits obtained at room temperature and at 100 °C were investigated by means of a high resolution field-emission scanning electron microscope (SEM) by S. Z. E. Abedin *et al.* Based on the SEM diagram (**Figure 2.21**), remarkably the crystallites become finer and deposition improved at 100 °C compared with the study done at room temperature [6].

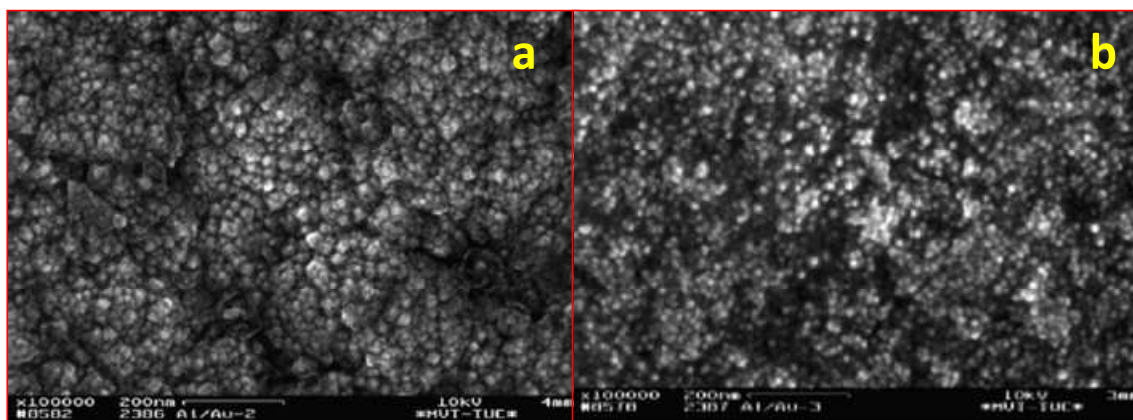


**Figure 2.21:** SEM micrographs of electrodeposited Al in the upper phase of the mixture  $\text{AlCl}_3$  and  $[\text{BMP}]\text{Tf}_2\text{N}$ : (a) at room temperature; (b) at 100 °C [6].

S. Caporali *et al.* [20] have carried out the electrodeposition of Aluminum in ionic liquid 1-butyl-3-methyl-imidazolium heptachloroaluminate ( $[\text{BMIM}]\text{Al}_2\text{Cl}_7$ ). The aluminum was deposited on carbon steel (UNI Fe360B) as protective coating against steel corrosion.

S. Caporali *et al.* have reported that the current efficiency for the electrochemical reduction of aluminum was nearly 100% in ionic liquid 1-butyl-3-methyl-imidazolium heptachloroaluminate ( $[\text{BMIM}]\text{Al}_2\text{Cl}_7$ ) [20]. The electroreduction process was carried out at constant current density ( $10 \text{ mA cm}^{-2}$ ) and controlling the time of deposition. Three series of samples for 1, 2 and 4 hours of deposition were shown in **Figure 2.22**.

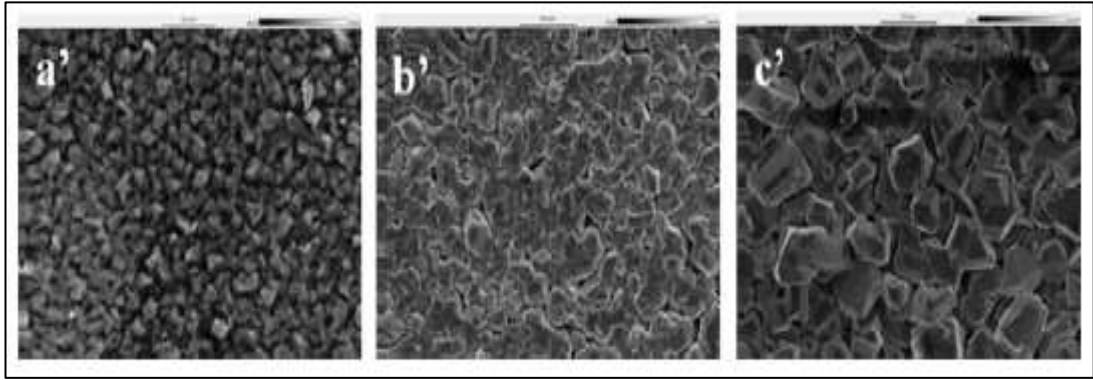


**Figure 2.22:** SEM micrographs obtained from the carbon steel samples coated with aluminum layers. The samples named a' are obtained after 1 hour deposition, b' after 2 hours and c' after 4 hours [20].

The electrochemical corrosion test on aluminum was studied by S. Caporali *et al.* [20]. Open-circuit potential curves (OCVs) were recorded in aerated 3.5 wt% NaCl aqueous solution as a function of time. In **Figure 2.23** shows the OCV curves obtained for the three different aluminated samples compared with the bare carbon steel and the pure aluminum. The bare carbon steel samples show a shift of the potential towards more negative values reaching the almost constant value of about -0.70 V/SCE after 5 hours. The aluminated samples are characterized by an initial period where the potential remains almost unchanged, followed by a shift towards more negative potentials. This behavior, very close to that of pure aluminum, can be related to the change of the surface due to the degradation of the thin aluminum oxide layer present on the sample and removed in the chloride containing solutions [20].

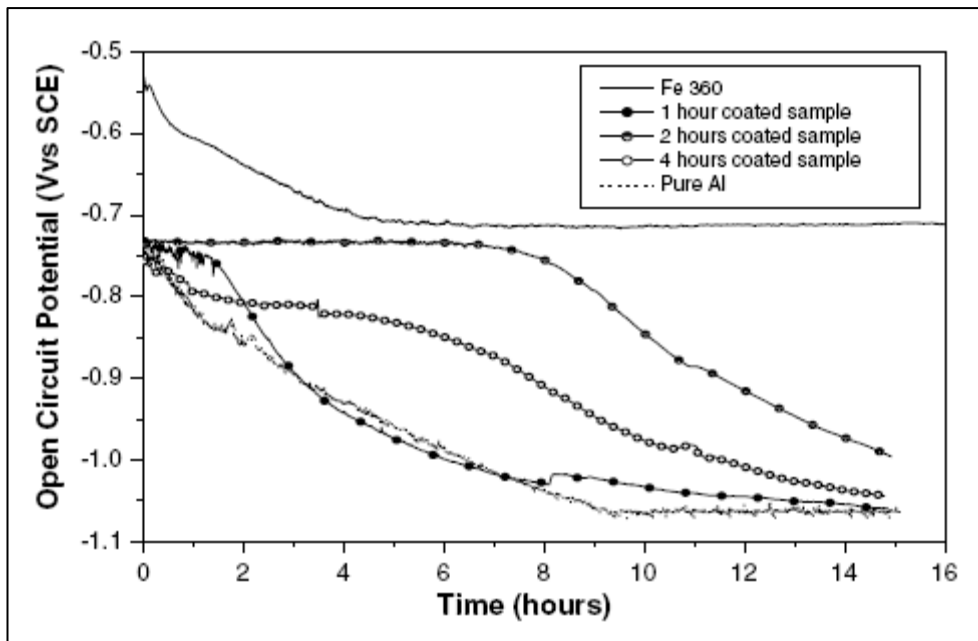


**Figure 2.23:** OCV curves of different thickness aluminum coated samples compared with the bare carbon steel and the pure aluminum in 3.5 wt% NaCl aqueous solution [20].

Neutral salt spray (NSS) test was also done by S. Caporali *et al.*[20], bare carbon steel and the three series of coated samples with different aluminum thickness, 10  $\mu\text{m}$ , 20  $\mu\text{m}$  and 40  $\mu\text{m}$  were prepared and subjected in the salt spray chamber up to 75 days (**Figure 2.24**).

The evolution of the corrosion spots was the same for all the samples, but the presence of thicker aluminum layer contribute to the slowing down of the corrosion process. After just 1 day, the bare carbon steel samples were completely covered by corrosion. On the other hand, the complete removal of the product with 10  $\mu\text{m}$  coating takes about 30 days (**Figure 2.25**). 20  $\mu\text{m}$  coating take about 70 days of exposition, while at the end of the experiment (75 days) the samples coated with 40  $\mu\text{m}$  of aluminum shown only about the 25% of the coating removed.

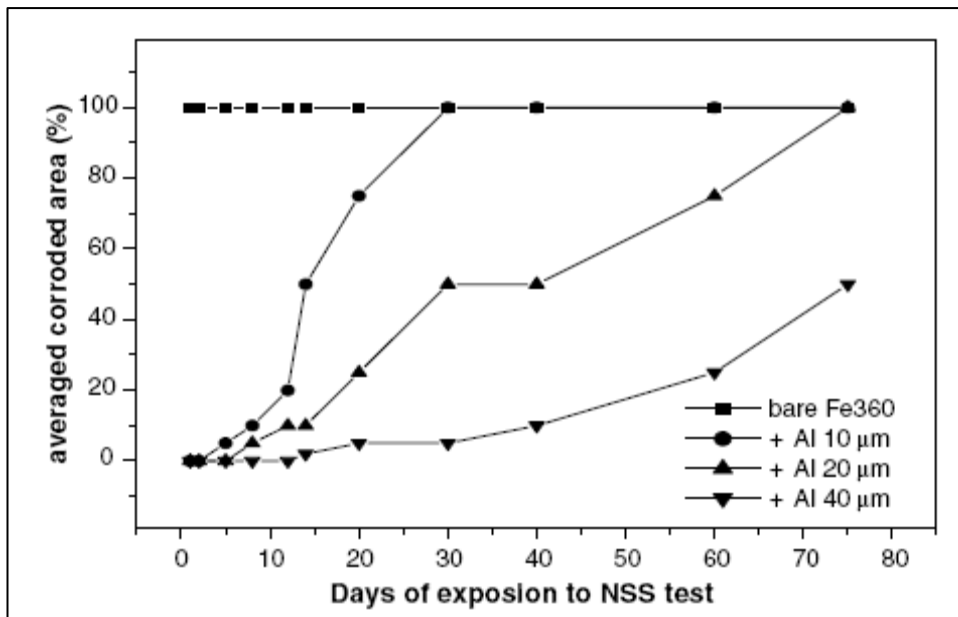


**Figure 2.24:** Salt spray test corrosion kinetics for the aluminum coated carbon steel [20].

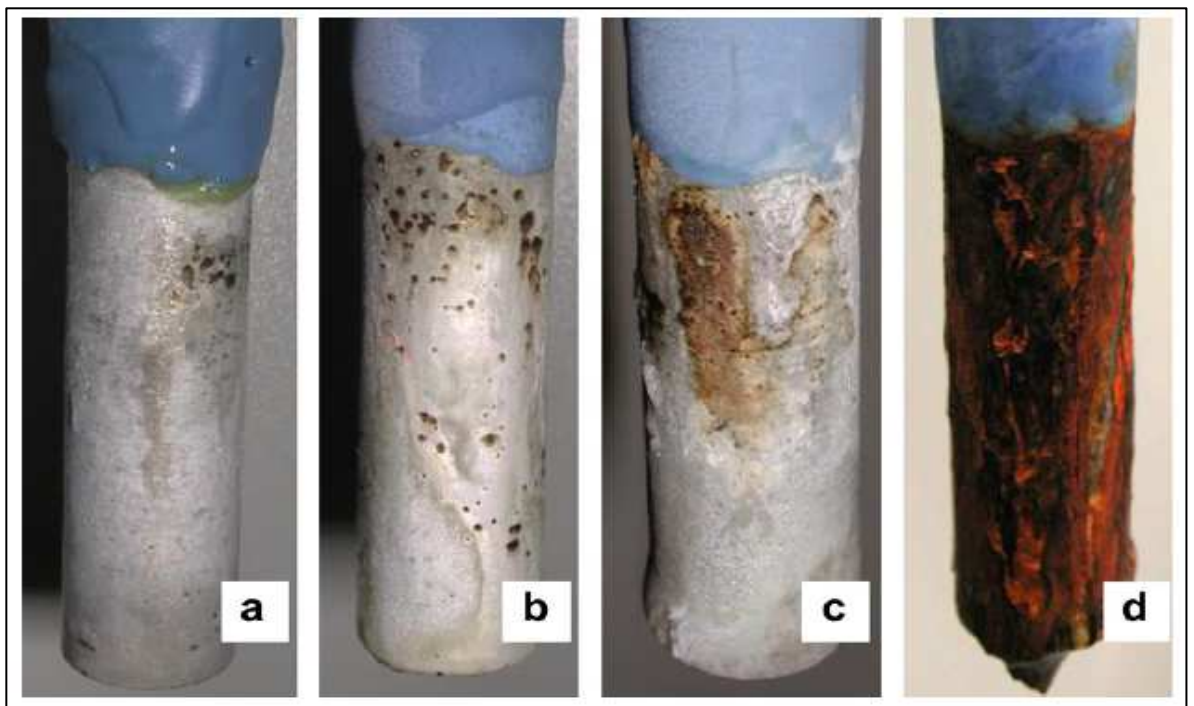


**Figure 2.25:** Sequence of images showing the process of degradation for a carbon steel sample coated with 10 μm of aluminum during the NSS test. The pictures are taken, respectively, after (a) 5, (b) 8, (c) 14, (d) 30 days of exposure [20].

T. Jiang *et al.* [21] have done the aluminum electrodeposition from acidic  $\text{AlCl}_3$ -[EMIm]Cl ionic liquids on aluminum substrates at above room temperatures (60 and 90 °C). The conductivities of 1.5: 1 and 2: 1  $\text{AlCl}_3$ / [EMIm]Cl ionic liquids were measured as a function of the temperature and electrolyte composition. As shown in **Figure 2.26**, the conductivities of ionic liquids increase as the electrolyte temperature increases. This is because the viscosity of the liquid decreases and hence the mobility of the ions increases. The activation energies determined from the slope of the Arrhenius plot (see the inset graph of **Figure 2.26**) are 14.3 kJ/mol for 1.5 :1  $\text{AlCl}_3$  / [EMIm]Cl and 14.6 kJ/mol for 2.0: 1  $\text{AlCl}_3$ / [EMIm]Cl, respectively [21]. In T. Jiang *et al.* study, it was found that 1.5: 1 and 2: 1  $\text{AlCl}_3$ / [EMIm]Cl ionic liquids are quite stable below 100 °C. However, they became dark brown quickly as the temperature increases above 160 °C. The change in the color was probably due to the chemical decomposition of [EMIm]Cl [21].

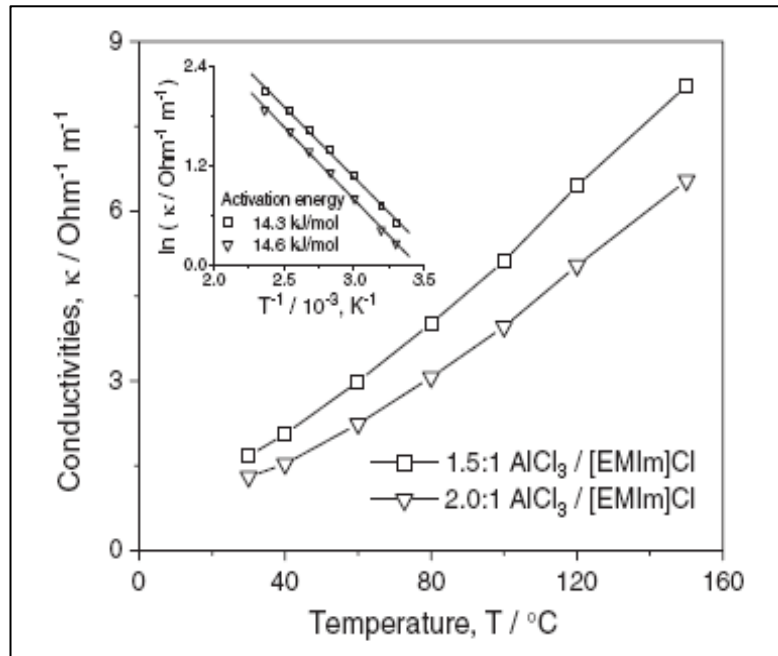


**Figure 2.26:** Electrical conductivities of  $\text{AlCl}_3$ -[EMIm]Cl ionic liquids as a function of the temperature and composition. The inset shows the Arrhenius plot of data [21].

Cyclic voltammetry study was done by T. Jiang *et al.* and the cyclic voltammogram was recorded on aluminum electrode with a scan rate of 100 mV/s (**Figure 2.27**). It is apparent that the cathodic process at  $C_1$  corresponds to the deposition of aluminum whereas the anodic peak at  $A_1$  was ascribed to the subsequent stripping of the deposited aluminum. The anodic oxidation current decreases to almost zero at +0.8 V due to passivation of the Al electrode. It is believed that the passivation behaviors attributed to  $AlCl_3$  precipitation on the electrode surface or to the adsorbed monovalent to trivalent aluminum intermediates. However, it is also possible that the decrease of anodic oxidation current is due to the presence of the oxides that were not completely removed from Al electrode by the pre-treatment. Another possibility is the film formation from the decomposition of the organic cation if the deposition is performed at current densities beyond the decomposition limit [21].

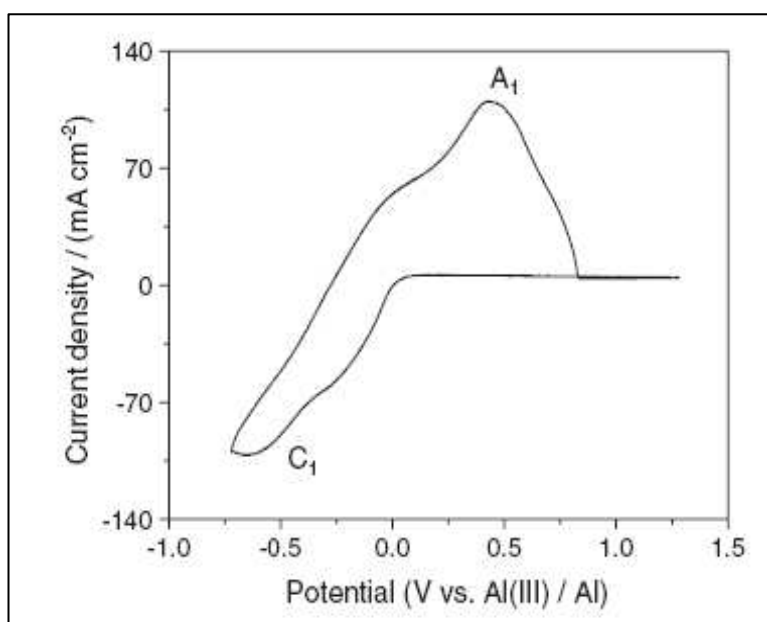


**Figure 2.27:** A typical voltammogram recorded on Al electrode in 2:1 molar ratio  $AlCl_3$ -[EMIm]Cl at 60 °C. Scan rate: 0.1 V/s [21].

The constant current deposition of aluminum from 2: 1  $AlCl_3$ - [EMIm]Cl was carried out on Al substrates by T. Jiang *et al.* **Figure 2.28** shows the surface morphologies of

the four representative aluminum deposits obtained at 20, 30, 50 and 70 mA/ cm<sup>2</sup>. With a current density of 20 mA/ cm<sup>2</sup>, the sample substrate was covered with non continuous aluminum deposits consisting of aluminum crystallites in the order of 30–50 μm in size. The deposits obtained at 30 and 50 mA/ cm<sup>2</sup> are quite smooth and have similar surface morphology, consisting of aluminum crystalline in the order of 5–10 μm. The deposit obtained at 70 mA/ cm<sup>2</sup> is much rougher, but it is still quite dense and well adherent. The results also show that the current efficiency increases from 85% to nearly 100% as the current density increases from 10 to 40 mA/ cm<sup>2</sup>. When the current density was raised further, the current efficiency decreases to a constant value of approximately 92% between 50–100 mA/ cm<sup>2</sup> [21].

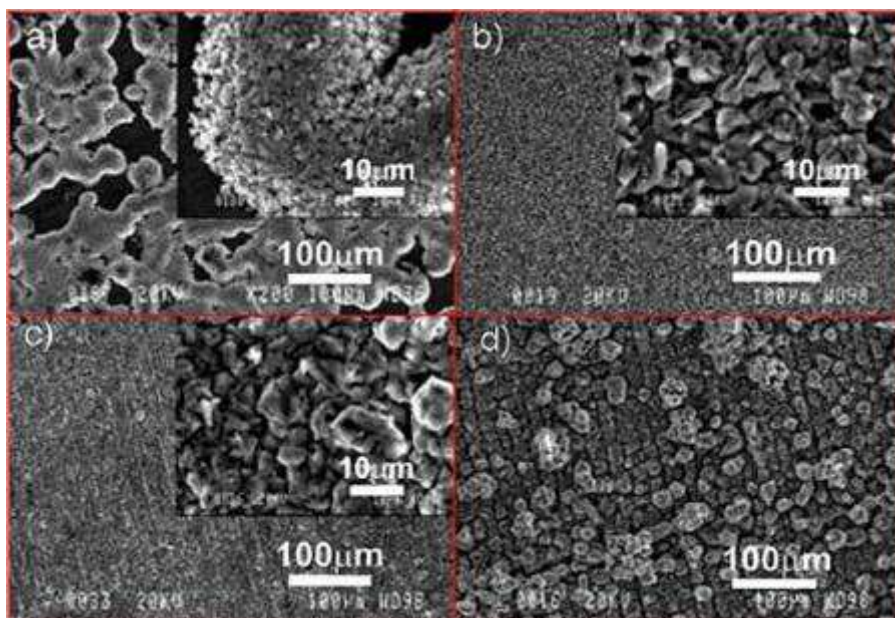


**Figure 2.28:** SEM micrographs of aluminum electrodeposits obtained on Al substrates from 2:1 molar ratio AlCl<sub>3</sub>-[EMIm]Cl at 90 °C with different current densities for 1 hour. a) 20 mA/ cm<sup>2</sup>, b) 30 mA/ cm<sup>2</sup>, c) 50 mA/ cm<sup>2</sup>, d) 70 mA/ cm<sup>2</sup> [21].

## 2.4.7 Electrodeposition of Palladium with Ionic Liquid

Y. Bando *et al.* [22] reported that it is not easy to obtain the Pd films without hydrogen embrittlement by electrodeposition from conventional aqueous plating baths since Pd has high catalytic activity against hydrogen evolution and absorbs great amount of hydrogen. As a result, the electrochemical reduction of palladium halide complexes was investigated by Y. Bando *et al.* in a hydrophobic room-temperature ionic liquid (RTIL), 1-n-butyl-1-methylpyrrolidinium bis(trifluoromethylsulfonyl)imide (BMPTFSI) [22]. Cyclic voltammetry experiments was carried out by Y. Bando *et al.*, **Figure 2.29** shows the cyclic voltammogram of the Pt electrode in 10 mM  $\text{PdCl}_4^{2-}$ /BMPTFSI. The reduction peak of  $\text{PdCl}_4^{2-}$  appeared at  $-1.8$  V, which was more negative than that for  $\text{PdBr}_4^{2-}$  by about 0.2 V. The deposition of metallic Pd was also possible from  $\text{PdCl}_4^{2-}$ /BMPTFSI. The shift in the peak potential can be attributed to the difference in donor property of the ligand. Since the donor number of  $\text{Cl}^-$  is larger than that of  $\text{Br}^-$ , the chlorocomplex is expected be more stabilized than the bromocomplex [22].

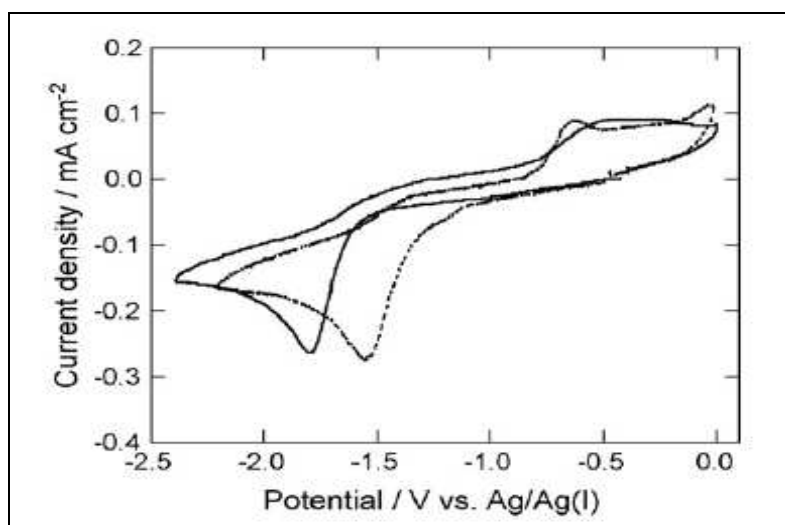


**Figure 2.29:** Cyclic voltammograms of a Pt electrode in BMPTFSI containing 10 mM  $\text{PdCl}_4^{2-}$  (—) and 10 mM  $\text{PdBr}_4^{2-}$  (- - -) at 25 °C. Scan rate: 50mVs<sup>-1</sup> [22].

Galvanostatic electrodeposition was carried out by Y. Bando *et al.* and the deposits show at the SEM images (**Figure 2.30**). Black and powdery deposits were obtained at higher current densities ( $-0.05 \text{ mAcm}^{-2}$ ). However, smooth deposits with brightness could be obtained at lower current densities ( $-0.01 \text{ mAcm}^{-2}$ ). The electrode reaction of  $\text{PdBr}_4^{2-}$  to metallic Pd was irreversible and the diffusion coefficient of  $\text{PdBr}_4^{2-}$  was about  $(1-2) \times 10^{-7} \text{ cm}^2 \text{ s}^{-1}$  at  $25^\circ \text{C}$ . It was suggested by Y. Bando *et al.* that the initial stage of the electrodeposition of Pd from  $\text{PdBr}_4^{2-}$ / BMPTFSI on the polycrystalline Pt electrode surface involves three-dimensional progressive nucleation under diffusion control [22].

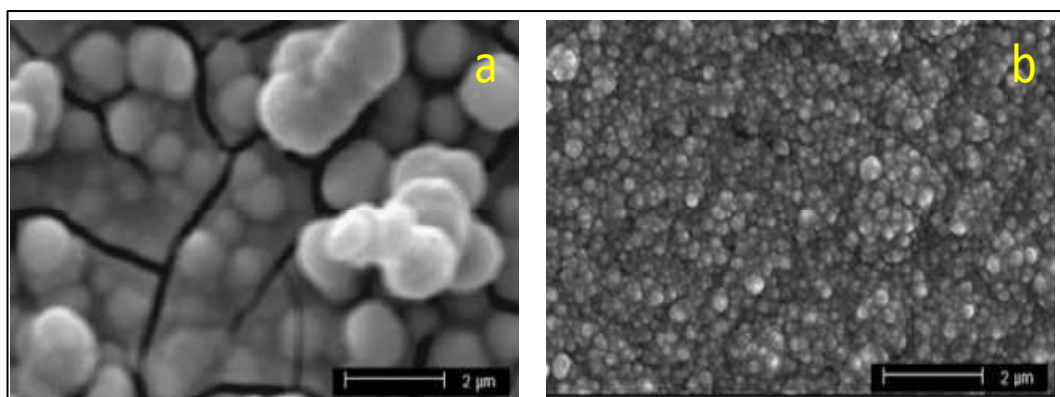


**Figure 2.30:** SEM images of the deposits on the Ni substrates by the galvanostatic electrodeposition in 10 mM  $\text{PdBr}_4^{2-}$ / BMPTFSI at  $25^\circ \text{C}$ . The current densities were (a)  $-0.05 \text{ mAcm}^{-2}$ , (b)  $-0.01 \text{ mAcm}^{-2}$  [22].

# 3. METHODOLOGY

## 3.1 Electrochemical Method

Voltammetry is an electrochemical method in which current is measured as a function of the applied potential. It is a branch of electrochemistry in which the electrode potential, or the faradaic current or both are changed with time. Normally, there is an interrelationship between all these three variables. The principle of this technique is a measurement of the diffusion controlled current flowing in an electrolysis cell in which one electrode is polarisable. In this technique a time dependent potential is applied to an electrochemical cell, and the current flowing through the cell is measured as a function of that potential. A plot of current which is directly proportional to the concentration of an electroactive species as a function of applied potential is called a voltammogram. The voltammogram provides quantitative and qualitative information about the species involved in the oxidation or reduction reaction or both at the working electrode [23, 24].

### 3.1.1 Cyclic Voltammetry

Cyclic voltammetry is a type of potentiodynamic electrochemical measurement. Cyclic voltammetry consists of cycling the potential of an electrode, which is immersed in an unstirred solution, and measuring the resulting current. The method uses a reference electrode (RE), working electrode (WE), and counter electrode (CE) which in combination are sometimes referred to as a three-electrode setup. Electrolyte is usually added to the test solution to ensure sufficient conductivity. Cyclic voltammetry is the most widely used technique for acquiring qualitative information about electrochemical reactions. Analysis of the current response can give considerable information about the

thermodynamics of redox processes, the kinetics of heterogeneous electron-transfer reaction and the coupled chemical reactions or adsorption processes. It is often the first electrochemical experiment performed in an electrochemical study especially for any new analyte since it offers a rapid location of redox potentials of the electro active species and convenient evaluation of the effect of media upon the redox process. In cyclic voltammetry, the electrode potential ramps linearly versus time as shown. This ramping is known as the experiment's scan rate (V/s). The potential is measured between the reference electrode and the working electrode and the current is measured between the working electrode and the counter electrode. The controlling potential which is applied across working electrode and reference electrode such as saturated calomel electrode (SCE) or a silver/silver chloride electrode (Ag/AgCl) can be considered an excitation signal. The excitation signal for CV is a linear potential scan with a triangular waveform as shown in **Figure 3.1**. This triangular potential excitation signal sweeps the potential of the electrode between 2 values, sometimes called the switching potentials. The excitation signal in **Figure 3.1** causes the potential first to scan negatively from +0.80 V to -0.20 V versus SCE at which point the scan direction is reversed, causing a positive scan back to original potential of +0.80 V. The scan rate, as reflected by the slope is 50 mV/s. A second cycle is indicated by the dashed line. Single or multiple cycles can be used. Modern instrumentation enables switching potentials and scan rate to be easily varied. A cyclic voltammogram is obtained by measuring the current at the working electrode during the potential scan. The current can be considered the response signal to the potential excitation signal. The voltammogram is a display of current (vertical axis) versus potential (horizontal axis). Because the potential varies linearly with time, the horizontal axis can also be thought of as time axis. This is helpful in understanding the fundamentals of the technique.

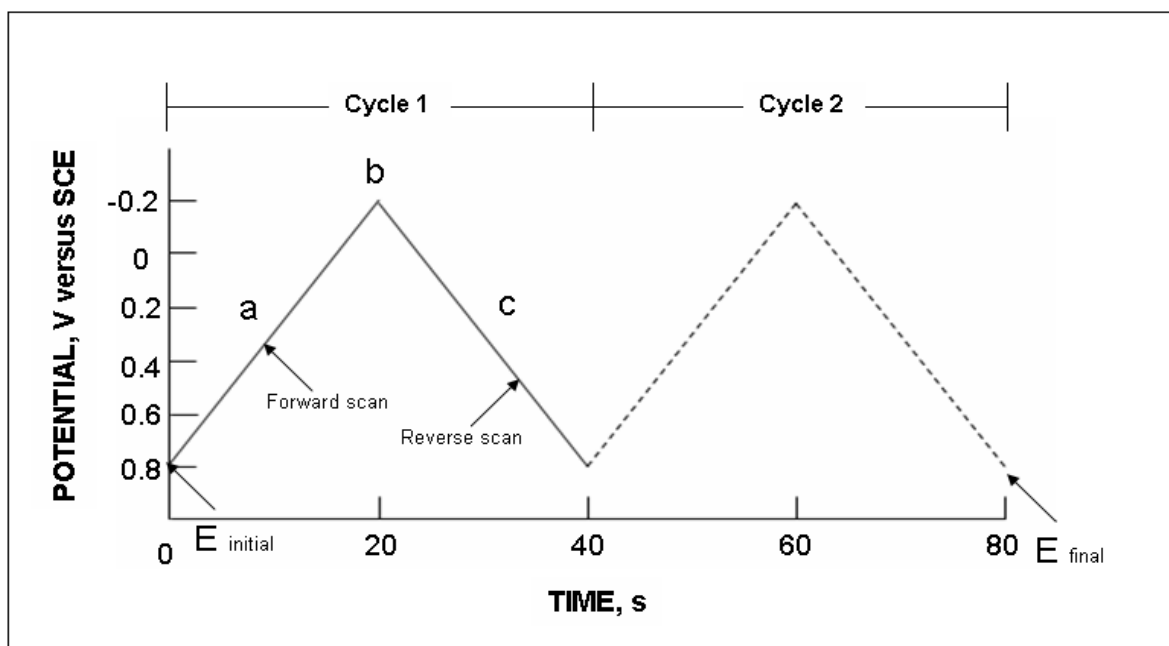


**Figure 3.1:** Typical excitation signal for cyclic voltammetry – a triangular potential waveform with switching potential at 0.8 and -0.2 V versus SCE

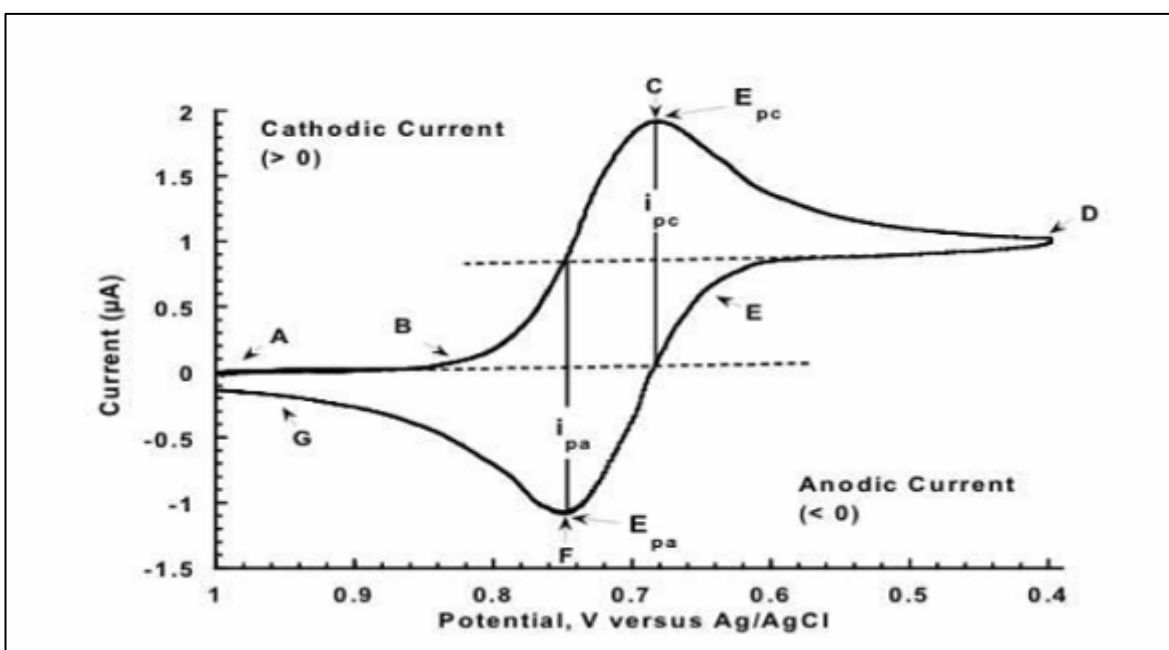


**Figure 3.2:** A typical cyclic voltammogram

**Figure 3.2** illustrates a typical cyclic voltammogram. In the parts “A”, “B” and “C”, the potential is applied and an increasing amount of current is observed. This is the cathodic part of the wave, where reduction of the electrolyte molecules is occurring. Maximum flow of electrons is observed at point “C”. After point “C”, potential is still applied, but the current associated with the reduction decreases due to depletion of electrolyte molecules at the electrode. Ion diffusion toward the electrode must occur before reduction. Here diffusion is slower than reduction and therefore there is a reduction in the current flow between the parts “C” and “D”. Parts “E”, “F” and “G” describe the reverse process. When the voltage is decreased, the reverse oxidation process occurs, and the electrolyte molecules are returned to their initial state. The important parameters of a cyclic voltammogram are the magnitudes of the anodic peak current ( $i_{pa}$ ) and cathodic peak current ( $i_{pc}$ ), and the anodic peak potential ( $E_{pa}$ ) and cathodic peak potential ( $E_{pc}$ ). These parameters are labeled in **Figure 3.2**. A redox couple in which both species rapidly exchange electrons with the working electrode is termed an electrochemically reversible couple. The formal reduction potential ( $E^\circ$ ) for a reversible couple is centered between  $E_{pa}$  and  $E_{pc}$  [13, 25-27].

$$E^\circ = \frac{E_{pa} + E_{pc}}{2} \quad (3.1)$$

The number of electrons transferred in the electrode reaction ( $n$ ) for a reversible couple can be determined from the separation between the peak potentials

$$\Delta E_p = E_{pa} - E_{pc} \cong \frac{0.059}{n} \quad (3.2)$$

The peak current for a reversible system is described by the Randles-Sevcik equation.

$$I_p = (2.69 \times 10^5) n^{3/2} A D^{1/2} C v^{1/2} \quad (3.3)$$

where;

$n$  = number of electron

$A$  = electrode area ( $\text{cm}^2$ )

$C$  = concentration ( $\text{mol cm}^{-3}$ )

$D$  = diffusion coefficient ( $\text{cm}^2 \text{s}^{-1}$ )

$\nu$  = scan rate ( $\text{V s}^{-1}$ )

Accordingly,  $I_p$  increases with  $\nu^{1/2}$  and is directly proportional to concentration. The relationship to concentration is particularly important in analytical application and in studies of electrode mechanisms. The value of  $i_{pa}$  and  $i_{pc}$  should be identical for a simple reversible (fast) couple. That is

$$\frac{i_{pa}}{i_{pc}} = 1 \quad (3.4)$$

However, the ratio of peak currents can be significantly influenced by chemical reactions coupled to the electrode process.

### 3.1.2 Chronoamperometry

Chronoamperometry (CA) is an electrochemical method in which a step potential is applied and the current,  $i$ , is measured as a function of time,  $t$ . This  $i$ - $t$  response is comprised of two components: the current due to charging of the double-layer and the other due to the electron transfer reaction with the electro active species. The results are most easily interpreted when a planar (flat) electrode is used in a quiet, unstirred solution, and the applied potential is sufficient to reduce or oxidize the electro active species as fast as it gets to the electrode surface, i.e., at a diffusion-controlled rate. When Current,  $i$ , vs. time  $t$ , response in the presence of an electro active species that

undergoes an electron transfer reaction at a diffusion-controlled rate, under these conditions, the current is given by the Cottrell relationship [13,15,28].

In electrochemistry, the Cottrell equation describes the change in electric current with respect to time in a controlled potential experiment, such as chronoamperometry. The current measured depends on the rate at which the analyte diffuses to the electrode. That is, the current is said to be "diffusion controlled." The Cottrell equation describes the case for an electrode that is planar [24, 29-34].

$$i(t) = \frac{nFAD^{1/2}C}{\pi^{1/2}t^{1/2}} \quad (3.5)$$

Where

$i$  = current, in unit A

$n$  = number of electrons (to reduce/oxidize one molecule of analyte  $j$ , for example)

$F$  = Faraday constant, 96,485 C/mol

$A$  = area of the (planar) electrode in  $\text{cm}^2$

$C$  = initial concentration of the reducible analyte  $j$  in  $\text{mol}/\text{cm}^3$ ;

$D$  = diffusion coefficient in  $\text{cm}^2/\text{s}$

$t$  = time in s

Application of Chronoamperometry are as follows:

- Analyze the shape of the current-time curve in order to study coupled chemical reactions.
- Determination of:  $n$  (moles of electrons);  $A$  (surface area of electrode);  $D$  (diffusion coefficient of analyte)

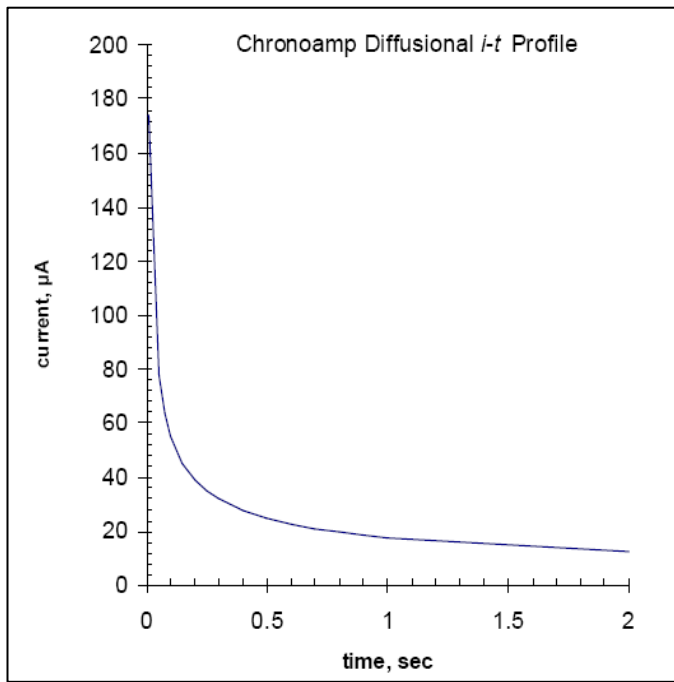


**Figure 3.3:** Chronoamperometry Diffusional  $i-t$  profile

## 3.2 Spectroscopy and Microscopy Analysis

### 3.2.1 Scanning Electron Microscopy (SEM)



**Figure 3.4:** SEM and EDX: Philips XL and EDAX Analyzer Genesis

The scanning electron microscope (SEM), **Figure 3.4**, is a type of electron microscope that images the sample surface by scanning it with a high-energy beam of electrons. The electrons interact with the atoms that make up the sample producing signals that contain information about the sample's surface morphology, composition and other properties such as electrical conductivity. The types of signals produced by an SEM include secondary electrons, back-scattered electrons (BSE), characteristic X-rays, light (cathodoluminescence), specimen current and transmitted electrons. Secondary electron detectors are common in all SEMs, but it is rare that a single machine would have detectors for all possible signals. The signals result from interactions of the electron beam with atoms at or near the surface of the sample. In the most common or standard detection mode, secondary electron imaging or SEI can produce very high-resolution images of a sample surface, revealing details about less than 1 to 5 nm in size. Due to

the very narrow electron beam, SEM micrographs have a large depth of field yielding a characteristic three-dimensional appearance useful for understanding the surface structure of a sample. A wide range of magnifications is possible, from about 10 times (about equivalent to that of a powerful hand-lens) to more than 500,000 times, about 250 times the magnification limit of the best light microscopes [35,36].

Back-scattered electrons (BSE) are beam electrons that are reflected from the sample by elastic scattering. BSE are often used in analytical SEM along with the spectra made from the characteristic X-rays. Because the intensity of the BSE signal is strongly related to the atomic number (Z) of the specimen, BSE images can provide information about the distribution of different elements in the sample. For the same reason, BSE imaging can image colloidal gold immuno-labels of 5 or 10 nm diameter which would otherwise be difficult or impossible to detect in secondary electron images in biological specimens. Characteristic X-rays are emitted when the electron beam removes an inner shell electron from the sample, causing a higher energy electron to fill the shell and release energy. These characteristic X-rays are used to identify the composition and measure the abundance of elements in the sample. Electron Gun- The source of electrons is located at the top of the column where electrons are emitted from a hot tungsten filament and accelerated down an evacuated column (**Figure 3.5**). The three gun components are the filament, the Wehnelt, which controls the number of electrons leaving the gun, and the anode, which accelerates the electrons to a selectable voltage between 1 – 30 kV. A vacuum is necessary because electrons can travel only short distances in air [37-39].

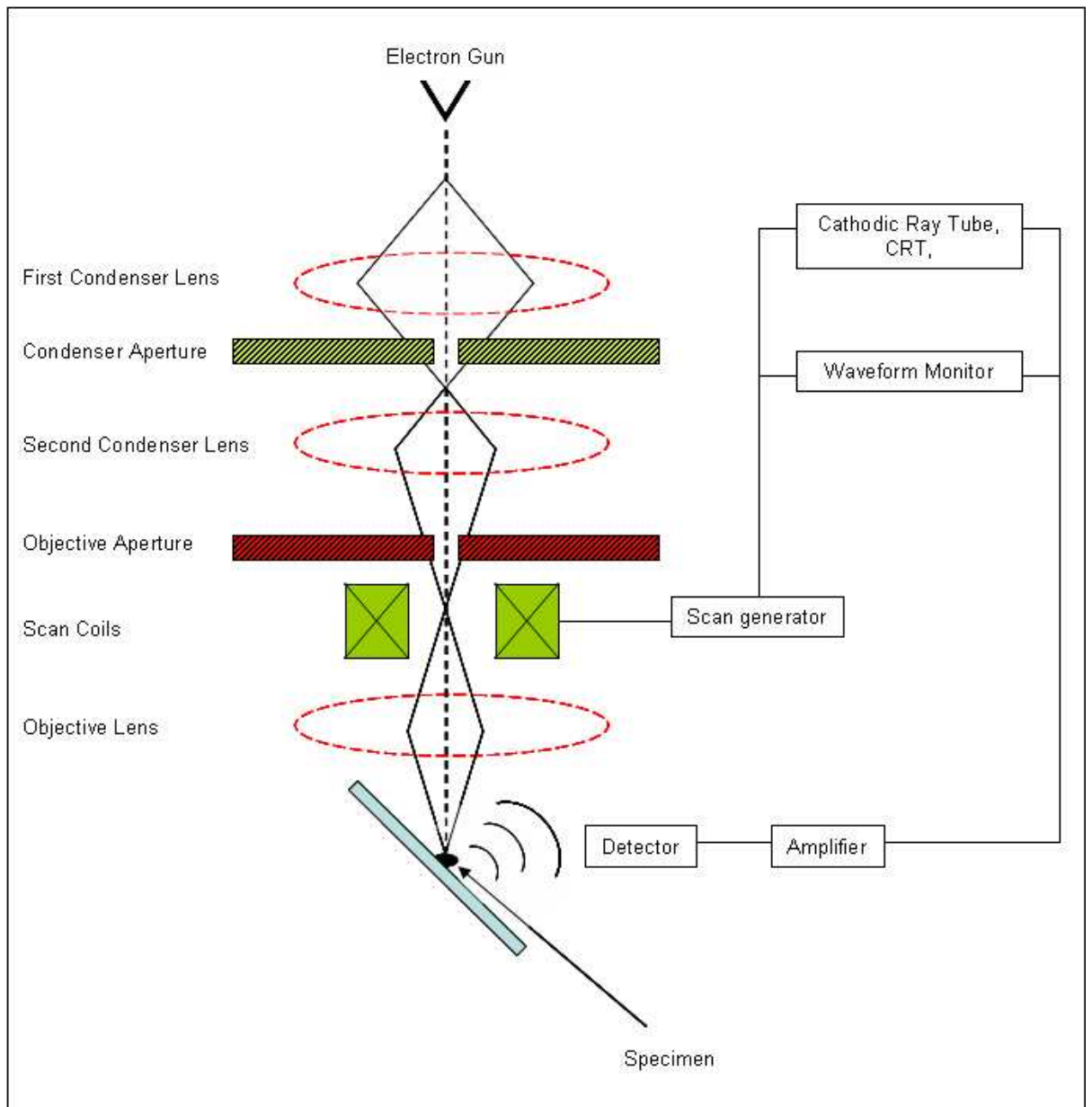


**Figure 3.5:** Schematic for an SEM

The main components of SEM (**Figure 3.5**) are as follows [35]:

**Electron Lenses-** Electron lenses are used to de-magnify the electron beam to a small spot about  $1\mu\text{m}$  in diameter. The condenser lens is located closest to the electron gun and the final or objective lens is located closest to the specimen. The objective lens moves the smallest spot formed by the beam up and down in space (working distance, WD) to meet the specimen surface, which is a focused condition.

**Scanning System-** The image is formed by pushing the beam across the specimen surface in a regular manner in synchronism with a beam scanning within the computer

monitor on the console. Scan coils, used to push or deflect the beam, are located within the objective lens.

***Objective Aperture-*** A foil with a small hole (~100  $\mu\text{m}$ ), located above the objective (final) lens. Its function is to limit the angular width of the electron beam to reduce aberrations and to improve depth-of-field in the image.

***Electron detector-*** Backscattered electrons are energetic enough to directly excite the detector, which is mounted on the bottom of the objective lens. Secondary electrons are drawn to the secondary electron detector by a positive charge placed in front of the detector. They are accelerated towards a scintillator screen where they produce light which is amplified to produce an electronic signal later sent to the computer to be displayed on the monitor.

***Vacuum system-*** Vacuum is produced by an oil diffusion pump backed by a mechanical pump. In the diffusion pump a stream of hot oil vapor strikes and pushes air molecules toward a mechanical pump that expels them from the system. A mechanical pump and valve system are used to pre-evacuate the system because a diffusion pump only operates after a vacuum is created.

### 3.2.2 Energy-dispersive X-ray spectroscopy (EDX)

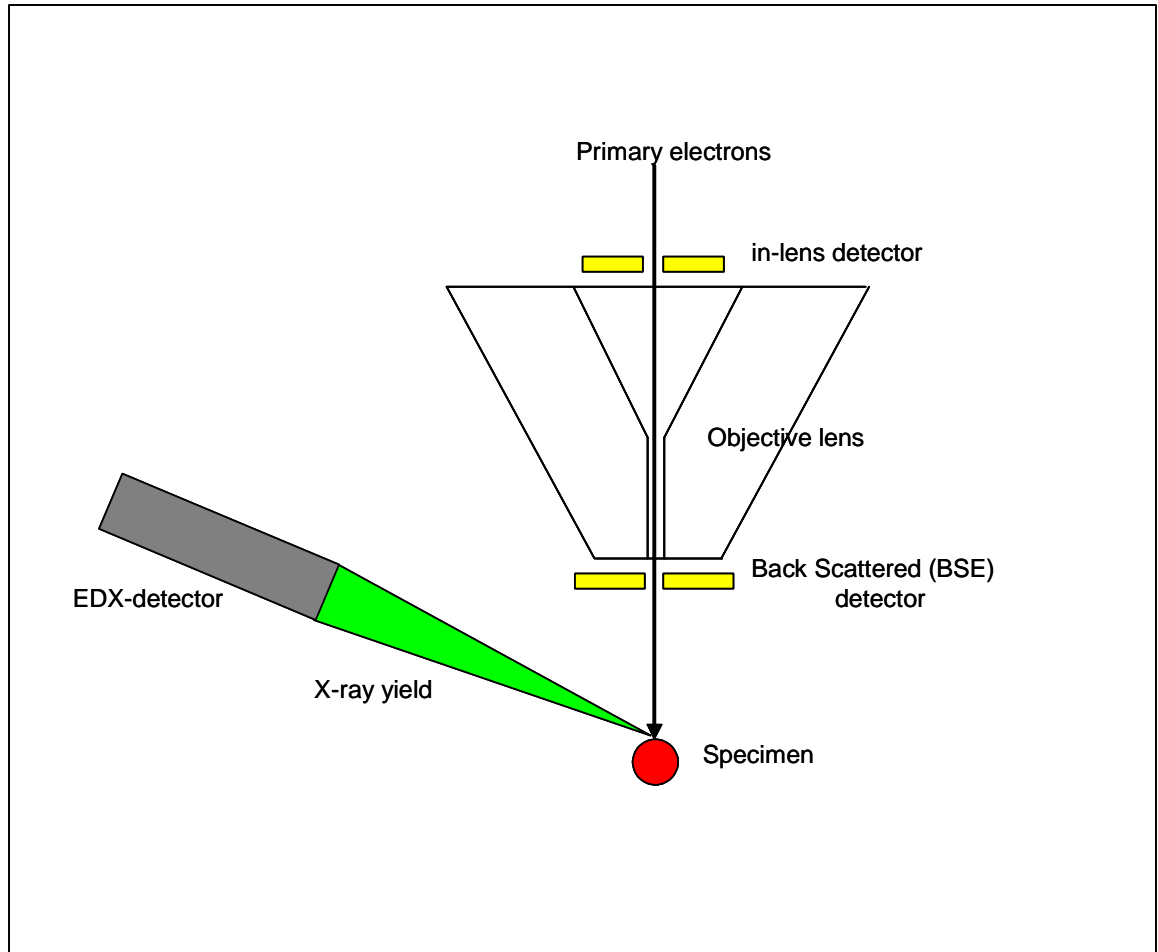


**Figure 3.6:** Schematic for an EDX

Energy dispersive X-ray spectroscopy (EDX) is an analytical technique used for the elemental analysis or chemical characterization of a sample as shown in **Figure 3.6**. It is one of the variants of XRF. EDX is a chemical microanalysis technique performed in conjunction with a scanning electron microscope (SEM). The technique utilizes x-rays that are emitted from the sample during bombardment by the electron beam to characterize the elemental composition of the analysed volume. Features or phases as small as about  $1\mu\text{m}$  can be analysed. When the sample is bombarded by the electron beam of the SEM, electrons are ejected from the atoms comprising the sample's surface. A resulting electron vacancy is filled by an electron from a higher shell, and an x-ray is emitted to balance the energy difference between the two electrons. The EDS x-ray detector measures the number of emitted x-rays versus their energy. The energy of the

x-ray is characteristic of the element from which the x-ray was emitted. A spectrum of the energy versus relative counts of the detected x-rays is obtained and evaluated for qualitative and quantitative determinations of the elements present in the sampled volume [35].

There are four primary components of the EDS setup: the beam source; the X-ray detector; the pulse processor; and the analyzer. A number of free-standing EDS systems exist. However, EDS systems are most commonly found integrated with scanning electron microscopes (SEM-EDS) and electron microprobes. Scanning electron microscopes are equipped with a cathode and magnetic lenses to create and focus a beam of electrons, and since the 1960s they have been equipped with elemental analysis capabilities. A detector is used to convert X-ray energy into voltage signals; this information is sent to a pulse processor, which measures the signals and passes them onto an analyzer for data display and analysis [40].

### 3.2.3 Atomic Force Microscope (AFM)



**Figure 3.7:** AFM: Digital Instruments Nano Scope 3a

The atomic force microscope (AFM) or scanning force microscope (SFM) as shown in **Figure 3.7** is a very high-resolution type of scanning probe microscopy, with resolution of fractions of a nanometer, more than 1000 times better than the optical diffraction limit. The precursor to the AFM, the scanning tunneling microscope, was developed by Gerd Binnig and Heinrich Rohrer in the early 1980s, a development that earned them the Nobel Prize for Physics in 1986. Binnig, Quate and Gerber invented the first AFM in 1986. The AFM is one of the foremost tools for imaging, measuring and manipulating matter at the nanoscale. The information is gathered by "feeling" the surface with a mechanical probe. Piezoelectric elements that facilitate tiny but accurate and precise movements on (electronic) command enable the very precise scanning. The AFM consists of a cantilever with a sharp tip (probe) at its end that is used to scan the

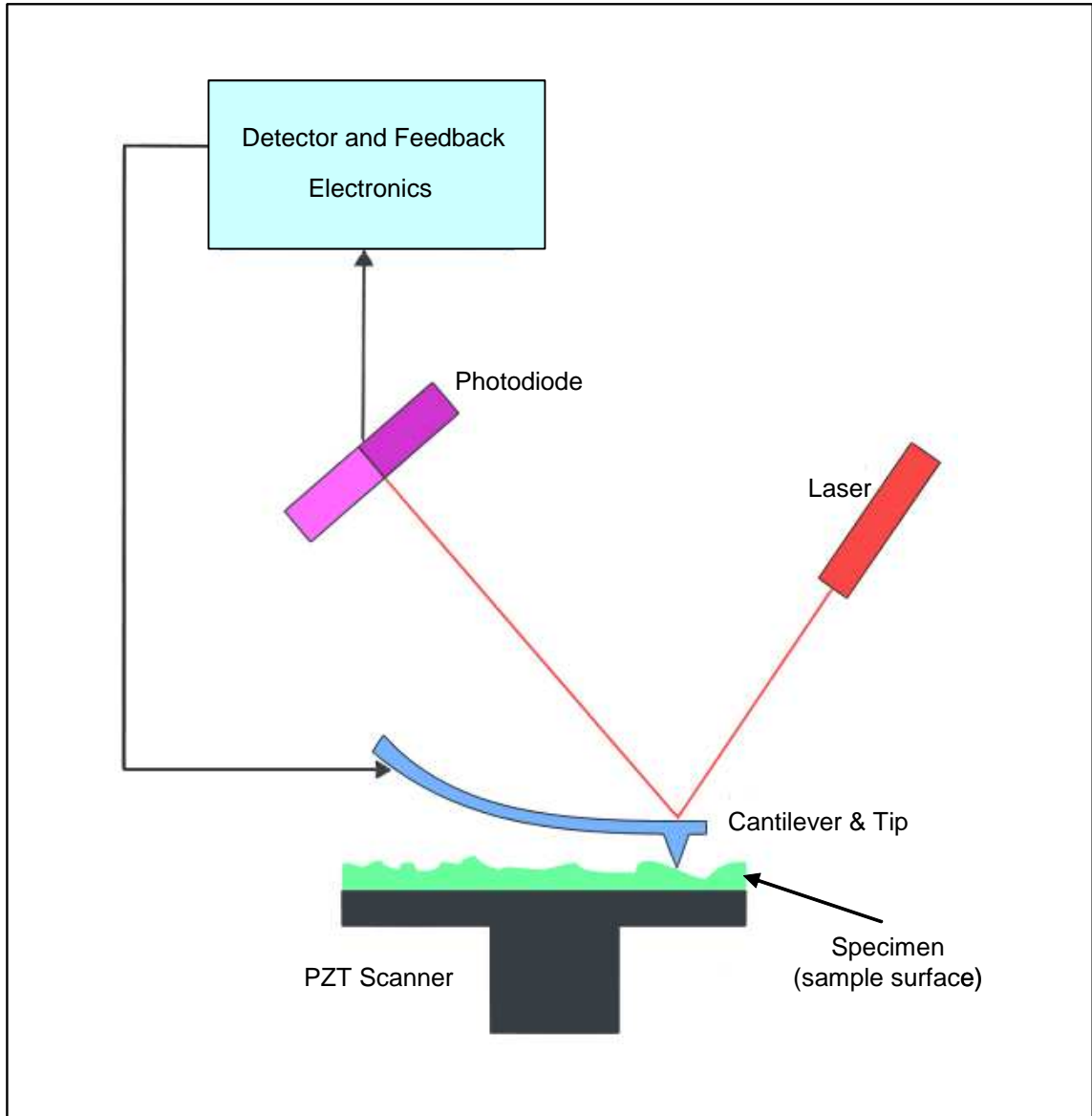


**Figure 3.8:** Schematic for an AFM

specimen surface as shown in **Figure 3.8**. The cantilever is typically silicon or silicon nitride with a tip radius of curvature on the order of nanometers. When the tip is brought into proximity of a sample surface, forces between the tip and the sample lead to a deflection of the cantilever according to Hooke's law. Depending on the situation, forces that are measured in AFM include mechanical contact force, Van der Waals forces, capillary forces, chemical bonding, electrostatic forces, magnetic forces (see magnetic force microscope, MFM), Casimir forces, solvation forces, etc. As well as force, additional quantities may simultaneously be measured through the use of specialized

types of probe (see scanning thermal microscopy, photothermal microspectroscopy, etc.). Typically, the deflection is measured using a laser spot reflected from the top surface of the cantilever into an array of photodiodes. Other methods that are used include optical interferometry, capacitive sensing or piezoresistive AFM cantilevers. These cantilevers are fabricated with piezoresistive elements that act as a strain gauge. Using a Wheatstone bridge, strain in the AFM cantilever due to deflection can be measured, but this method is not as sensitive as laser deflection or interferometry. If the tip was scanned at a constant height, a risk would exist that the tip collides with the surface, causing damage. Hence, in most cases a feedback mechanism is employed to adjust the tip-to-sample distance to maintain a constant force between the tip and the sample. Traditionally, the sample is mounted on a piezoelectric tube, that can move the sample in the z direction for maintaining a constant force, and the x and y directions for scanning the sample. Alternatively a 'tripod' configuration of three piezo crystals may be employed, with each responsible for scanning in the x,y and z directions. This eliminates some of the distortion effects seen with a tube scanner. In newer designs, the tip is mounted on a vertical piezo scanner while the sample is being scanned in X and Y using another piezo block. The resulting map of the area  $s = f(x,y)$  represents the topography of the sample. The AFM can be operated in a number of modes, depending on the application. In general, possible imaging modes are divided into static (also called contact) modes and a variety of dynamic (or non-contact) modes where the cantilever is vibrated [35,41].

### 3.2.4 Fourier Transform Infrared Spectroscopy (FTIR)



**Figure 3.9:** FTIR: Perkin Elmer Spectrum RX1

FTIR (Fourier Transform Infrared) Spectroscopy (**Figure 3.9**), or simply FTIR Analysis is a failure analysis technique that provides information about the chemical bonding or molecular structure of materials, whether organic or inorganic. It is used in failure analysis to identify unknown materials present in a specimen, and is usually conducted to complement EDX analysis. The technique works on the fact that bonds and groups of bonds vibrate at characteristic frequencies. A molecule that is exposed to infrared rays absorbs infrared energy at frequencies which are characteristic to that molecule. During FTIR analysis, a spot on the specimen is subjected to a modulated IR beam. The specimen's transmittance and reflectance of the infrared rays at different frequencies is translated into an IR absorption plot consisting of reverse peaks. The resulting FTIR spectral pattern is then analyzed and matched with known signatures of identified materials in the FTIR library. Unlike SEM inspection or EDX analysis, FTIR

spectroscopy does not require a vacuum, since neither oxygen nor nitrogen absorbs infrared rays. FTIR analysis can be applied to minute quantities of materials, whether solid, liquid, or gaseous. When the library of FTIR spectral patterns does not provide an acceptable match, individual peaks in the FTIR plot may be used to yield partial information about the specimen. Radiation of all frequencies from the IR source is reflected into the interferometer where it is modulated by the moving mirror on the left as shown in **Figure 3.10**. The modulated radiation is then reflected from the two mirrors on the right through the sample in the compartment at the bottom. After passing through the sample, the radiation falls on the detector. A data acquisition system attached to the detector records the signal and stores it in the memory of a computer as an interferogram [35,42].

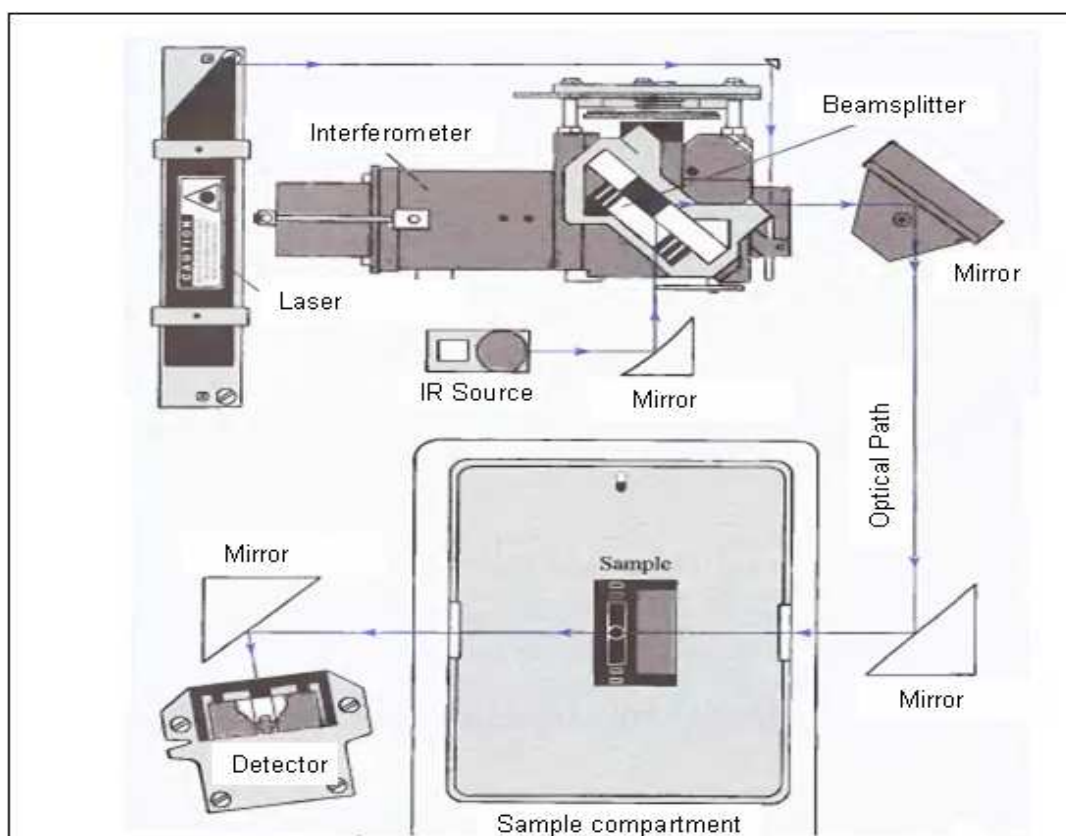


**Figure 3.10:** Instrument diagram for a basic FTIR spectrometer.

### 3.3 Wetting Balance Test

Tin electrodeposition has been gaining a significant role in Semiconductor assembly process since the past few decades. Tin electrodeposition in semiconductor industry (**Figure 3.11**) is the process of applying a coat of metal over the leads of an IC to:

- 1) Protect the leads against corrosion;
- 2) Improve the solderability of the leads;
- 3) Improve the appearance of the leads.



**Figure 3.11:** Semiconductor component that electroplated with tin

The wetting balance test, sometimes called a meniscograph (**Figure 3.12 and 3.13**) is one of the methods used to test the solderability of IC leads. The wetting balance test is classified in ANSI/ J-STD-002 as a “Test without establishes Accept/Reject Criterion”. This test method is recommended for engineering evaluations only and not as a production pass/fail monitor. The wetting balance test is a device which measures the forces exerted on a surface by the metallurgical wetting of solder and then plots these forces with respect to time. The method of measuring the forces is an LVDT (linear variable differential transformer) attached to the sample which is suspended in molten solder. **Figure 3.13** shows a schematic of the apparatus. To begin the test, the part to be tested is loaded into the weighing system. The solder pot containing the molten solder, which is part of the test equipment, is then raised at the controlled rate to the surface to be tested. The depth to which the part is immersed in the solder and dwell time of the

surface in the solder bath are set by gauge user. Initially, forces on the weighing machine are upward due to buoyancy of the sample and friction with the solder. As wetting proceeds the forces change direction, pulling downward due to the surface tension of the meniscus which forms between the solder and the part being tested.

**Figure 3.14 and 3.15** show a typical curve generated by the instrument [43-48].

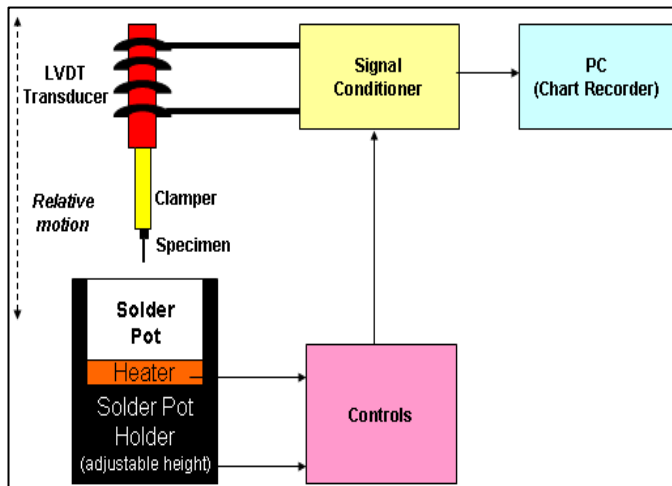


**Figure 3.12:** Schematic of wetting balance gauge



**Figure 3.13:** RHESCA SAT-5100 wetting balance gauge

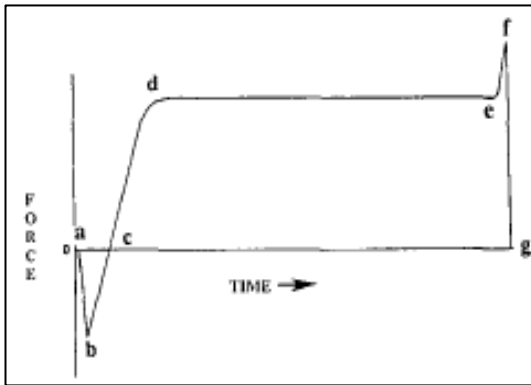


**Figure 3.14:** Typical wetting balance curve

The lettered points represent the following actions or occurrences.

- a. Immersion into the solder begins.*
- b. Maximum buoyant/frictional force prior to wetting.*
- c. Solder surface is normal to the surface being tested.*
- d. Maximum wetting force achieved due to meniscus rise and equilibrium is established.*
- e. Solder pot withdrawal begins.*
- f. Maximum withdrawal force is achieved and the molten solder fractures.*
- g. Solder contact is fully broken and force returns to near zero (actual zero is not achieved due to weight of solder deposited on part)*

One commonly used performance measure is the time to cross the zero axis of wetting force. This point indicates the transition from non-wetting ( $F < 0$ ) to wetting ( $F > 0$ ).

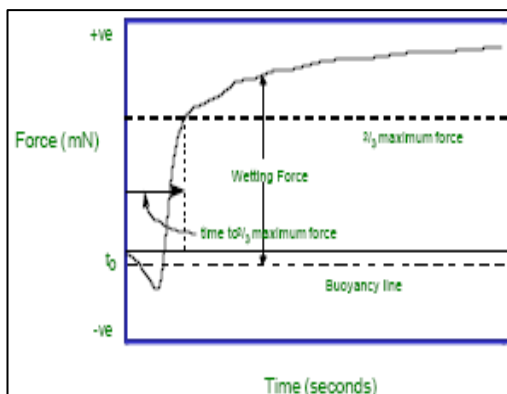


**Figure 3.15:** Typical wetting balance curve

## 3.4 Electrochemical Experiments

The electrochemical experiments were carried out using an Autolab PGSTAT 10 potentiostat as shown in **Figure 3.16**. The electrochemical behavior of tin reduction and oxidation was studied in the water and air stable ionic liquid 1-butyl-1-methyl-pyrrolidinium trifluoro-methanesulfonate, (BMPOTF) which was purchased from Merck KGaA and Tin Methane Sulfonate,  $(\text{CH}_3\text{SO}_3)_2\text{Sn}$  that was supplied by OM Group, Inc. The working electrode was a copper rod; the counter electrode was a platinum wire. The potential is measured between the reference electrode and the working electrode and the current is measured between the working electrode and the counter electrode. The reference electrode was silver chloride (Ag-AgCl) electrode due to its non-toxic character.

### 3.4.1 Reagent and Chemicals

The reagents and chemicals used throughout the experiments:

Component	Percent (%)
Stannous Methane Sulfonate, $(\text{CH}_3\text{SO}_3)_2\text{Sn}$	$\leq 55$
Water, $\text{H}_2\text{O}$	$\leq 30$
Methane Sulfonic Acid, $\text{CH}_3\text{SO}_3\text{H}$	$\geq 15$

**Table 3.1:** Component of Tin Methane Sulfonate

Component	Percent (%)
Assay (electrophoresis)	$\geq 98$
Water, $\text{H}_2\text{O}$	$\leq 1$
Halides	$\leq 0.1$

**Table 3.2:** Component of Ionic Liquid: 1-butyl-1-methyl-pyrrolidinium trifluoro-methanesulfonate, (BMPOTF)

## 3.5 Cyclic Voltammetry and Chronoamperometry

### Experiments

The 3-electrode cell with a volume of 50 cm<sup>3</sup> was used in this experiment (**Figure 3.17**). 15 cm<sup>3</sup> of electrolyte was placed in the cell which contained counter electrode, working electrode and reference electrode. The working electrode was a copper rod with diameter of 4 mm and exposed area of 0.1257 cm<sup>2</sup> (**Figure 3.18**). Before each experiment, the copper rod was prepared as follows: wet grinding with SiC type abrasive paper grade 100, 1000 and 1200 to a mirror finish. Cleaning 10 minutes in ethanol and then de-scaled with 10% Methane Sulfonic Acid (10%) and final rinsing in de-ionized water. The counter electrode was a platinum wire with 4 cm length and 0.1 mm diameter (**Figure 3.19**). The working electrode potentials reported herein were measured against Ag|AgCl reference electrode and correspond to this scale (**Figure 3.20**). The electrochemical experiments were carried out using an Autolab PGSTAT 10 potentiostat. All experiments were conducted at room temperature, 29 ± 1 °C in a mixture of BMPOTF ionic liquid and MSA based tin methane sulfonate salts. Tin Methane Sulfonate, (CH<sub>3</sub>SO<sub>3</sub>)<sub>2</sub>Sn, was added in the desired amounts. No organic additives were included in the solutions in this study. The electrolyte volume for the mixture was fixed at 15 mL in these experiments as shown in **Table 3.3**. Molarity of stannous (Sn<sup>2+</sup>) was calculated based on **Equation 3.6**.

$$\begin{aligned}
Y \text{ M Sn}^{2+} &= Y \frac{\text{mol}}{\text{L}} \times \frac{118.710 \text{ g}}{\text{mol}} \\
&= \frac{118.710 \text{ Y g}}{\text{L}} \times V \text{ L} \\
&= 118.710 \text{ Y.V g} \times \frac{1 \text{ L}}{300 \text{ g}} \\
&= 0.3957 \text{ Y.V L}
\end{aligned}
\tag{3.6}$$

Where,

$Y$  = Desired Molarity of  $\text{Sn}^{2+}$ ;

Tin, Sn atomic weight = 118.710 g/mol;

$V$  = Volume of electrolyte make-up in L;

Concentration of tin metal in Tin Methane Sulfonate Salt = 300 g/L

Stannous, $\text{Sn}^{2+}$ Concentration (Molarity)	Tin Methane Sulfonate Salt Volume (mL)	Ionic Liquid, BMPOTF volume (mL)
0.1	0.59	14.41
0.2	1.19	13.81
0.3	1.78	13.22
0.4	2.37	12.63
0.5	2.97	12.03

**Table 3.3:** Quantity of tin methane sulfonate and ionic liquid-BMPOTF in 15 mL electrolyte

### 3.5.1 Oxygen Removal:

The electrochemical reduction of oxygen usually proceeds via two well separated two-electron steps. The first step corresponds to the formation of hydrogen peroxide:



and the second step corresponds to the reduction of the peroxide:



The exact stoichiometry of these steps is dependent on the medium of electrode. The large background current accruing from this stepwise oxygen reduction interferes with the measurement of many reducible analytes. In addition, the products of the oxygen reduction may affect the electrochemical process under in verification [15]. As a result, Precaution measure was taken to eliminate oxygen from the system by purging high purity nitrogen through the solution prior to the experiments for 3 minutes.



**Figure 3.16:** Cyclic voltammetry and Chronoamperometry experiments set up



**Figure 3.17:** 3-electrode cell, A:Counter electrode, B:Reference electrode, C:Working electrode

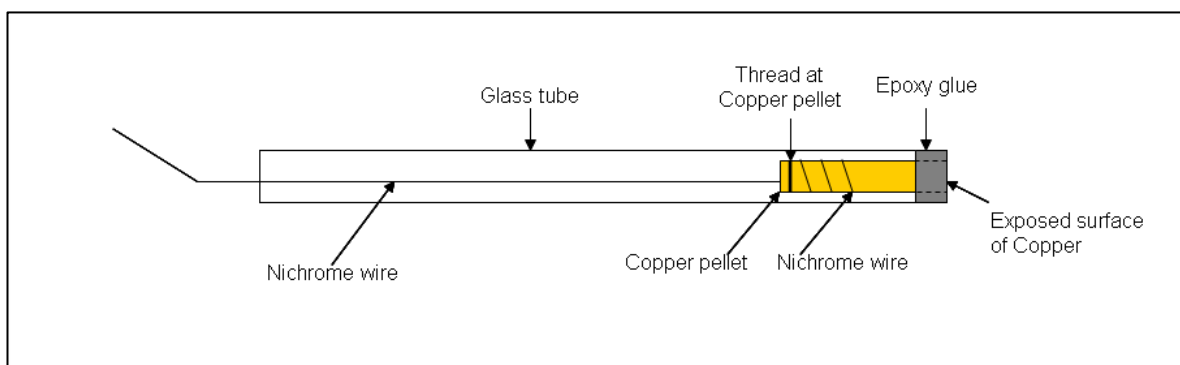


**Figure 3.18:** Structure of working electrode- Copper

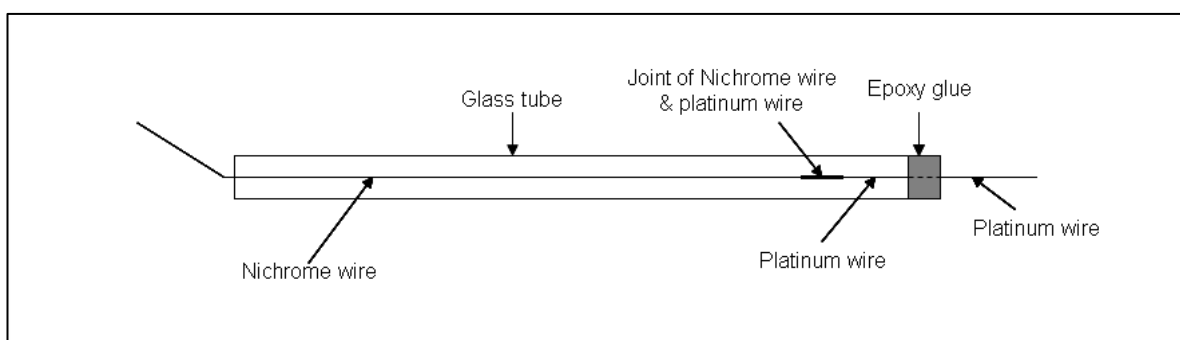


**Figure 3.19:** Structure of counter electrode- Platinum wire

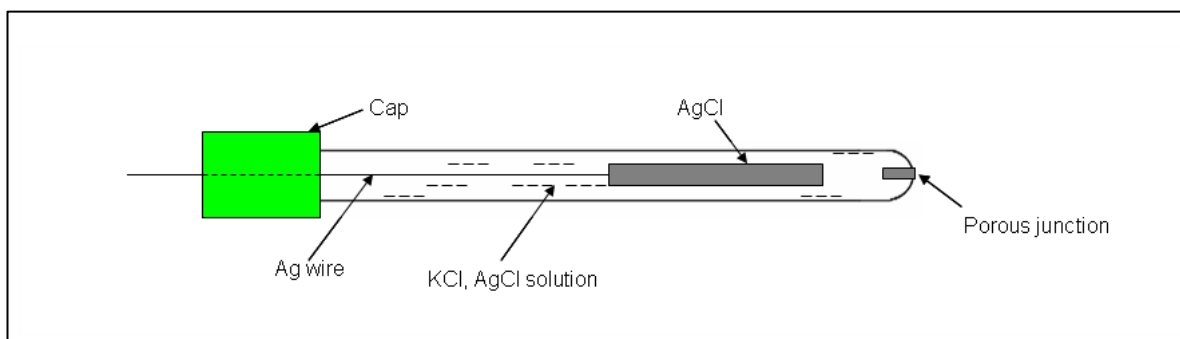


**Figure 3.20:** Structure of Silver-silver chloride reference electrode

### 3.5.2 NiChrome wire

Nichrome is a brand name for a nickel-chromium resistance wire, a non-magnetic alloy of nickel and chromium. A common alloy is 80% nickel and 20% chromium, by weight, but there are many others to accommodate various applications. It is silvery-grey in colour, is corrosion resistant, and has a high melting point of about 1400 °C (2552 °F). Due to its relatively high resistivity and resistance to oxidation at high temperatures, it is widely used in heating elements, such as in hair dryers, electric ovens and toasters. Typically, Nichrome is wound in wire coils to a certain electrical resistance, and current passed through to produce heat. The properties of Nichrome wire as follows [49-51]:

Material property	Value	Units
Modulus of elasticity	$2.2 \times 10^{11}$	Pa
Specific gravity	8.4	None
Density	8400	kg/ m <sup>3</sup>
Melting point	1400	°C
Electrical resistivity at room temperature	$1.0 \times 10^{-6}$ to $1.5 \times 10^{-6}$	Ωm
Specific heat	450	Jkg <sup>-1</sup> °C <sup>-1</sup>
Thermal conductivity	11.3	Wm <sup>-1</sup> °C <sup>-1</sup>
Thermal expansion	$14 \times 10^{-6}$	°C <sup>-1</sup>
Standard ambient temperature and pressure		

**Table 3.4:** Physical properties for Nichrome

### 3.6 Electroplating experiments

Copper panels were used as the substrate for tin electroplating experiments (**Figure 3.6 and 3.7**). Their dimension was 20 mm × 20 mm. Precautionary measures were taken to eliminate oxygen from the system by bubbling high purity nitrogen through the solution prior to the experiments for 3 minutes. Before each experiment, the copper panel was prepared as follows: Cleaning 10 minutes in ethanol and then de-scaled with 10% Methane Sulfonic Acid (10%) and final rinsing in de-ionized water and dried by using an air dryer.

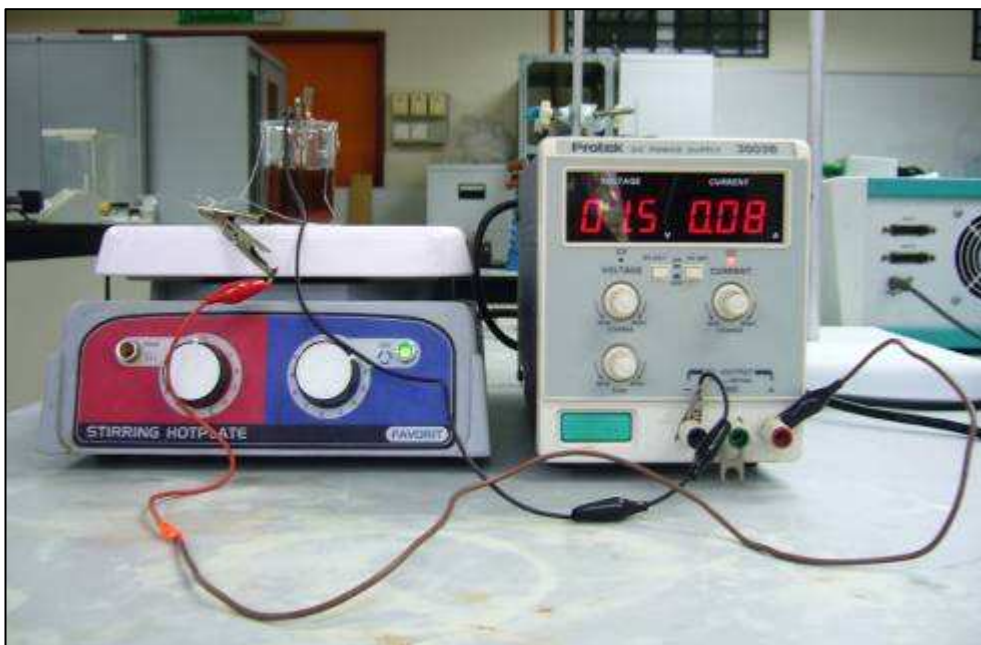


**Figure 3.21:** Electroplating experiments set up

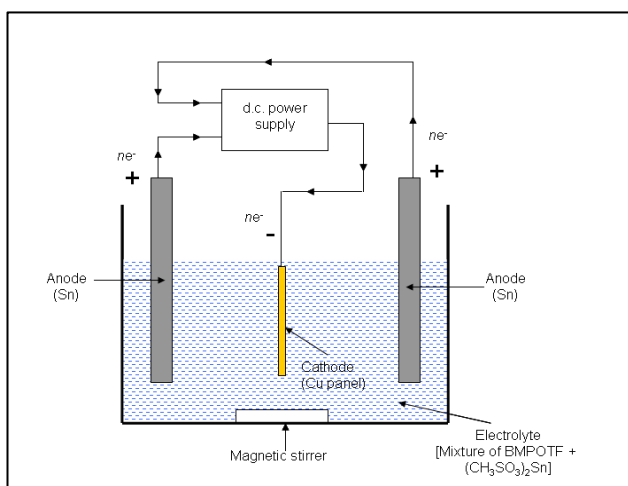


**Figure 3.22:** Schematic for an electroplating experiments

The panels were weighted and attached to the circuit with a wire electrical contact. It was placed in the cell with a tin anode on both of its adjacent side. After electrodeposition, the panel was removed, rinsed in hot de-ionized water, dried and weighted. By using Faraday's law of electrolysis, the increase in mass of the copper panels after electrodeposition and the charge passed, the current efficiency can be estimated. Stannous ions, Sn(II) was introduced into the BMPOTF ionic liquid along with (CH<sub>3</sub>SO<sub>3</sub>)<sub>2</sub>Sn. The tin concentration was varied from 0.1 M to 0.5 M with 0.1 M interval. The cell has a volume of 80 cm<sup>3</sup> and 40 cm<sup>3</sup> of solutions were used. Scanning electron microscopy (SEM), Energy dispersive X-ray spectroscopy (EDX) and Atomic force microscopy (AFM) were used to examine the surface morphology and analyze the elemental compositions of the electrodeposits.

# 4. RESULT AND DISCUSSION

## 4.1 Cyclic voltammetry

Stannous ions, Sn(II) was introduced into the BMPOTF ionic liquid along with  $(\text{CH}_3\text{SO}_3)_2\text{Sn}$ . The tin concentration was varied from 0.1 M to 0.5 M with 0.1 M interval. Cyclic voltammetry was swept from 0 to -1.0 V vs. Ag|AgCl then the sweep direction was reversed. The potential sweep rate was remained at  $50 \text{ mVs}^{-1}$  throughout the experiments. The diffusion coefficient of stannous ions in BMPOTF ionic liquid was calculated from the Randles-Sevcik equation.

$$I_p = (2.69 \times 10^5) n^{3/2} A D^{1/2} C \nu^{1/2} \quad (4.1)$$

where;

$I_p$  = peak current density ( $\text{A}/\text{cm}^2$ )

$n$  = number of electron

$A$  = electrode area ( $\text{cm}^2$ ),  $0.1257 \text{ cm}^2$

$C$  = concentration ( $\text{mol cm}^{-3}$ )

$D$  = diffusion coefficient ( $\text{cm}^2 \text{ s}^{-1}$ )

$\nu$  = scan rate ( $\text{V s}^{-1}$ )

**Figure 4.1-4.5** show the voltametric response for BMPOTF with different tin concentration. Cyclic voltammetry was swept from 0 to -1.0 V vs. Ag|AgCl then the sweep direction was reversed. The potential sweep rate was remained at  $50 \text{ mVs}^{-1}$  throughout the experiments. Increasing stannous concentration produces a stronger reduction and oxidation peak. A single reduction and oxidation peak were observed in the cyclic voltammetry of tin deposition and dissolution at a copper substrate.

The forward sweep from 0 to -1 V vs. Ag-AgCl shows a reduction peak for tin deposition corresponding to a two-electron step:



On reversing the potential sweep from -1.0 V to 0 V vs. Ag-AgCl, a single stripping peak was observed confirming the two-electron oxidation of metallic to stannous ions via the reverse reaction:

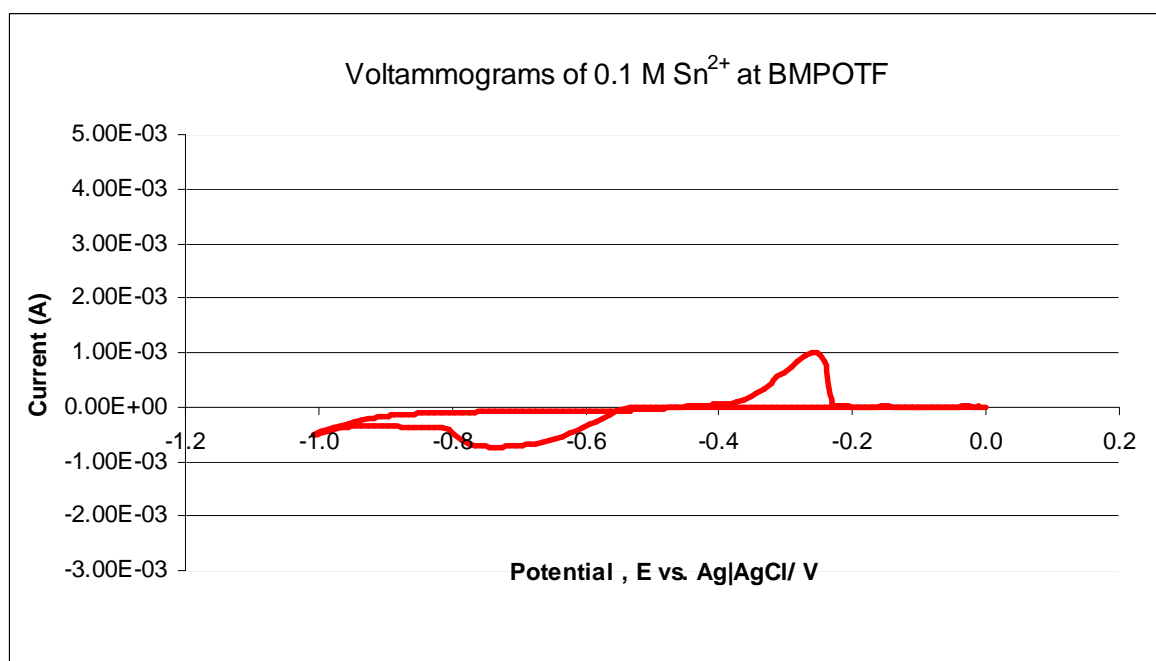


**Figure 4.1:** Voltammograms of 0.1 M  $\text{Sn}^{2+}$  at BMPOTF, potential sweep rate at 50  $\text{mVs}^{-1}$

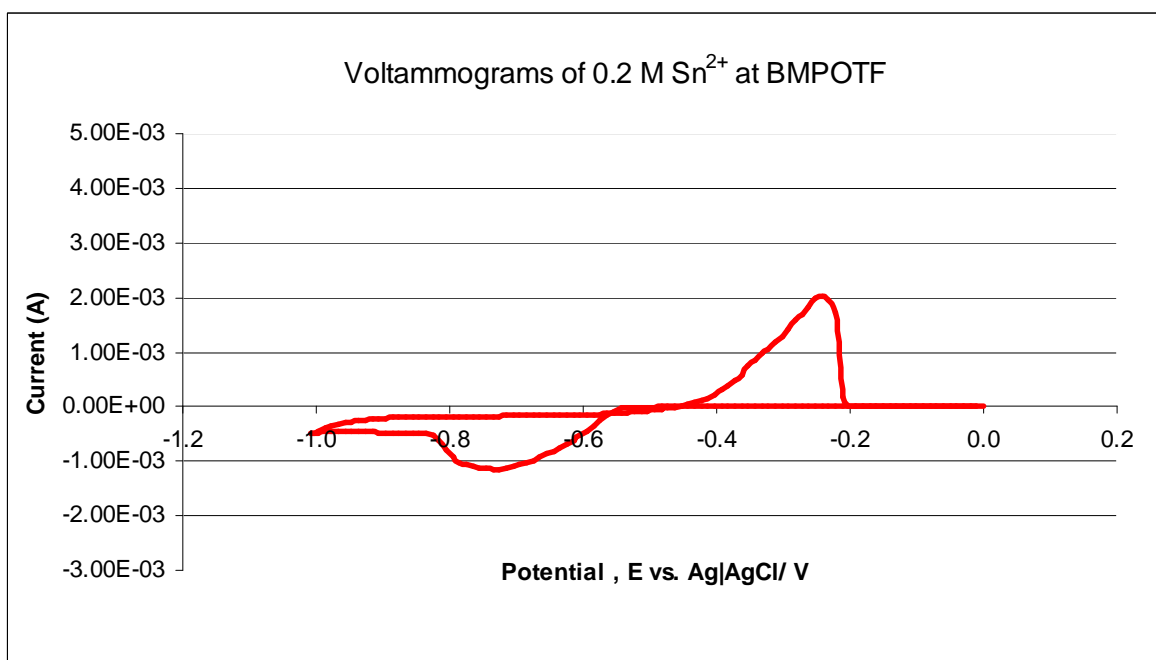


**Figure 4.2:** Voltammograms of 0.2 M Sn<sup>2+</sup> at BMPOTF, potential sweep rate at 50 mVs<sup>-1</sup>

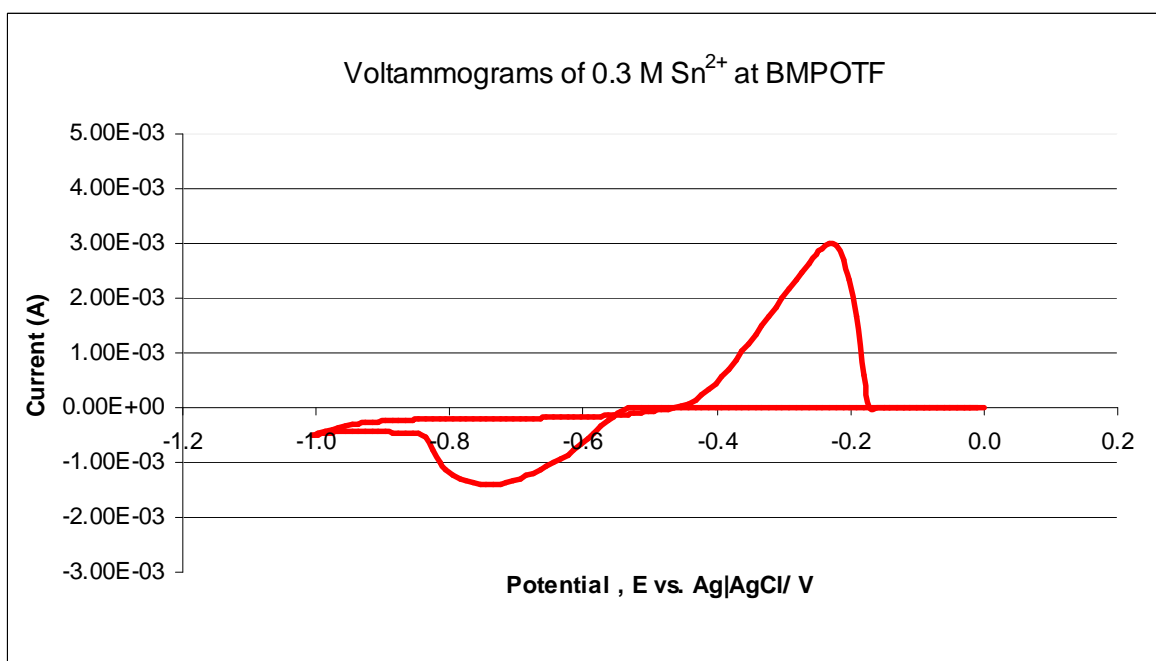


**Figure 4.3:** Voltammograms of 0.3 M Sn<sup>2+</sup> at BMPOTF, potential sweep rate at 50 mVs<sup>-1</sup>

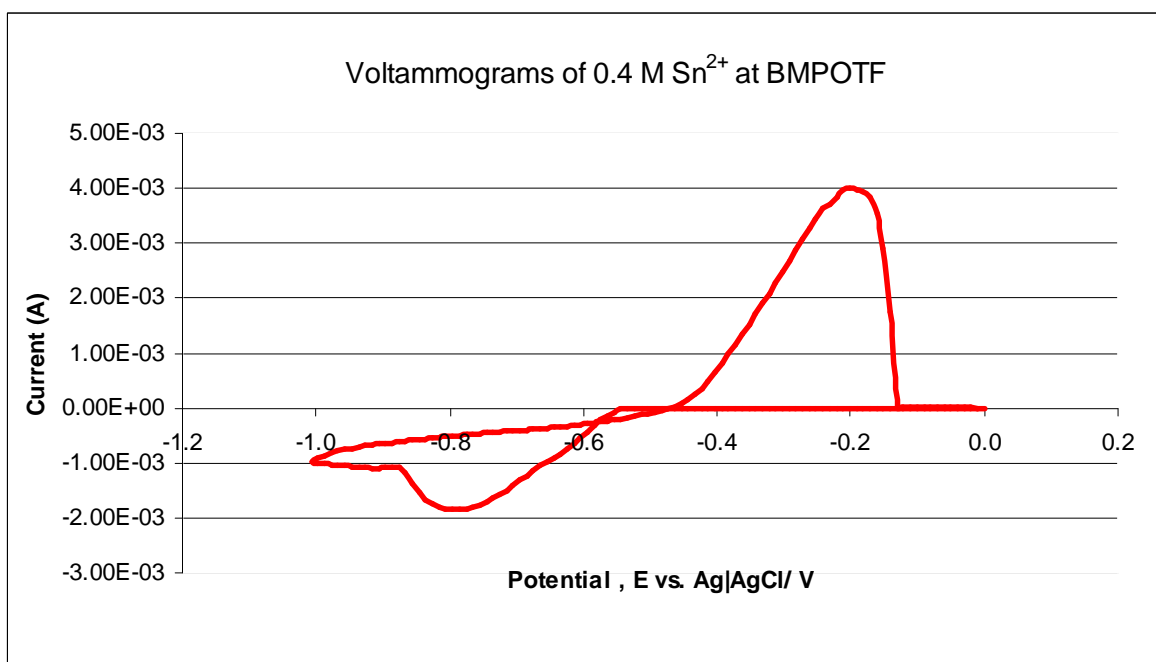


**Figure 4.4:** Voltammograms of 0.4 M Sn<sup>2+</sup> at BMPOTF, potential sweep rate at 50 mVs<sup>-1</sup>

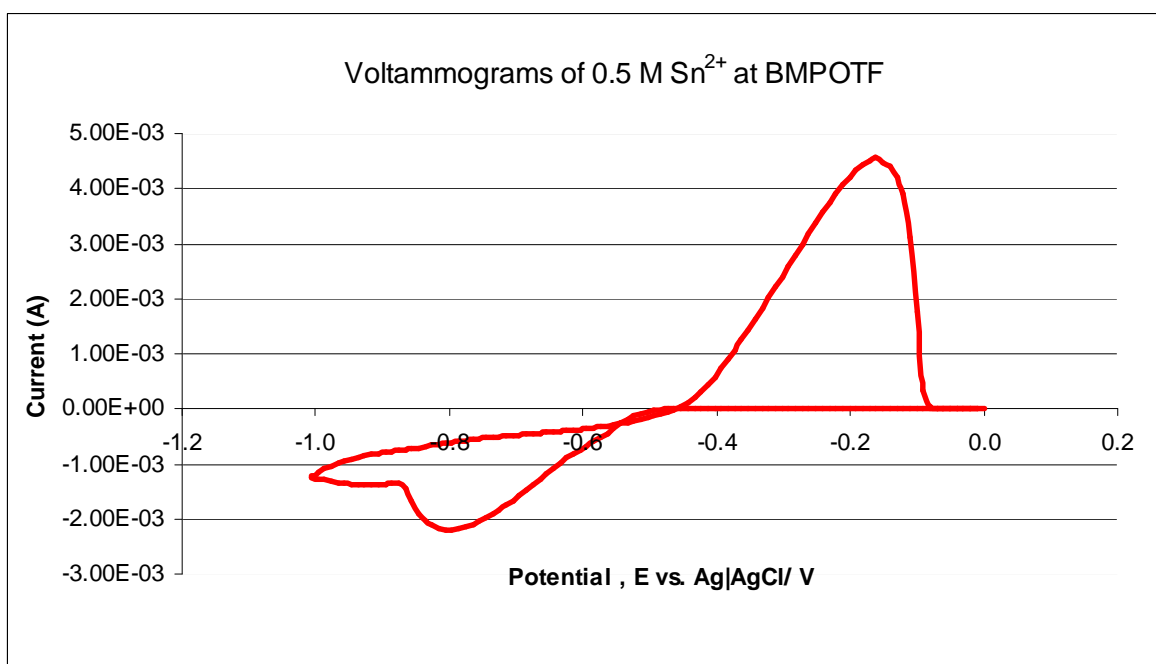


**Figure 4.5:** Voltammograms of 0.5 M Sn<sup>2+</sup> at BMPOTF, potential sweep rate at 50 mVs<sup>-1</sup>

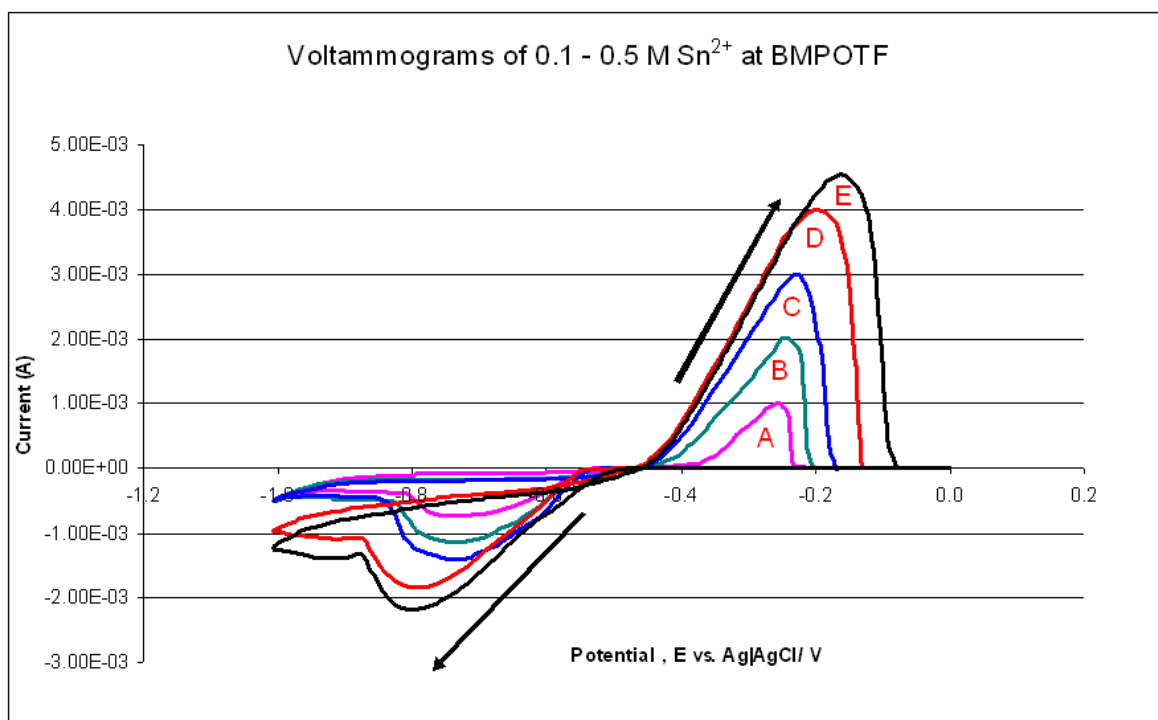


**Figure 4.6:** Cyclic voltammogram at  $50 \text{ mVs}^{-1}$  for solution  $X \text{ M } (\text{CH}_3\text{SO}_3)_2\text{Sn}$ , A=0.1M, B=0.2M, C=0.3M, D=0.4M, E=0.5M

Concentration (mol/dm <sup>3</sup> )	Peak Current (A)	Electrode area (cm <sup>2</sup> )	Current Density (mA/cm <sup>2</sup> )	Potential sweep rate, (mVs <sup>-1</sup> )	Diffusion of coefficient, (cm <sup>2</sup> /s)
0.1	0.0009890	0.1257	7.86919	50	2.1394E-07
0.2	0.0020180	0.1257	16.05665	50	2.2268E-07
0.3	0.0029910	0.1257	23.79854	50	2.1742E-07
0.4	0.0039980	0.1257	31.81095	50	2.1851E-07
0.5	0.0045680	0.1257	36.34628	50	1.8256E-07
			Average		<b>2.11E-07</b>

**Table 4.1:** Peak current density and tin diffusion coefficient obtained at different  $\text{Sn}^{2+}$  concentration

The diffusion coefficient of stannous ions in BMPOTF ionic liquid is approximately

$2.11 \times 10^{-7} \text{ cm}^2/\text{s}$  and was calculated from the Randles-Sevcik equation:

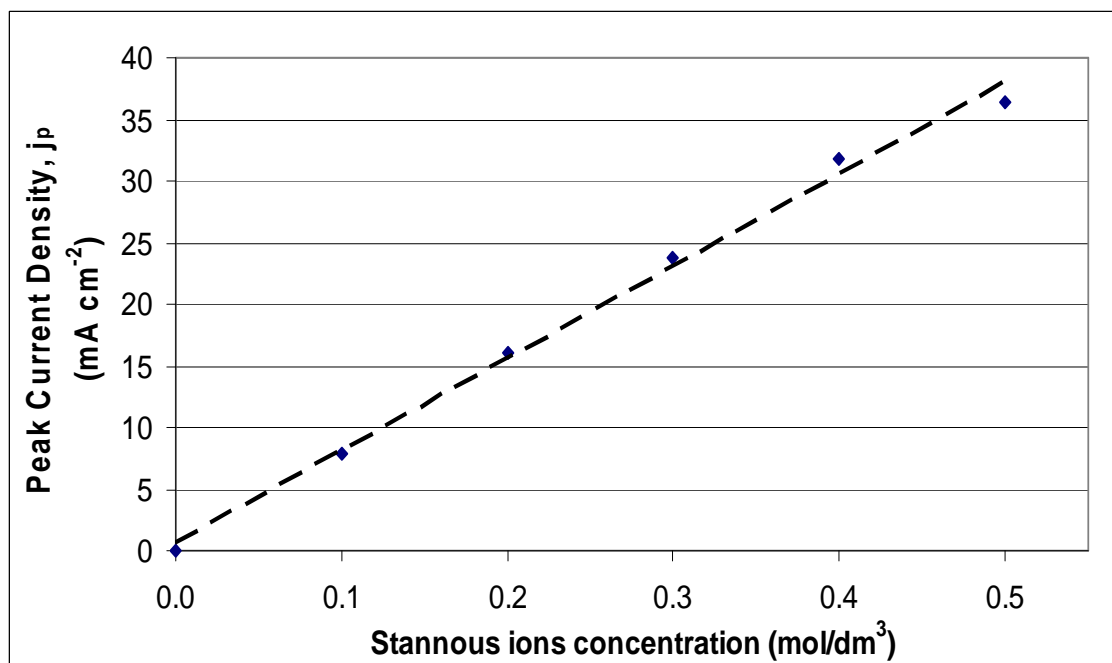


**Figure 4.7:** Effect of  $\text{Sn}^{2+}$  concentration on peak current density

Based on data in **Table 4.1**, tin diffusion coefficient,  $D$  has dropped when the mixture of BMPOTF and MSA tin had reached 0.5 M  $\text{Sn}^{2+}$ . From **Figure 4.7**,  $I_p$  increases with directly proportional to stannous concentration. The relationship to concentration is particularly important in analytical application and in studies of electrode mechanisms.

## 4.2 Chronoamperometry

As is known, the extent of diffusion layer thickness is time dependent [30]. Thus, the diffusion coefficient,  $D$  was counter evaluated by performing chronoamperometry experiments. **Figure 4.8-4.17** show an  $i$ - $t$  transient during the reduction of Tin ions ( $\text{Sn}^{2+}$ ) on working electrode at potential -0.8 V vs. SCE. By selecting the data points from the experimental data detected in **Table 4.2-4.6**, a Cottrell plot is obtained as current vs. minus square root of time.

The diffusion of coefficient was computed with the Cottrell equation as below:

$$i(t) = \frac{nFAD^{1/2}C}{\pi^{1/2}t^{1/2}} \quad (4.4)$$

Where

$i$  = current, in unit A

$n$  = number of electrons (to reduce/oxidize one molecule of analyte  $j$ , for example)

$F$  = Faraday constant, 96,485 C/mol

$A$  = area of the (planar) electrode in  $\text{cm}^2$ , 0.1257  $\text{cm}^2$

$C$  = initial concentration of the reducible analyte  $j$  in  $\text{mol}/\text{cm}^3$ ;

$D$  = diffusion coefficient in  $\text{cm}^2/\text{s}$

$t$  = time in s

Time (s)	$t^{-1/2}$ ( $s^{-1/2}$ )	Current (A)	Electrode area ( $cm^2$ )	Current Density ( $A/cm^2$ )	Diffusion of coefficient, ( $cm^2/s$ )
0	-	2.832E-04	0.1257	0.00225	-
1	1.0000	9.480E-05	0.1257	0.00075	3.0393E-07
2	0.7071	6.145E-05	0.1257	0.00049	2.5541E-07
3	0.5774	4.904E-05	0.1257	0.00039	2.4400E-07
4	0.5000	4.068E-05	0.1257	0.00032	2.2386E-07
5	0.4472	3.603E-05	0.1257	0.00029	2.1951E-07
6	0.4082	3.273E-05	0.1257	0.00026	2.1737E-07
7	0.3780	3.024E-05	0.1257	0.00024	2.1648E-07
8	0.3536	2.813E-05	0.1257	0.00022	2.1409E-07
9	0.3333	2.641E-05	0.1257	0.00021	2.1230E-07
10	0.3162	2.497E-05	0.1257	0.00020	2.1086E-07
11	0.3015	2.372E-05	0.1257	0.00019	2.0931E-07
12	0.2887	2.266E-05	0.1257	0.00018	2.0838E-07
13	0.2774	2.169E-05	0.1257	0.00017	2.0684E-07
14	0.2673	2.085E-05	0.1257	0.00017	2.0583E-07
15	0.2582	2.011E-05	0.1257	0.00016	2.0515E-07
				<b>Average</b>	<b>2.2355E-07</b>

**Table 4.2:** Chronoamperometry data of 0.1 M  $Sn^{2+}$  at BMPOTF

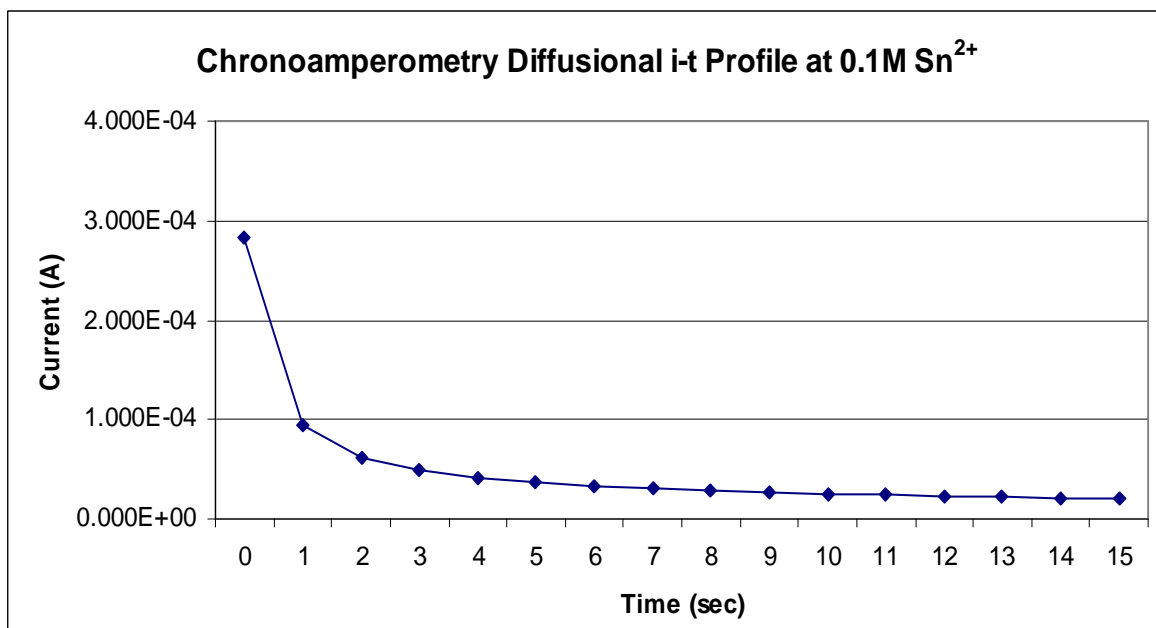


**Figure 4.8:** Chronoamperometry profile  $i$  vs.  $t$ , 0.1 M Sn<sup>2+</sup> at BMPOTF

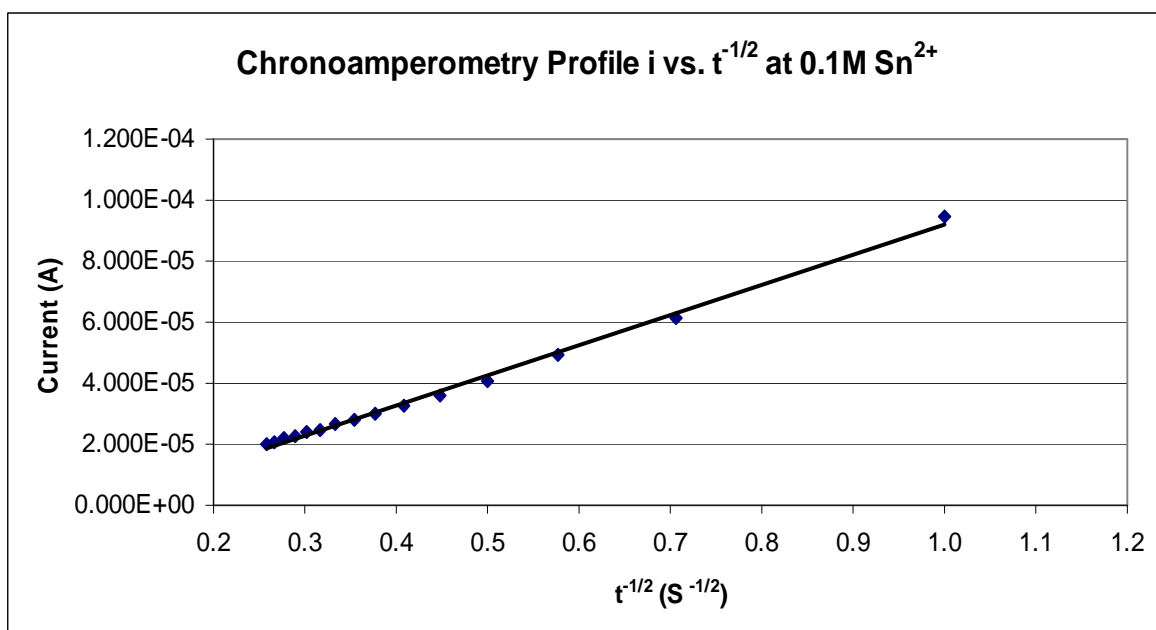


**Figure 4.9:** Chronoamperometry profile  $i$  vs.  $t^{-1/2}$ , 0.1 M Sn<sup>2+</sup> at BMPOTF

Time (s)	$t^{-1/2}$ (s <sup>-1/2</sup> )	Current (A)	Electrode area (cm <sup>2</sup> )	Current Density (A/cm <sup>2</sup> )	Diffusion of coefficient, (cm <sup>2</sup> /s)
0	-	4.833E-04	0.1257	0.00385	-
1	1.0000	2.010E-04	0.1257	0.00160	3.4158E-07
2	0.7071	1.253E-04	0.1257	0.00100	2.6548E-07
3	0.5774	1.003E-04	0.1257	0.00080	2.5517E-07
4	0.5000	8.665E-05	0.1257	0.00069	2.5392E-07
5	0.4472	7.720E-05	0.1257	0.00061	2.5195E-07
6	0.4082	6.996E-05	0.1257	0.00056	2.4829E-07
7	0.3780	6.454E-05	0.1257	0.00051	2.4652E-07
8	0.3536	6.079E-05	0.1257	0.00048	2.4995E-07
9	0.3333	5.633E-05	0.1257	0.00045	2.4145E-07
10	0.3162	5.338E-05	0.1257	0.00042	2.4091E-07
11	0.3015	5.061E-05	0.1257	0.00040	2.3821E-07
12	0.2887	4.833E-05	0.1257	0.00038	2.3698E-07
13	0.2774	4.684E-05	0.1257	0.00037	2.4115E-07
14	0.2673	4.534E-05	0.1257	0.00036	2.4333E-07
15	0.2582	4.383E-05	0.1257	0.00035	2.4363E-07
				<b>Average</b>	<b>2.5323E-07</b>

**Table 4.3:** Chronoamperometry data of 0.2 M Sn<sup>2+</sup> at BMPOTF

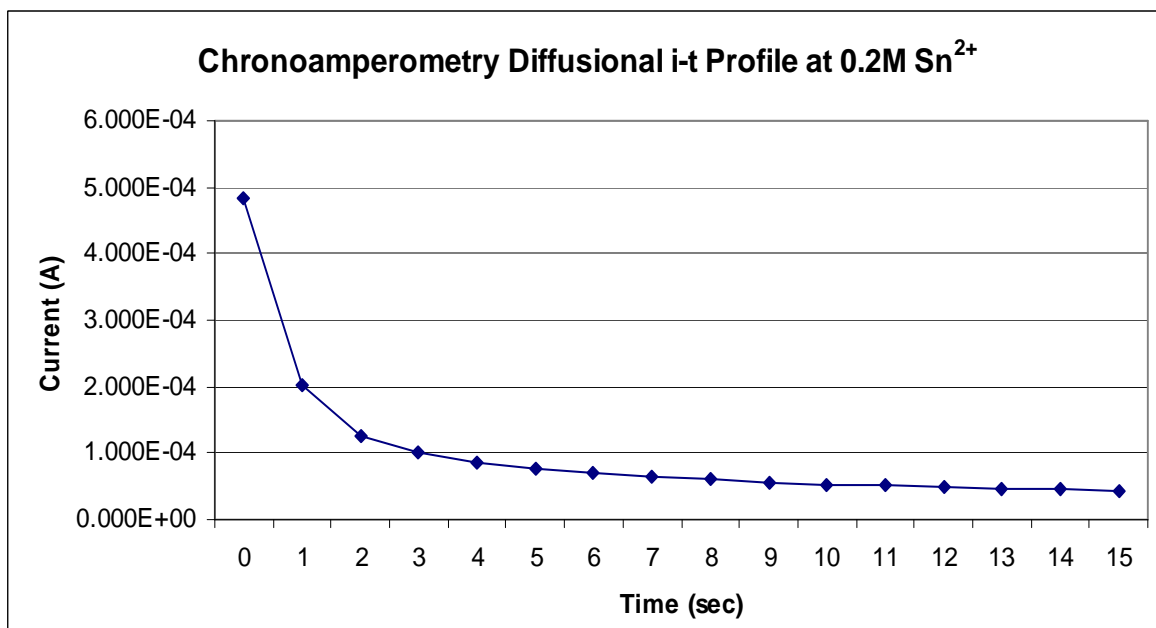


**Figure 4.10:** Chronoamperometry profile  $i$  vs.  $t$ , 0.2 M Sn<sup>2+</sup> at BMPOTF

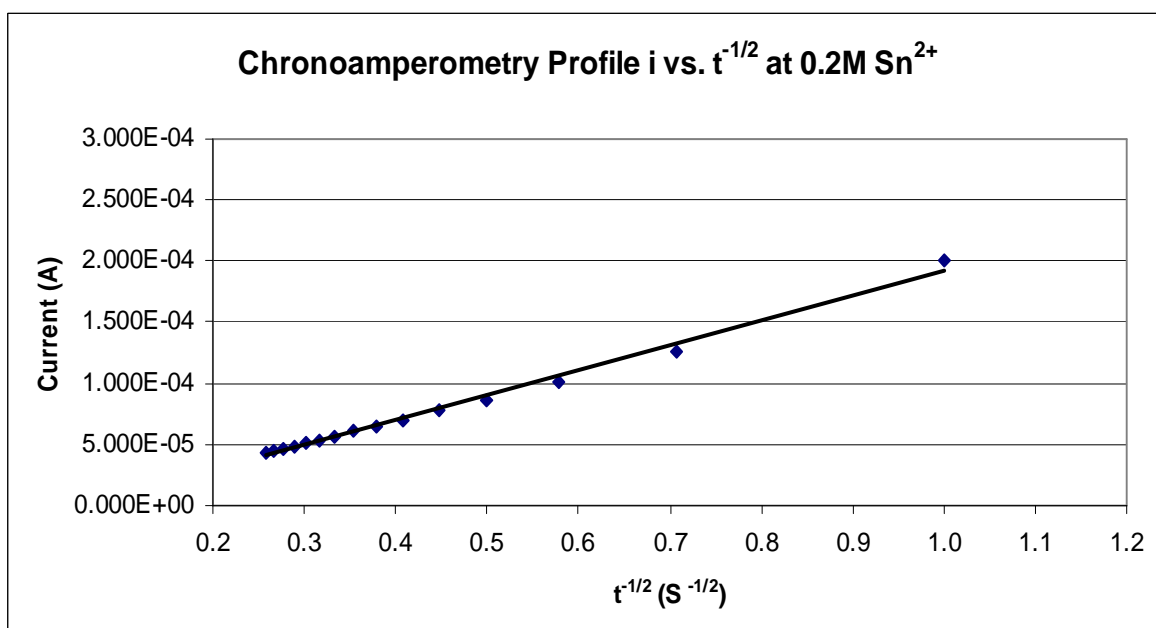


**Figure 4.11:** Chronoamperometry profile  $i$  vs.  $t^{-1/2}$ , 0.2 M Sn<sup>2+</sup> at BMPOTF

Time (s)	$t^{-1/2}$ (s <sup>-1/2</sup> )	Current (A)	Electrode area (cm <sup>2</sup> )	Current Density (A/cm <sup>2</sup> )	Diffusion of coefficient, (cm <sup>2</sup> /s)
0	-	7.466E-04	0.1257	0.00594	-
1	1.0000	3.329E-04	0.1257	0.00265	4.1643E-07
2	0.7071	2.110E-04	0.1257	0.00168	3.3459E-07
3	0.5774	1.662E-04	0.1257	0.00132	3.1139E-07
4	0.5000	1.394E-04	0.1257	0.00111	2.9208E-07
5	0.4472	1.211E-04	0.1257	0.00096	2.7554E-07
6	0.4082	1.095E-04	0.1257	0.00087	2.7033E-07
7	0.3780	1.006E-04	0.1257	0.00080	2.6620E-07
8	0.3536	9.394E-05	0.1257	0.00075	2.6528E-07
9	0.3333	8.669E-05	0.1257	0.00069	2.5416E-07
10	0.3162	8.207E-05	0.1257	0.00065	2.5310E-07
11	0.3015	7.810E-05	0.1257	0.00062	2.5212E-07
12	0.2887	7.570E-05	0.1257	0.00060	2.5840E-07
13	0.2774	7.258E-05	0.1257	0.00058	2.5733E-07
14	0.2673	6.986E-05	0.1257	0.00056	2.5675E-07
15	0.2582	6.634E-05	0.1257	0.00053	2.4806E-07
				<b>Average</b>	<b>2.8078E-07</b>

**Table 4.4:** Chronoamperometry data of 0.3 M Sn<sup>2+</sup> at BMPOTF

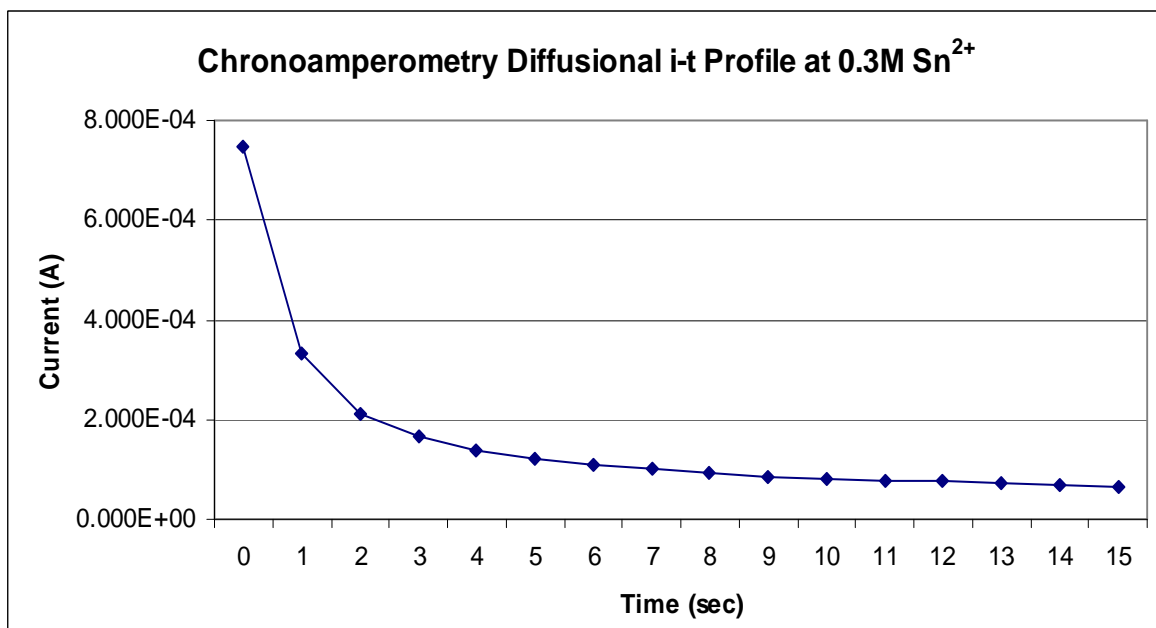


**Figure 4.12:** Chronoamperometry profile  $i$  vs.  $t$ , 0.3 M Sn<sup>2+</sup> at BMPOTF

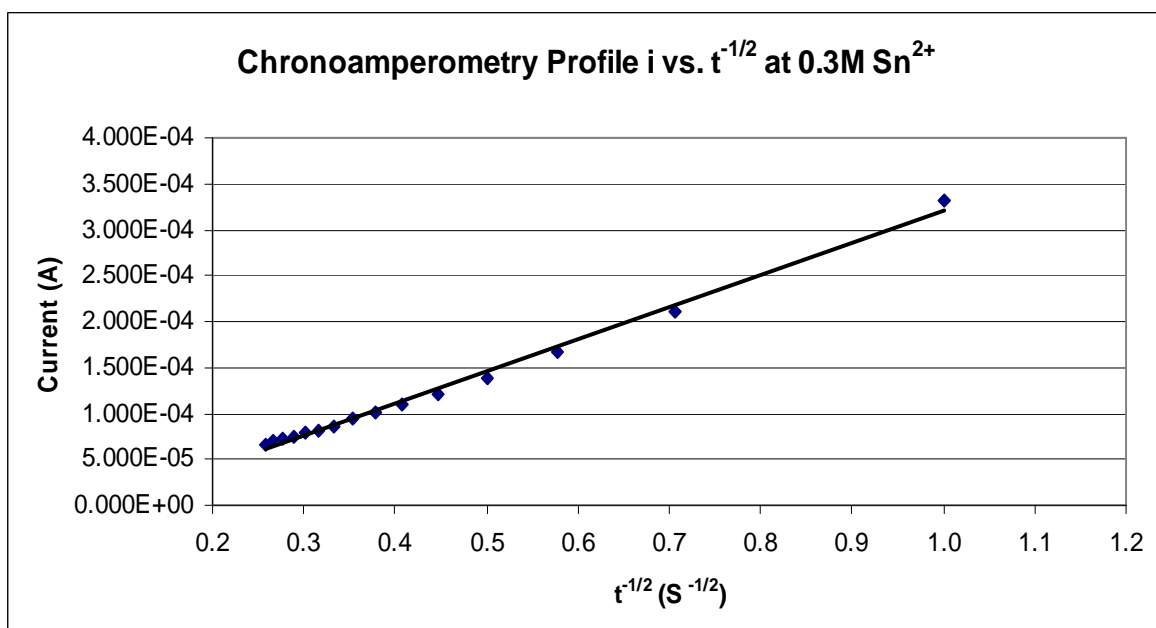


**Figure 4.13:** Chronoamperometry profile  $i$  vs.  $t^{-1/2}$ , 0.3 M Sn<sup>2+</sup> at BMPOTF

Time (s)	$t^{-1/2}$ (s <sup>-1/2</sup> )	Current (A)	Electrode area (cm <sup>2</sup> )	Current Density (A/cm <sup>2</sup> )	Diffusion of coefficient, (cm <sup>2</sup> /s)
0	-	9.165E-04	0.1257	0.00729	-
1	1.0000	4.473E-04	0.1257	0.00356	4.2290E-07
2	0.7071	2.882E-04	0.1257	0.00229	3.5112E-07
3	0.5774	2.306E-04	0.1257	0.00183	3.3720E-07
4	0.5000	1.958E-04	0.1257	0.00156	3.2414E-07
5	0.4472	1.691E-04	0.1257	0.00135	3.0220E-07
6	0.4082	1.514E-04	0.1257	0.00120	2.9070E-07
7	0.3780	1.384E-04	0.1257	0.00110	2.8341E-07
8	0.3536	1.276E-04	0.1257	0.00102	2.7532E-07
9	0.3333	1.176E-04	0.1257	0.00094	2.6309E-07
10	0.3162	1.116E-04	0.1257	0.00089	2.6325E-07
11	0.3015	1.061E-04	0.1257	0.00084	2.6174E-07
12	0.2887	1.016E-04	0.1257	0.00081	2.6182E-07
13	0.2774	9.768E-05	0.1257	0.00078	2.6218E-07
14	0.2673	9.409E-05	0.1257	0.00075	2.6197E-07
15	0.2582	9.109E-05	0.1257	0.00072	2.6307E-07
				<b>Average</b>	<b>2.9494E-07</b>

**Table 4.5:** Chronoamperometry data of 0.4 M Sn<sup>2+</sup> at BMPOTF

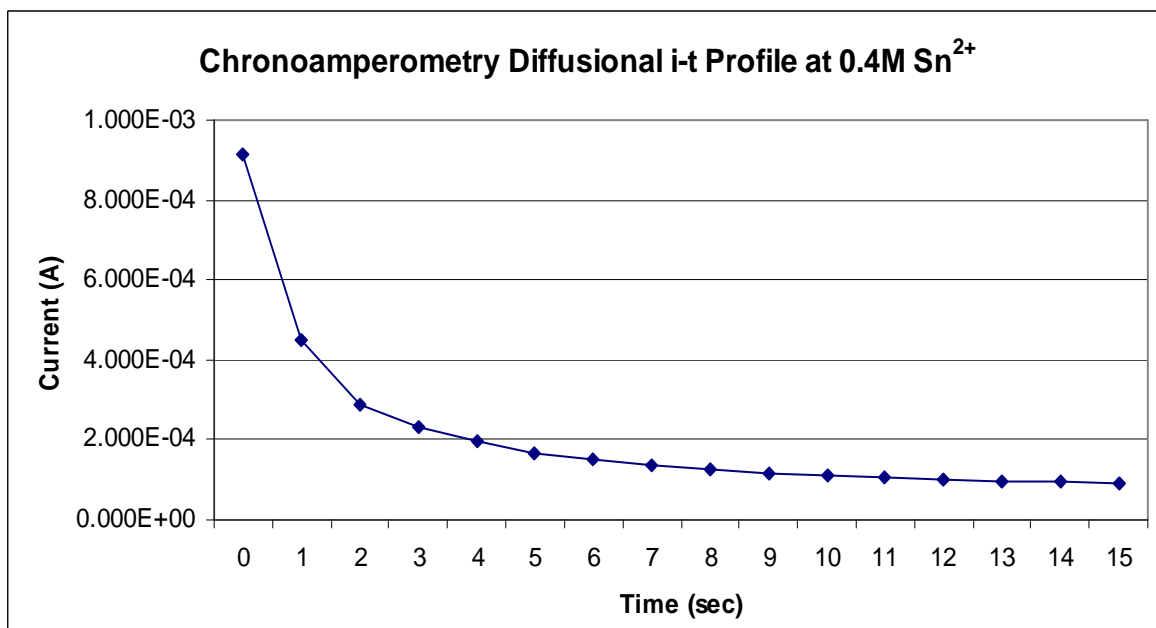


**Figure 4.14:** Chronoamperometry profile  $i$  vs.  $t$ , 0.4 M Sn<sup>2+</sup> at BMPOTF

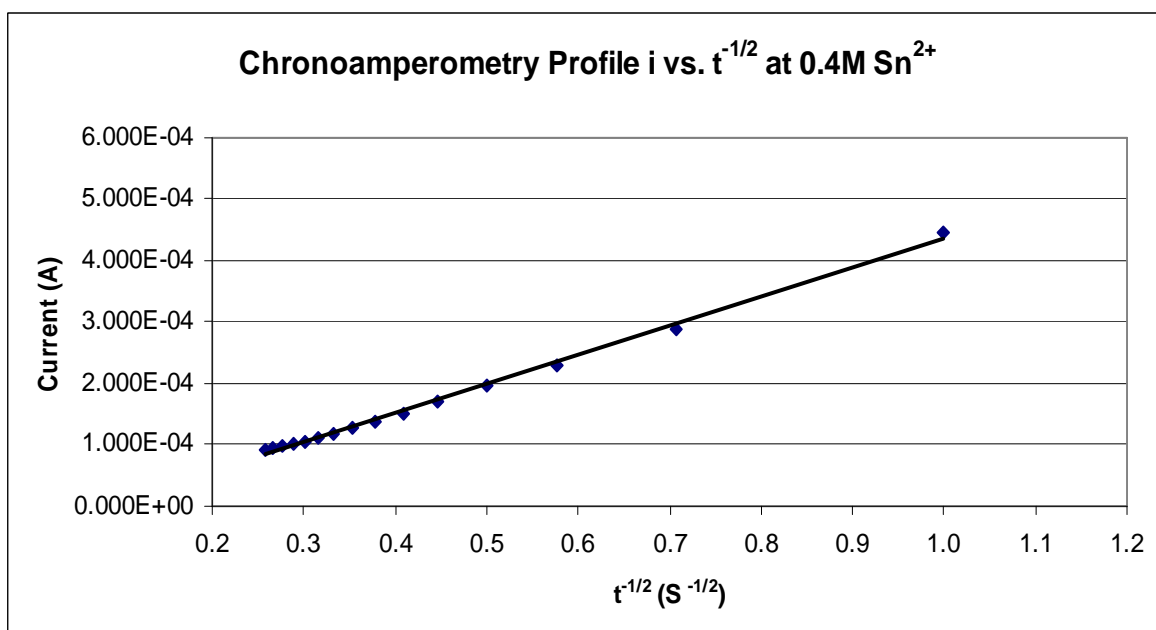


**Figure 4.15:** Chronoamperometry profile  $i$  vs.  $t^{-1/2}$ , 0.4 M Sn<sup>2+</sup> at BMPOTF

Time (s)	$t^{-1/2}$ (s <sup>-1/2</sup> )	Current (A)	Electrode area (cm <sup>2</sup> )	Current Density (A/cm <sup>2</sup> )	Diffusion of coefficient, (cm <sup>2</sup> /s)
0	-	9.698E-04	0.1257	0.00772	-
1	1.0000	5.325E-04	0.1257	0.00424	3.8358E-07
2	0.7071	3.227E-04	0.1257	0.00257	2.8174E-07
3	0.5774	2.570E-04	0.1257	0.00204	2.6805E-07
4	0.5000	2.198E-04	0.1257	0.00175	2.6142E-07
5	0.4472	1.943E-04	0.1257	0.00155	2.5535E-07
6	0.4082	1.741E-04	0.1257	0.00139	2.4602E-07
7	0.3780	1.610E-04	0.1257	0.00128	2.4545E-07
8	0.3536	1.509E-04	0.1257	0.00120	2.4643E-07
9	0.3333	1.416E-04	0.1257	0.00113	2.4411E-07
10	0.3162	1.340E-04	0.1257	0.00107	2.4290E-07
11	0.3015	1.281E-04	0.1257	0.00102	2.4418E-07
12	0.2887	1.237E-04	0.1257	0.00098	2.4839E-07
13	0.2774	1.186E-04	0.1257	0.00094	2.4736E-07
14	0.2673	1.141E-04	0.1257	0.00091	2.4656E-07
15	0.2582	1.112E-04	0.1257	0.00088	2.5091E-07
				<b>Average</b>	<b>2.6083E-07</b>

**Table 4.6:** Chronoamperometry data of 0.5 M Sn<sup>2+</sup> at BMPOTF

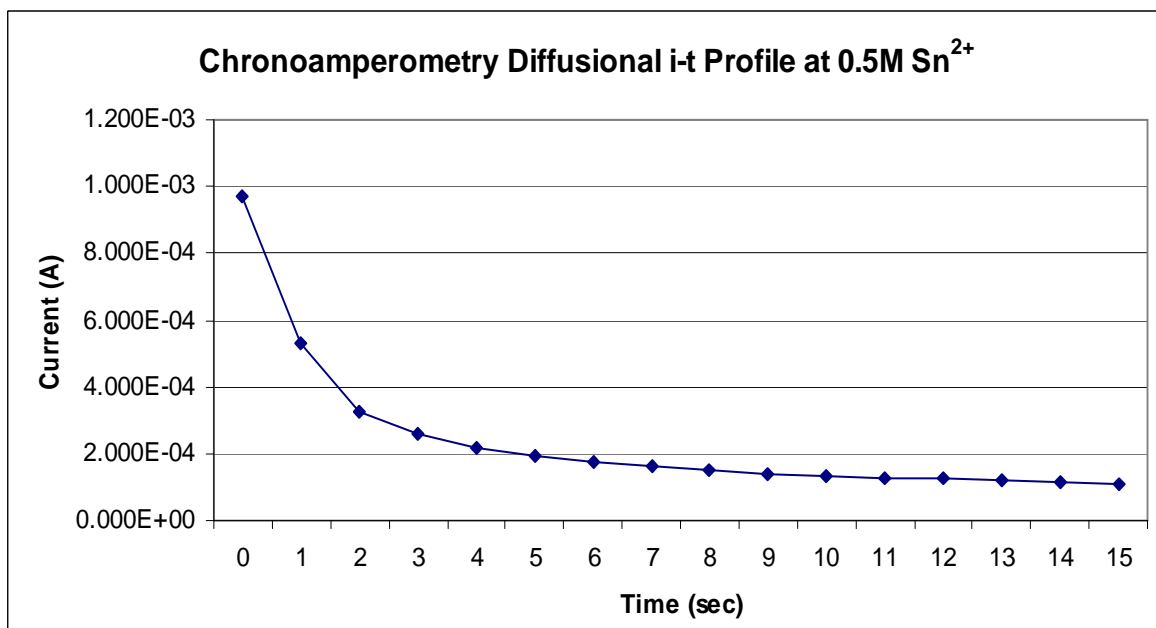


**Figure 4.16:** Chronoamperometry profile  $i$  vs.  $t$ , 0.5 M Sn<sup>2+</sup> at BMPOTF

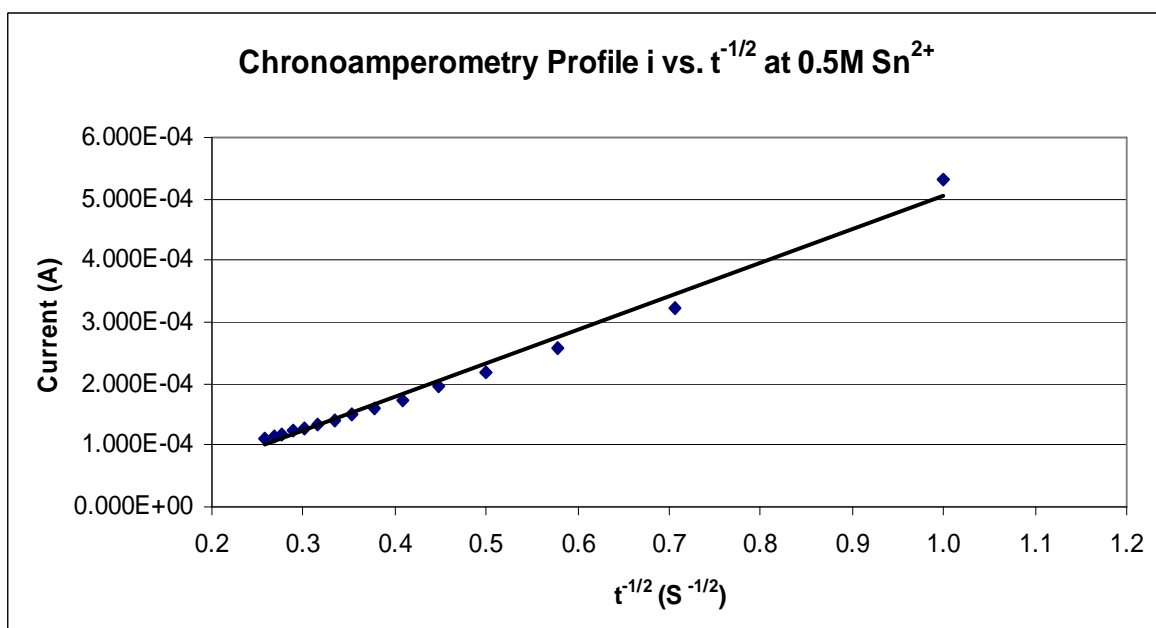


**Figure 4.17:** Chronoamperometry profile  $i$  vs.  $t^{-1/2}$ , 0.5 M Sn<sup>2+</sup> at BMPOTF

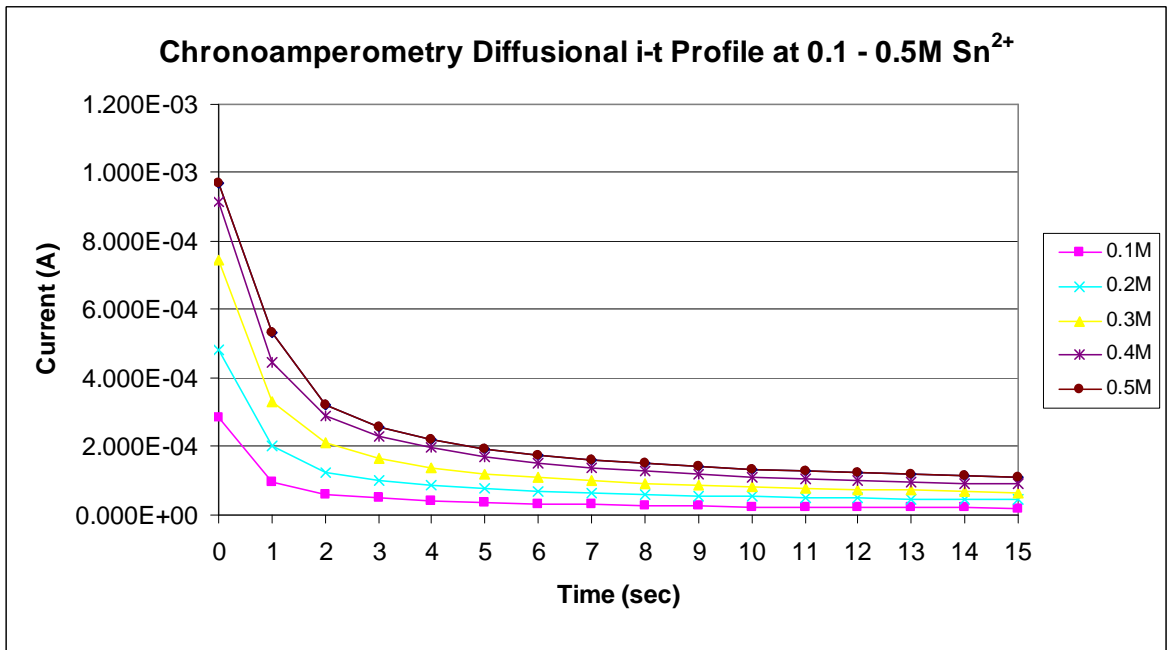


**Figure 4.18:** Chronoamperometry diffusional i-t profile from 0.1-0.5 M Sn<sup>2+</sup> at BMPOTF

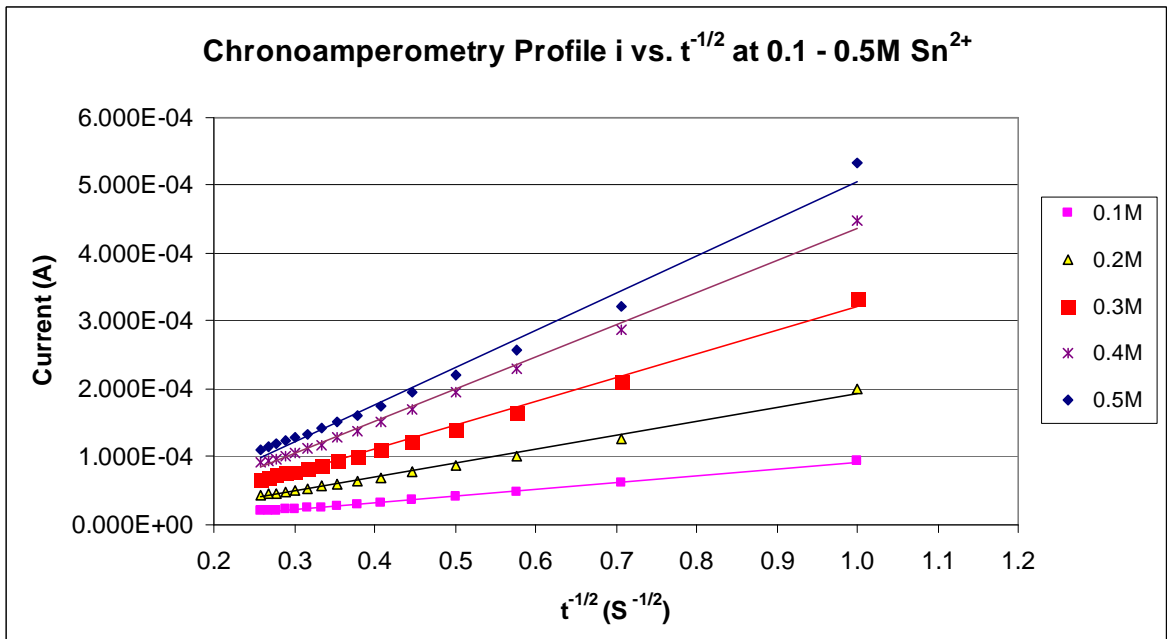


**Figure 4.19:** Chronoamperometry profile i vs.  $t^{-1/2}$  from 0.1-0.5 M Sn<sup>2+</sup> at BMPOTF

Sn <sup>2+</sup> Molarity (mol/ dm <sup>3</sup> )	Sn <sup>2+</sup> Dif. coefficient, <i>D</i> (cm <sup>2</sup> /s)
0.1	<b>2.2355E-07</b>
0.2	<b>2.5323E-07</b>
0.3	<b>2.8078E-07</b>
0.4	<b>2.9494E-07</b>
0.5	<b>2.6083E-07</b>
<b>Average</b>	<b>2.63 × 10<sup>-07</sup></b>

**Table 4.7:** Tin diffusion coefficient obtained at different Sn<sup>2+</sup> concentration through Chronoamperometry- Cottrell equation

No	Electrolyte	Anions	Reference	Sn <sup>2+</sup> Dif. coefficient, <i>D</i> (cm <sup>2</sup> /s)
1	Aqueous, CH <sub>3</sub> SO <sub>3</sub> H	CH <sub>3</sub> SO <sub>3</sub> <sup>-</sup>	[3]	6.5 × 10 <sup>-6</sup>
2	1-ethyl-3-methylimidazolium tetrafluoroborate, [EMIm]BF <sub>4</sub>	BF <sub>4</sub> <sup>-</sup>	[8]	6.1 × 10 <sup>-7</sup>
3	1-n-butyl-1-methylpyrrolidinium bis (trifluoromethylsulfonyl) imide, BMPTFSI	TFSI	[9]	1.0 × 10 <sup>-7</sup>
4	AlCl <sub>3</sub> with 1-methyl-3-ethyl imidazolium chloride, AlCl <sub>3</sub> -MeEtImCl	SnCl <sub>4</sub> <sup>2-</sup>	[7]	5.3 × 10 <sup>-7</sup>
5	1-butyl-1-methyl-pyrrolidinium trifluoro-methanesulfonate, BMPOTF	CH <sub>3</sub> SO <sub>3</sub> <sup>-</sup> and OTF <sup>-</sup>	This work- Cyclic voltammetry	2.11 × 10 <sup>-7</sup>
			This work- Chronoamperometry	2.63 × 10 <sup>-7</sup>

**Table 4.8:** Tin diffusion coefficient based on literature review

The chronoamperograms revealed the presence of mixture of MSA tin and BMPOTF ionic liquid over the concentration range of 0.1-0.5 M. Plotting the net current vs. the minus square root of time gives a straight line. This indicates that a diffusion controlled process is dominant for tin as was demonstrated previously using cyclic voltammetry.

The values obtained from chronoamperometric experiment for the diffusion coefficient was having slight drop from 0.4 to 0.5 M of Sn<sup>2+</sup>. This was in good agreement with the results obtained from cyclic voltammetry.

The dependency of the Diffusion coefficient to the viscosity and the radius of the diffusing species can be explained by the Stoke-Einstein equation,  $D = kT / 6 \eta r$  where  $k$  = Boltzmann constant,  $T$  = Kelvin temperature,  $\eta$  = viscosity of the solvent,  $r$  = dynamic radius of the diffusing species.

Hussey *et al.* [7] found that the Tin(II) exists as  $\text{SnCl}_4^{2-}$  in  $\text{AlCl}_3$  with 1-methyl-3-ethyl imidazolium chloride ionic liquid and the low values of the diffusion coefficient was due to the increased viscosity of the ionic liquid. They also suggest that there is some degree of association between the Tin(II) with chloroaluminate ions such as  $\text{AlCl}_4^-$  and  $\text{Al}_2\text{Cl}_7^-$ , which contribute to the low value of the diffusion coefficient.

W. Yang *et al.* [8] used tetrafluoroborate,  $\text{BF}_4^-$  based ionic liquid, where the diffusion coefficient was higher than calculated from the chloroaluminate ionic liquid by Hussey. From the Stoke-Einstein equation, it can be seen that the smaller Tin(II) tetrafluoroborate species will contribute to a slightly higher diffusion coefficient value for the Tin(II) species.

Studies using trifluoromethylsulfonyl imide ionic liquids from Tachikawa *et al.* [9] and this work using trifluoromethylsulfonate ionic liquid gave smaller diffusion coefficient for the Tin(II) species. It can be suggested that the complexation between the Tin(II) with trifluoromethylsulfonate and trifluoromethylsulfonyl imide, which is larger than the chloride ion and the tetrafluoroborate ion, has increased the radius of the Tin(II) species in solution. This contributes to the lower diffusion coefficient compared to the chloride and tetrafluoroborate based ionic liquids in the works previously reported [7,8].

### 4.3 Electroplating experiments

In electroplating industry, metals are electrodeposited using constant current (galvanostatic) methods. Constant current electrodeposition of tin on polished copper electrodes with area  $8 \text{ cm}^2$  were carried out using current densities of 1, 2, 3, 4, 5, 6, and 7  $\text{A/ dm}^2$  (ASD). Stannous ions, Sn(II) was introduced into the BMPOTF ionic liquid along with  $(\text{CH}_3\text{SO}_3)_2\text{Sn}$ . The tin concentration was varied from 0.1 M to 0.5 M with 0.1 M interval.

The panels were weighted and attached to the circuit with a wire electrical contact. It was placed in the cell with a tin anode on both of its adjacent side. After electrodeposition, the panel was removed, rinsed in hot de-ionized water, dried and weighted. By using Faraday's law of electrolysis, the increase in mass of the copper panels after electrodeposition and the charge passed, the current efficiency can be estimated.

The current efficiency is defines as the proportion of the current that is used in a specified reaction: the unused part in this process is considered a waste. Thus, the current efficiency,  $\epsilon$  is defined as the ratio of the specified chemical change to the total chemical change [9]. Thus,

$$\epsilon (\%) = \frac{\text{Actual reaction}}{\text{Total reaction}} \times 100 \quad (4.5)$$

The actual change is the mass of metal deposited or dissolved at the consumable anode, and theoretical change is the corresponding mass to be expected from Faraday's law of reaction if there were no side reaction. The efficiencies are not always 100% as hydrogen and oxygen are evolved at the cathode and the anode respectively.

Faraday's Law:

$$Q = I \cdot t \quad (4.6)$$

$$\begin{aligned} m &= \frac{Q}{qn} \cdot \frac{M}{N_A} = \frac{1}{qn} \cdot \frac{QM}{N_A} \\ &= \frac{1}{F} \cdot \frac{QM}{n} = \frac{1}{96,485 \text{ C} \cdot \text{mol}^{-1}} \cdot \frac{QM}{n} \end{aligned} \quad (4.7)$$

Where,

**m** is the mass of the substance produced at the electrode (in grams);

**Q** is the total electric charge that passed through the solution (in coulombs);

**q** is the electron charge =  $1.602 \times 10^{-19}$  coulombs per electron;

**n** is the valence number of the substance as an ion in solution (electrons per ion),

**F** =  $qN_A = 96,485 \text{ C} \cdot \text{mol}^{-1}$  is Faraday's constant,

**M** is the molar mass of the substance (in grams per mole), and

**N<sub>A</sub>** is Avogadro's number =  $6.023 \times 10^{23}$  ions per mole

Scanning electron microscopy (SEM), Energy dispersive X-ray spectroscopy (EDX) and Atomic Force Microscopy (AFM) were used to examine the surface morphology and analyze the elemental compositions of the electrodeposits.

No.	Current Density (A/dm <sup>2</sup> )	Stannous Ions Concentration (mol/dm <sup>3</sup> )				
		0.1	0.2	0.3	0.4	0.5
1	1.0	99.5	99.6	98.9	98.2	94.8
2	2.0	99.9	98.2	98.2	97.9	87.7
3	3.0	99.8	96.4	98.0	97.8	81.1
4	4.0	99.2	98.7	97.9	97.0	72.7
5	5.0	99.6	98.6	97.0	96.9	66.3
6	6.0	99.70	97.7	96.9	96.0	61.7
7	7.0	98.7	97.6	96.3	94.6	58.3

**Table 4.9:** Current efficiency obtained at different Sn<sup>2+</sup> concentration

Theoretically, electrodeposition at higher current density (HCD) will decrease the current efficiency due to hydrogen evolution. However, tin electro deposition via the mixture of ionic liquid BMPOTF and Methane Sulfonic Acid (MSA) based tin methane sulfonate salts has shown excellent current efficiency which is as high as 99.9%.

Based on result in **Table 4.9**, the average current efficiency was  $97 \pm 2\%$  when electrodeposited with Sn<sup>2+</sup> concentration in the range of 0.1 - 0.4 M, and at 1 to 7 ASD. The deposit was dense, fine and in polygonal grain structure as revealed in **Figure 4.20, 4.23, 4.26 and 4.29**, SEM images @ 3500X. The grain size of tin had increased from 1-2  $\mu\text{m}$  to  $\approx 5 \mu\text{m}$  proportional to current density change. There was no copper element observed from the tin plated surface via EDX analysis at 20 keV. It had proven that the tin deposit on copper substrate is dense and compact.

However, there was a sudden drop for current efficiency when deposited with 0.5 M MSA tin. The similar phenomenon happened in cyclic voltammetry and chronoamperometry experiments whereby the stannous diffusion coefficient dropped when the mixture of BMPOTF and MSA tin had reached 0.5 M Sn<sup>2+</sup>. It was believed

that the mixture of BMPOTF and MSA tin has reached saturated point at 0.5M Sn<sup>2+</sup>. The ion H<sup>+</sup> from acid was reduced to hydrogen gas during tin deposition. The hydrogen gas was co-deposited onto the copper substrate, thus causing the tin deposit was dull, porous and had poor reflectivity as shown in **Figure 4.32**. The copper element was revealed at the tin plated surface when analyzed under 20 keV EDX as shown in **Figure 4.33 and 4.34**.

The SEM results that obtained in this work is similar to the study which carried out by Q. B. Zhang *et al.* [18]. Q. B. Zhang *et al.* have done the copper electrodeposition in an electrolyte which contains mixture of ionic liquid 1-butyl-3-methylimidazolium hydrogen sulfate-[BMIM]HSO<sub>4</sub>, sulfuric acid, hydrated copper sulfate and distilled water. The surface morphology of the copper deposition in Q. B. Zhang *et al.* study showing that the grain is finer and dense with the increasing of ionic liquid ratio in electrolyte. It was believed that the ionic liquid is an efficient leveling agent in copper electrodeposition, leading to more leveled and fine grained cathodic deposits. The ionic liquid also inhibits crystal growth and promotes nucleation of copper, leading to finer grained copper deposits [18].

Representative AFM images of the tin deposition are seen in **Figure 4.35-4.39**. The copper samples were plated at different Sn<sup>2+</sup> concentration in BMPOTF ionic liquid at 1 ASD. These images parallel the SEM images in **Figure 4.20, 4.23, 4.26, 4.29 and 4.32** but AFM images give a perspective of the third (**Z**) dimension. The roughness is increasing proportional to Sn<sup>2+</sup> concentration. The smooth and fine structure can be observed from **Figure 4.35 and 4.36**. The roughness of deposit become slightly greater when plated at 0.3 and 0.4 M Sn<sup>2+</sup> (**Figure 4.37 and 4.38**). The larger tin crystal and deep crevice found at the sample plated at 0.5 M Sn<sup>2+</sup> (**Figure 4.39**).

The AFM surface morphology analysis in this work is identical with the study that carried out by M. J. Deng *et al.* [4]. M. J. Deng *et al.* has done the investigation on electrodeposition behavior of nickel. It was reported that the roughness of the nickel-deposited surface increased as the deposition potential and current density increased [4].

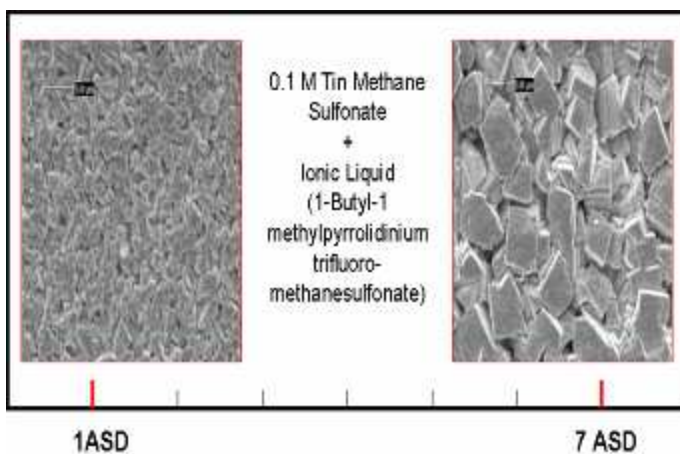


**Figure 4.20:** SEM for 0.1 M  $\text{Sn}^{2+}$  at BMPOTF with 1 ASD and 7 ASD electrodeposition

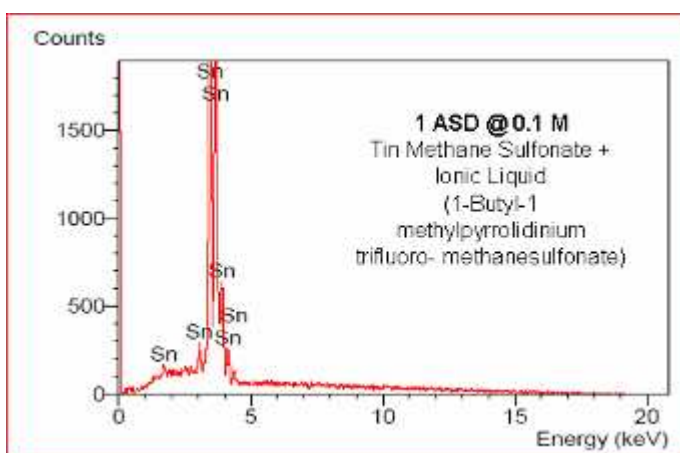


**Figure 4.21:** EDX for 0.1 M  $\text{Sn}^{2+}$  at BMPOTF with 1 ASD electrodeposition

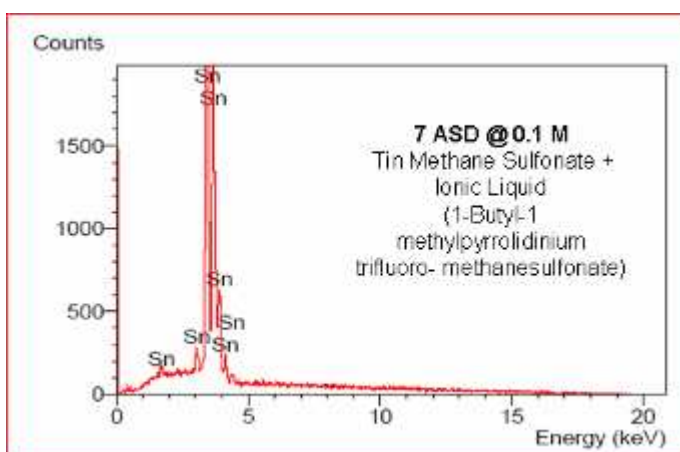


**Figure 4.22:** EDX for 0.1 M  $\text{Sn}^{2+}$  at BMPOTF with 7 ASD electrodeposition







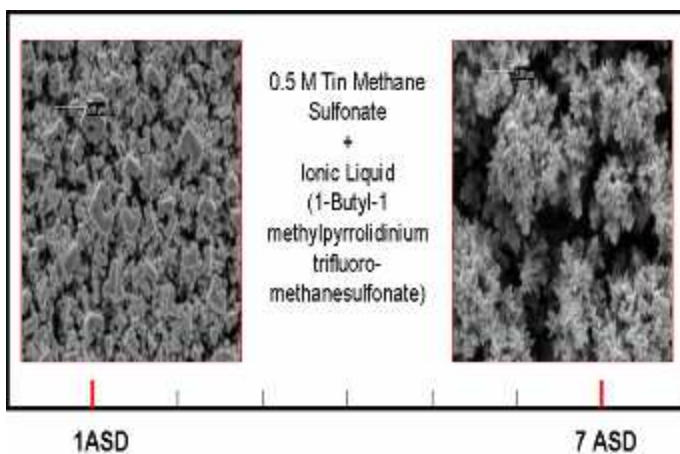


**Figure 4.32:** SEM for 0.5 M Sn<sup>2+</sup> at BMPOTF with 1 ASD and 7 ASD electrodeposition

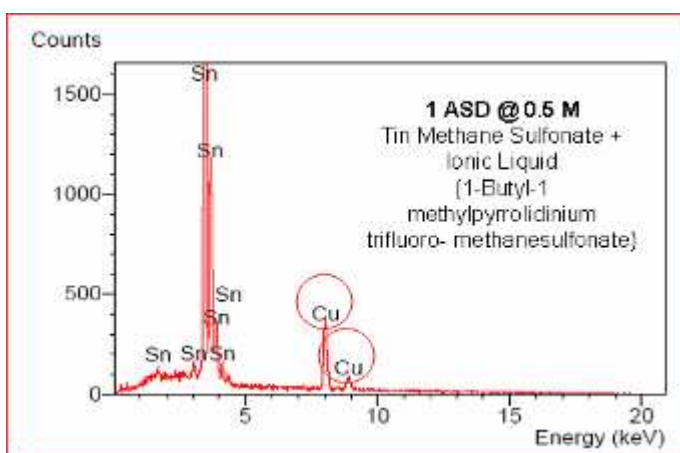


**Figure 4.33:** EDX for 0.5 M Sn<sup>2+</sup> at BMPOTF with 1 ASD electrodeposition

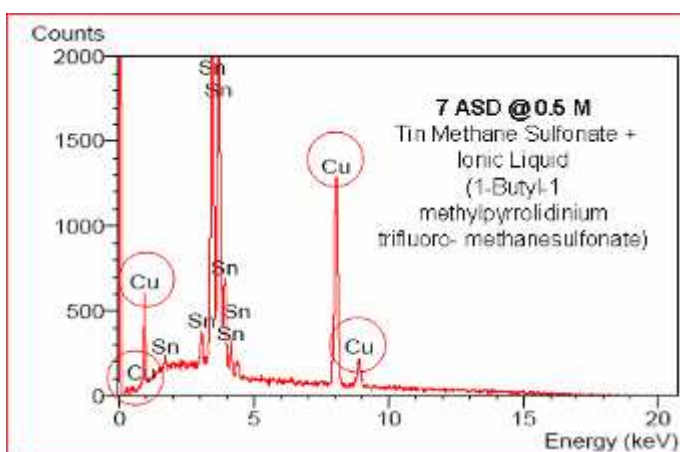


**Figure 4.34:** EDX for 0.5 M Sn<sup>2+</sup> at BMPOTF with 7 ASD electrodeposition

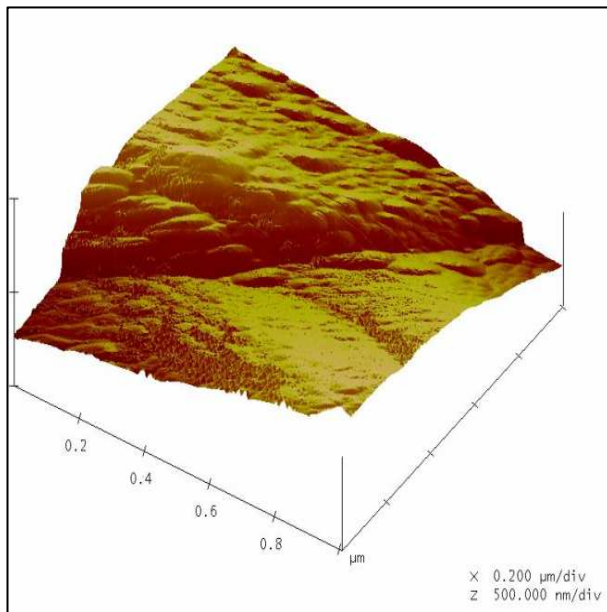


**Figure 4.35:** AFM for 0.1 M Sn<sup>2+</sup> at BMPOTF with 7 ASD electrodeposition

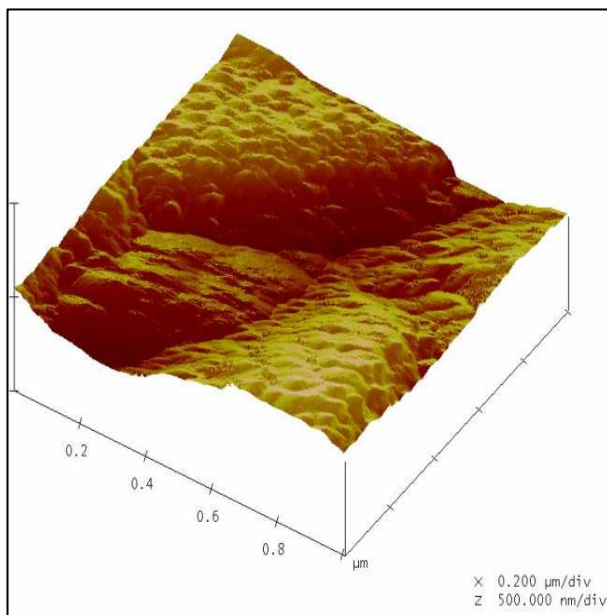


**Figure 4.36:** AFM for 0.2 M Sn<sup>2+</sup> at BMPOTF with 7 ASD electrodeposition

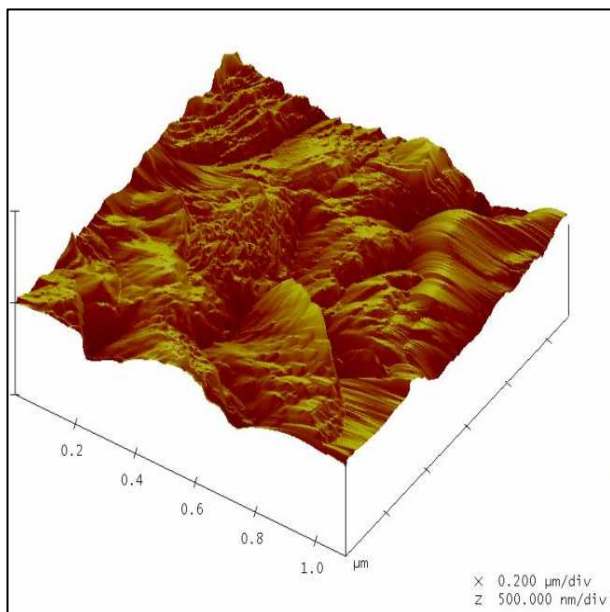


**Figure 4.37:** AFM for 0.3 M  $\text{Sn}^{2+}$  at BMPOTF with 7 ASD electrodeposition

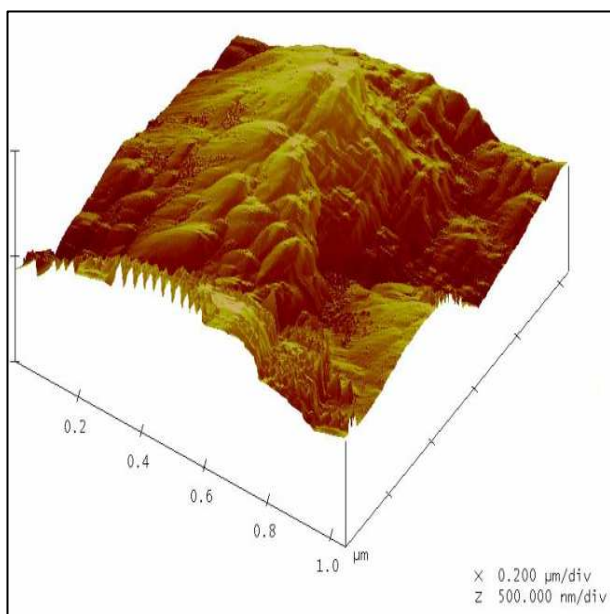


**Figure 4.38:** AFM for 0.4 M  $\text{Sn}^{2+}$  at BMPOTF with 7 ASD electrodeposition

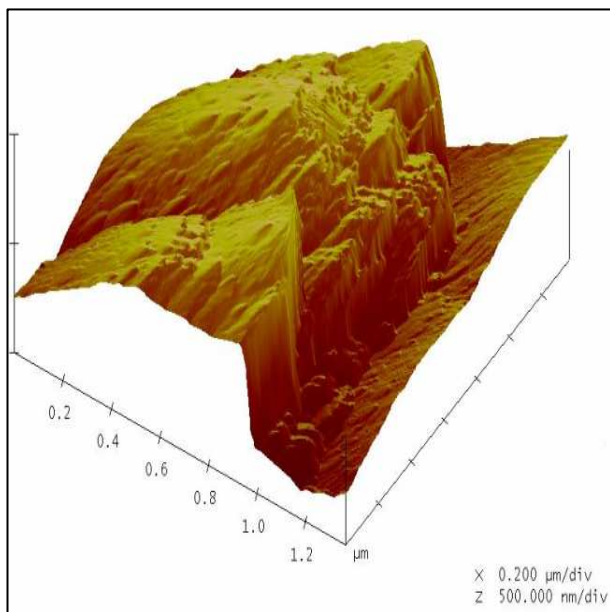


**Figure 4.39:** AFM for 0.5 M  $\text{Sn}^{2+}$  at BMPOTF with 7 ASD electrodeposition

## 4.4 FTIR analysis on electrolyte

Ionic liquid, 1-butyl-1-methyl-pyrrolidinium trifluoro-methanesulfonate, (BMPOTF) as well as the mixture of BMPOTF and Tin Methane Sulfonate,  $(\text{CH}_2\text{SO}_3)_2\text{Sn}$  with various stannous ions concentration were examined using Fourier Transform Infrared (FTIR) analysis. The IR spectra of blank solution with 0 M stannous ions was presented in **Figure 4.40**, infrared spectrum with 0.1 M and 0.5 M of Stannous ions were revealed in **Figure 4.41** and **4.42** respectively.

The free O-H stretch, a sharp peak at  $3600\text{-}3500\text{ cm}^{-1}$  are presented at all infrared spectrum, from **Figure 4.40-4.42**. Based on the FTIR result, it could be concluded that water was presented in all samples. However, the absorption of infrared radiation or the percent transmittance (%T) is getting stronger with the increasing of stannous ions. Based on the chemical technical data sheet, Tin Methane Sulfonate,  $(\text{CH}_2\text{SO}_3)_2\text{Sn}$  contains 30% of water. Water content would be introduced together with tin methane sulfonate into electrolyte by means of increasing the stannous concentration.

On the other hand, the absorption of infrared radiation for sulfonate ions, with S=O stretch which occurs at 1150-1350  $\text{cm}^{-1}$  and S-O stretch at 630-650  $\text{cm}^{-1}$  was increased proportionally with the increasing of stannous concentration. The phenomenon is attributable to sulfonate ions and methane sulfonic acid in tin methane sulfonate. Based on the chemical technical data sheet, Tin Methane Sulfonate,  $(\text{CH}_2\text{SO}_3)_2\text{Sn}$  contains 15% of Methane sulfonic acid. It means the acid concentration will increase proportionally with the tin methane sulfonate in electrolyte.

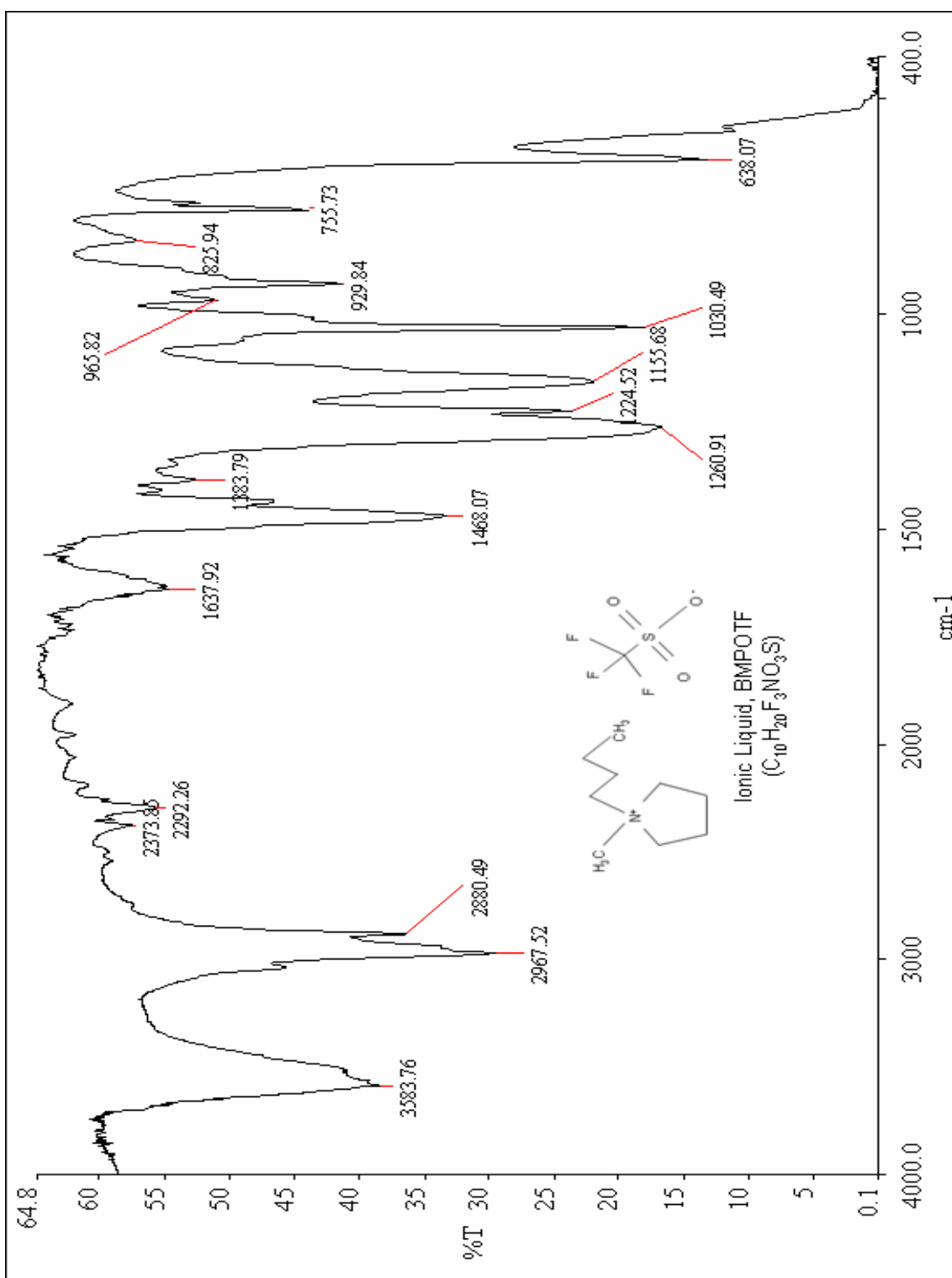


**Figure 4.40:** FTIR of pure Ionic Liquid – BMPOTF only

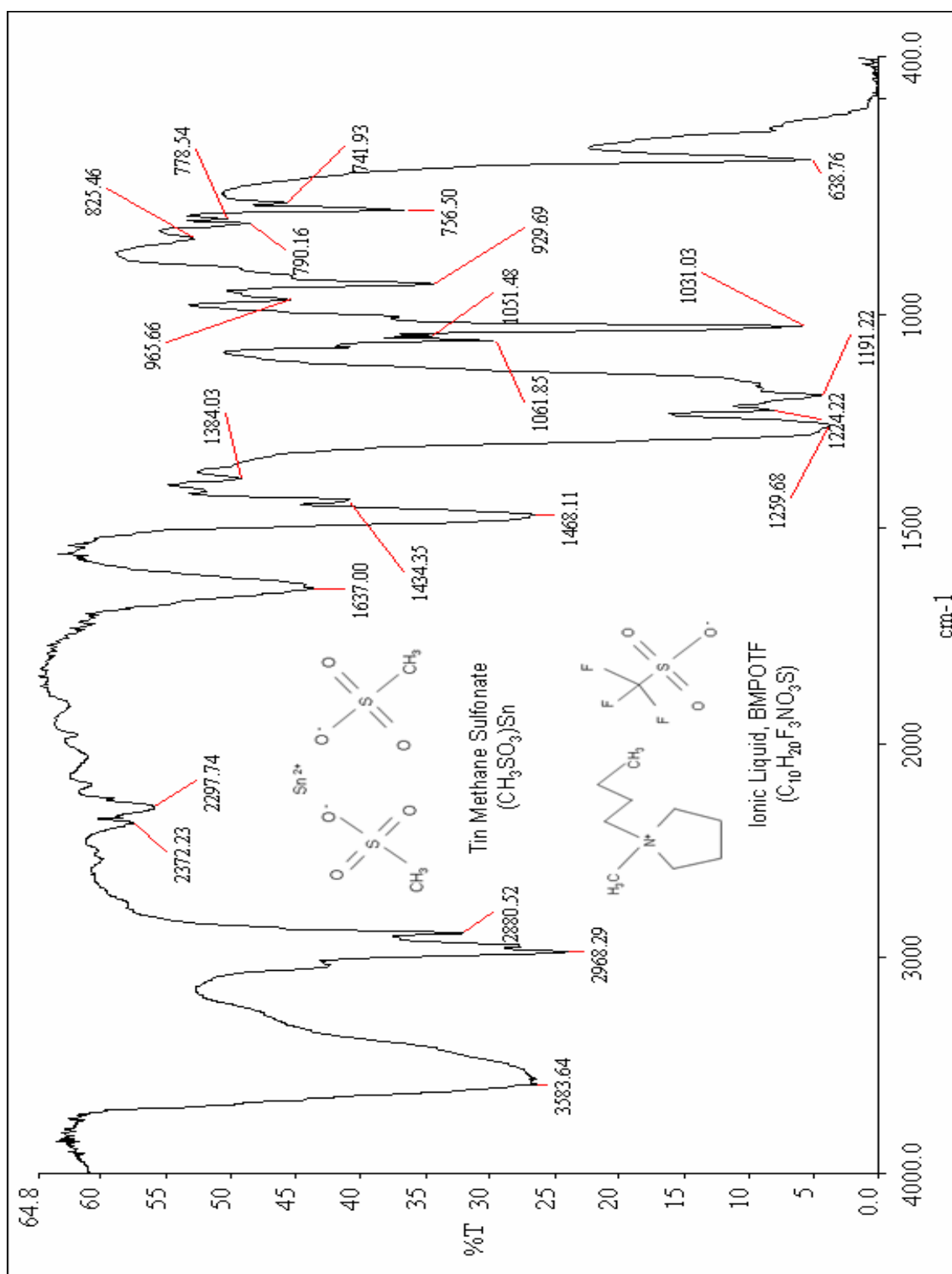


**Figure 4.41:** FTIR of Mixture of Ionic Liquid – BMPOTF and 0.1 M Tin Methane Sulfonate

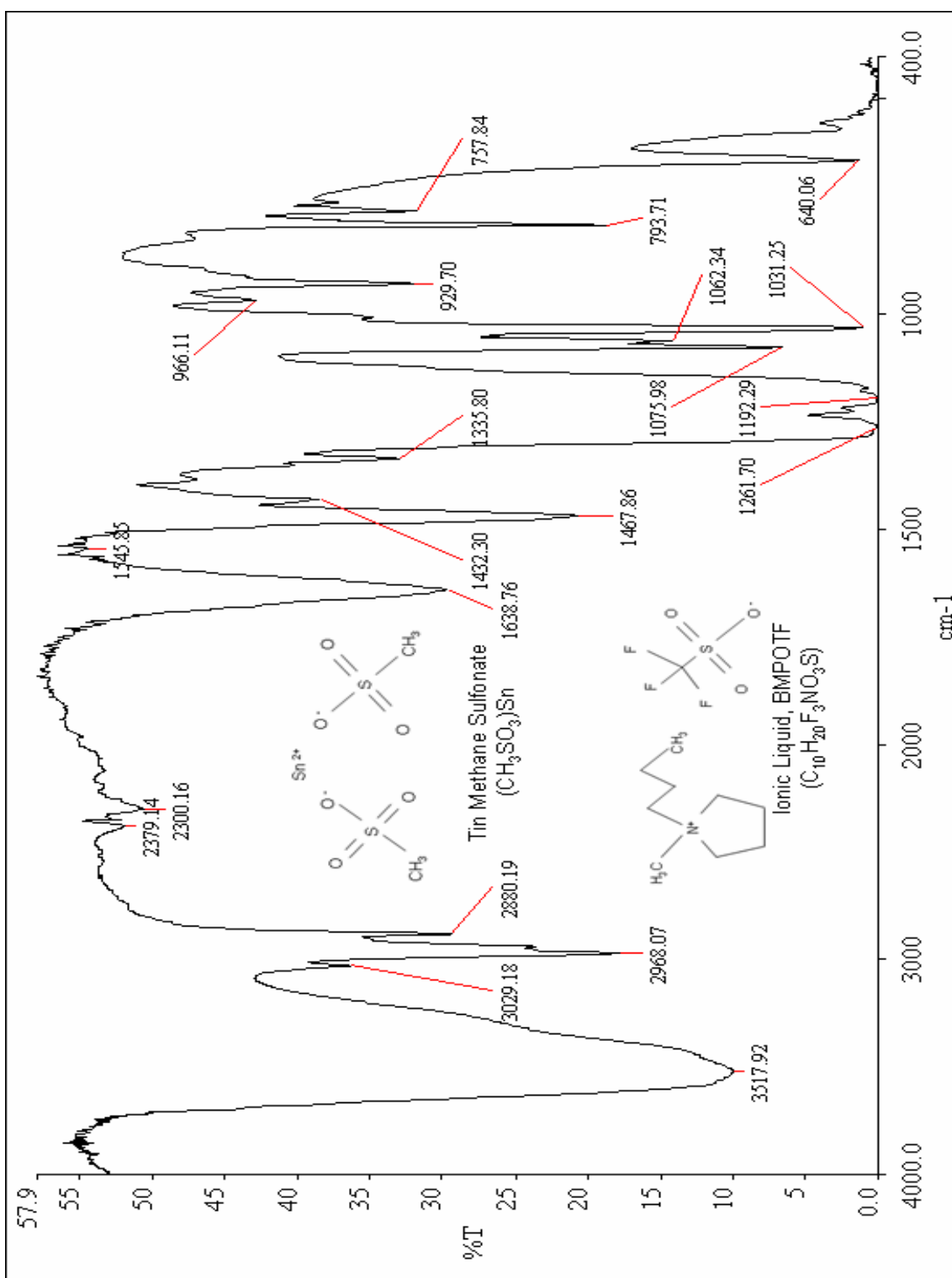


**Figure 4.42:** FTIR of Mixture of Ionic Liquid – BMPOTF and 0.5 M Tin Methane Sulfonate

## 4.5 Reliability Test

### 4.5.1 Results and Discussion for Wetting Balance Test

Wetting balance test had been carried out on the copper panels with dimension 20 mm X 20 mm that electrodeposited with 0.4 M  $\text{Sn}^{2+}$  in different electrolyte (**Figure 4.43 and 4.44**). Group 1 was the samples that plated in the mixture of Ionic Liquid (IL) - BMPOTF and Tin MSA . Group 2 was the samples that plated in the conventional Methane Sulfonic Acid (MSA) based tin plating electrolyte with the addition of commercial proprietary additive.

Each group of Sample had been tested with

- 245 °C with Pb-free SAC (Sn-Ag-Cu) molten solder

Sample size for each group of sample is 5 units

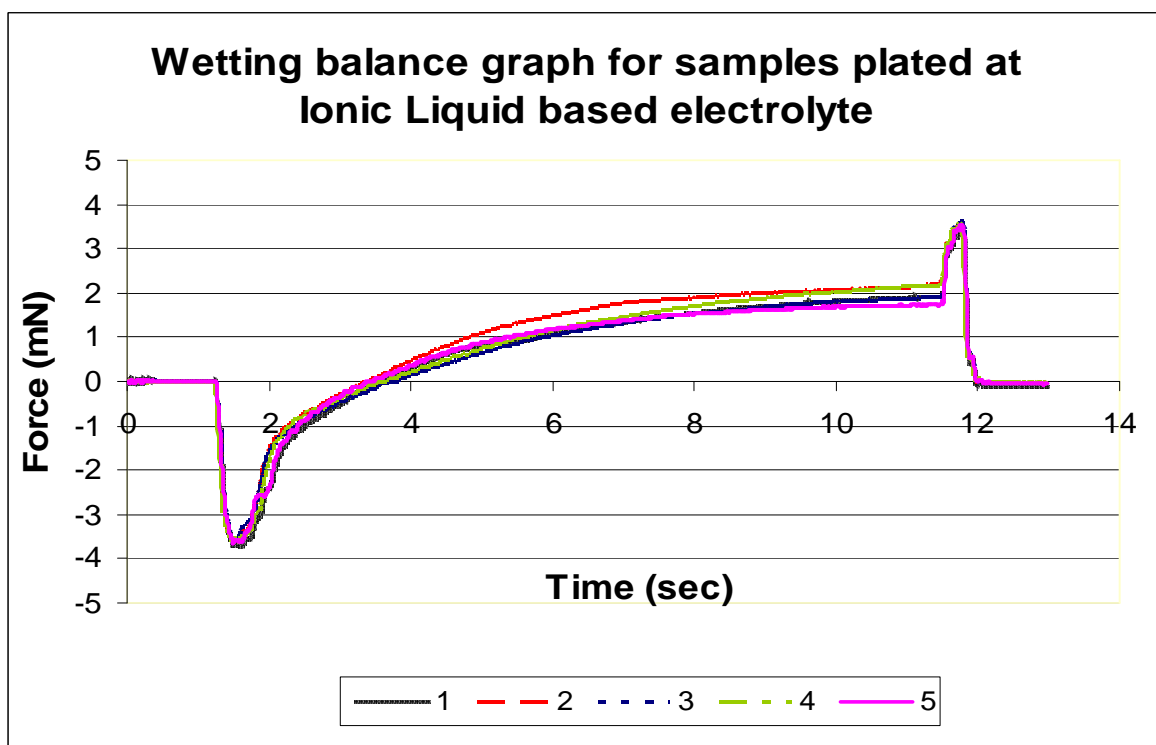


**Figure 4.43:** Wetting balance graph for samples plated at Ionic Liquid based electrolyte

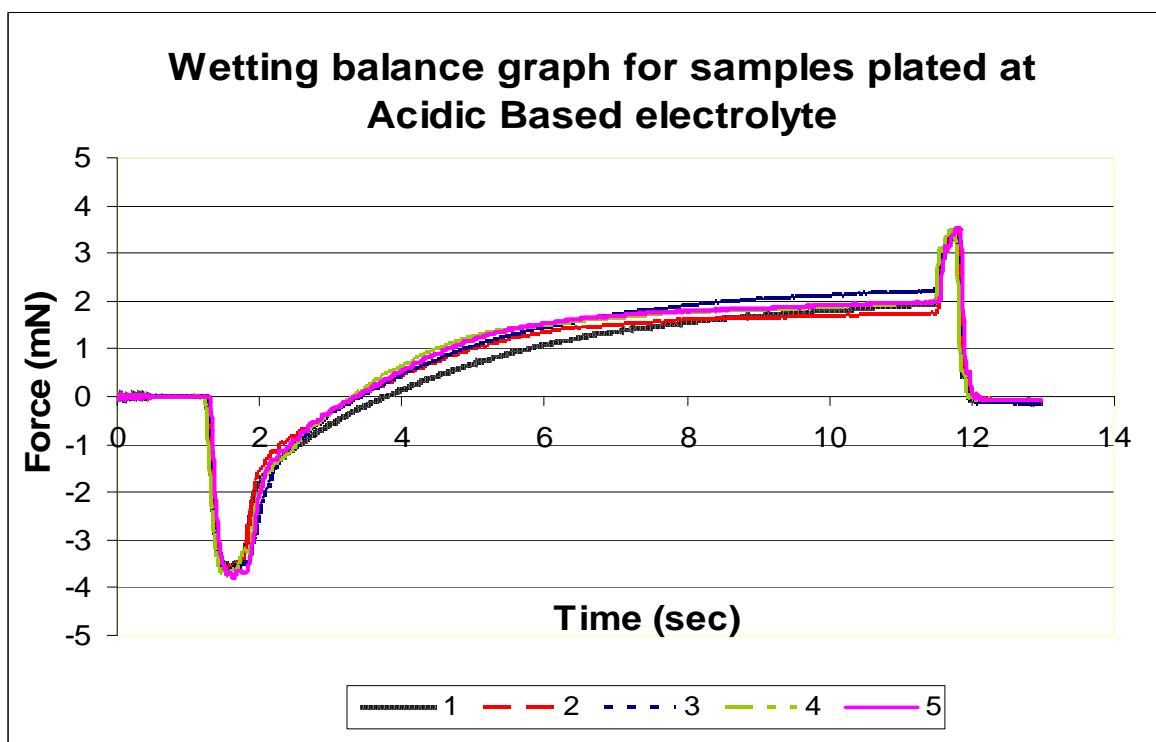


**Figure 4.44:** Wetting balance graph for samples plated at Acidic based electrolyte

Sample	Time-to-zero, To (Seconds)	
	IL Based (Group 1)	Acidic Based (Group 2)
1	2.331	2.152
2	2.106	2.528
3	2.460	2.184
4	2.118	2.017
5	2.203	2.085
Average	<b>2.244</b>	<b>2.193</b>

**Table 4.10:** Time-to-zero reading for IL based and Acidic based plated samples

In order to prove the similarity in term of solderability between IL plated and acidic (MSA) plated samples (**Table 4.10**), hypothesis test was carried out (**Figure 4.45**).

$$H_0: u_1 = u_2$$

$$H_1: u_1 \neq u_2$$

$u_1$  = wetting balance time for IL based plated samples

$u_2$  = wetting balance time for acidic (MSA) based plated samples

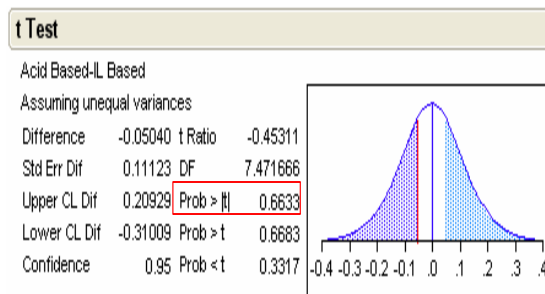
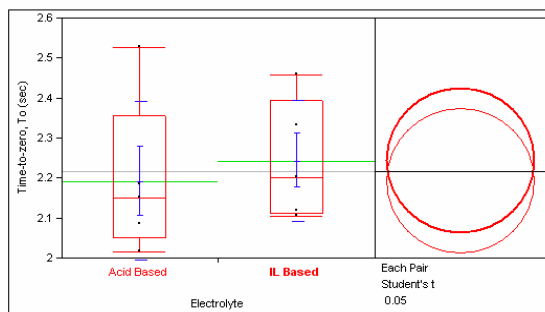


**Figure 4.45:** t Test diagram

From the mean comparison and t-Test diagram, p-value for t-Test is 0.6633 which is greater than 0.05; null hypothesis cannot be rejected (**Figure 4.45**). There is no significant difference in term of solderability and wetting balance time between IL plated and acidic (MSA) plated samples.

## 5. CONCLUSION

### 5.1 Project Conclusion and overall discussion

The electrodeposition of tin in the mixture of water and air stable ionic liquid- 1-butyl-1-methyl-pyrrolidinium trifluoro-methane sulfonate and Methane Sulfonic Acid (MSA) based tin methane sulfonate salts shows the promising result in this study. The deposit was dense, fine and in polygonal grain structure.

In cyclic voltammetry and chronoamperometry studies, it has shown that the diffusion coefficient of stannous ions in BMPOTF ionic liquid is approximately  $2 \times 10^{-7} \text{ cm}^2/\text{s}$  and was calculated from the Randles-Sevcik and Cottrell equation. Diffusion coefficient of  $\text{Sn}^{2+}$ ,  $D$  has dropped when the mixture of BMPOTF and MSA tin had reached 0.5 M  $\text{Sn}^{2+}$ .

In electroplating studies, the average current efficiency are above 95% when electrodeposited with  $\text{Sn}^{2+}$  concentration in the range of 0.1 - 0.4M, and at 1 to 7 ASD. The deposit was dense, fine and in polygonal grain structure. The grain size of tin had increased from 1-2  $\mu\text{m}$  to  $\approx 5 \mu\text{m}$  proportional to current density change.

However, there was a sudden drop for current efficiency when deposited with 0.5 M MSA tin. The similar phenomenon happened in cyclic voltammetry experiments whereby the stannous diffusion coefficient dropped when the mixture of BMPOTF and MSA tin had reached 0.5 M  $\text{Sn}^{2+}$ . It was believed that the mixture of BMPOTF and MSA tin has reached saturated point at 0.5M  $\text{Sn}^{2+}$ . The ion  $\text{H}^+$  from acid was reduced to gas hydrogen during tin deposition. The hydrogen gas was co-deposited onto the copper substrate, thus causing the tin deposit dull, porous and had poor reflectivity.

Wetting balance test, one of the methods used to test the solderability of IC leads had been carried out on the copper panels with dimension 20 mm × 20 mm that electrodeposited with 0.4 M Sn<sup>2+</sup> in different electrolyte. Group 1 was the samples that plated in the mixture of Ionic Liquid (IL) -BMPOTF and MSA Tin. Group 2 was the sample that plated in the conventional Methane Sulfonic Acid (MSA) based tin plating electrolyte with the addition of commercial proprietary additive. By using the statistical t-Test diagram, there is no significant difference in term of solderability/ wetting balance time between IL plated and acidic (MSA) plated samples. It has proven that Ionic Liquid is able to achieve electroplating industrial standard or more specifically semiconductor's electroplating standard.

A main reproach is that the cost of ionic liquids is too high at the moment. Indeed, 500 gram of costs up to RM 4000. One has to bear in mind that currently one pays more or less the salary of the chemist in the laboratory who synthesizes the liquid from the educts. If a large scale production line was available, operated automatically, the costs would be reduced drastically. There is a dispute in the community about what future prices will be. One should not forget that ionic liquids electrolyte is additive-free and they can easily be recycled. Thus the overall costs for a process will decide whether an ionic liquids process will be established or not.

The dream would be that there will be – like water – one ionic liquid that is suited as a general liquid for all electrochemical reactions. It cannot be excluded that such a liquid will be produced in the future, but at present the field is in rather a developmental state. We ourselves were pretty surprised when we realized that the anion of an ionic liquid can have a dramatic effect on the electrodeposition of metals. A deeper understanding of

ionic liquids will be required before ionic liquids become standard electrolytes for electroplating.

## 6. PUBLICATION

1. Yang Kok Kee, Koay Hun Lee, Wan Jeffrey Basirun , Electrodeposition of tin using Tin (II) Methanesulfonate from mixture of Ionic Liquid and Methane Sulfonic Acid , *Advances In Materials And Processing Technologies (AMPT) 2009*.
2. Yang Kok Kee, Koay Hun Lee, Wan Jeffrey Basirun , Electrodeposition of tin using Tin (II) Methanesulfonate from mixture of Ionic Liquid and Methane Sulfonic Acid , *Patent Application, 2009, Status: Pending*
3. Yang Kok Kee, Koay Hun Lee, Wan Jeffrey Basirun , Voltammetry and Chronoamperometry of Tin (II) Methanesulfonate in Ionic Liquid and Methane Sulfonic Acid (MSA) solvent, *3<sup>rd</sup> International Conference on Functional Materials and Devices 2010 (ICFMD-2010)*.

## 7. REFERENCES

- [1] B. T. K. Barry, C. J. Thwaites (1983). *Tin and its alloys and compounds*. John Wiley & Sons.
- [2] China Mining Organization from URL: <http://www.chinamining.org>. Retrieved February 16, 2009.
- [3] C. T. J. Low, F. C. Walsh (2008). The stability of an acidic tin methanesulfonate electrolyte in the presence of a hydroquinone antioxidant. *Electrochim Acta*, 53, 5280-5286.
- [4] M. J. Deng, I. W. Sun, P. Y. Chen, J. K. Chang, W. T. Tsai (2008). Electrodeposition behavior of nickel in the water-and-air stable 1-ethyl-3-methylimidazolium- dicyanamide room-temperature ionic liquid., *Electrochim Acta*, 53, 5812-5818.
- [5] F. Endres, D. MacFarlane, A. Abbott (2008). *Electrodeposition from Ionic Liquids*. Clausthal-Zellerfeld- WILEY-VCH.
- [6] S. Z. E. Abedin, E. M. Moustafa, R. Hempelmann, H. Natter, F. Andres (2005). Additive free electrodeposition of nanocrystalline aluminum in a water and air stable ionic liquid. *Electrochem Commun*, 7, 1111-1116.
- [7] C. L. Hussey, X. H. Xu (1993). The electrochemistry of Tin in the Aluminum Chloride-1-Methyl-3-ethylimidazolium chloride molten salt. *J Electrochem Soc*, 140:3, 618-626.
- [8] W. Z. Yang, H. Chang, Y. M. Tang, J. T. Wang, Y. X. Shi (2008). Electrodeposition of Tin and Antimony in 1-ethyl-3-methylimidazolium tetrafluoroborate ionic liquids. *J Appl Electrochem*, 38, 537-542.

- [9] N. Tachikawa, N. Serizawa, Y. Katayama, T. Miura (2008). Electrodeposition of Sn (II)/ Sn in a hydrophobic room-temperature ionic liquid. *Electrochim Acta*, 53, 6530-6534.
- [10] A. C. Tan (1993). *Tin and Solder Plating in the Semiconductor Industry*. London-Chapman & Hall.
- [11] D. Pletcher, F. C. Walsh (1990). *Industrial Electrochemistry*. 2<sup>nd</sup> edn. KLUWER, THE LANGUAGE OF SCIENCE.
- [12] N. Kanani (2004). *Electroplating: Basic principles, processes and practice*. Berlin-ELSEVIER.
- [13] A. J. Bard, L. R. Faulkner (2001). *Electrochemical Methods – Fundamental and Applications*. 2<sup>nd</sup> edn. Texas. John Wiley & Sons.
- [14] E. Raub, K. Müller (1967). *Fundamentals of Metal Deposition*. Schwanisch Gmund- ELSEVIER PUBLISHING COMPANY.
- [15] C. M. A. Brett, A. M. O. Brett (1994). *Electrochemistry Principles, Methods and Applications*. Coimbra-Oxford University Press.
- [16] M. Paunovic, M. Schlesinger (2006). *Fundamentals of Electrochemical Deposition*. 2<sup>nd</sup> edn. NJ- Wiley Interscience.
- [17] L. J. Durney (1984). *Electroplating Engineering Handbook*. 4<sup>th</sup> edn. New York-Van Norstrand Reinhold.
- [18] Q. B. Zhang, Y. X. Hua, Y. T. Wang, H. J. Lu, X. Y. Zhang (2009). Effects of ionic liquid additive [BMIM]HSO<sub>4</sub> on copper electro-deposition from acidic sulfate electrolyte. *Hydrometallurgy*, 98, 291–297.
- [19] C. Su, M. An, P. Yang, H. Gu, X. Guo (2010). Electrochemical behavior of cobalt from 1-butyl-3-methylimidazolium tetrafluoroborate ionic liquid. *Appl Surf Sci*, 256, 4888–4893.

- [20] S. Caporali, A. Fossati, A. Lavacchi, I. Perissi, A. Tolstogousov, U. Bardi (2007). Aluminum electroplated from ionic liquids as protective coating against steel corrosion. *Corros Sci*, 50, 534–539.
- [21] T. Jiang, M. J. C. Brym, G. Dubé, A. Lasia, G. M. Brisard (2006). Electrodeposition of aluminum from ionic liquids: Part I—electrodeposition and surface morphology of aluminum from aluminum chloride (AlCl<sub>3</sub>)–1-ethyl-3-methylimidazolium chloride ([EMIm]Cl) ionic liquids. *Surf Coat Tech*, 201, 1–9.
- [22] Y. Bando, Y. Katayama, T. Miura (2007). Electrodeposition of palladium in a hydrophobic 1-n-butyl-1-methylpyrrolidinium bis(trifluoromethylsulfonyl) imide room-temperature ionic liquid. *Electrochim Acta*, 53, 87–91.
- [23] G. M. Brisard (2007). An Electroanalytical Approach for Investigating the Reaction Pathway of Molecules at Surfaces. *Elec Soc S*, Summer 2007, 23-25.
- [24] P. M. S. Monk (2001). *Fundamentals of Electroanalytical Chemistry*. Manchester-John Wiley and Sons.
- [25] C. Yang, P. Xie (2007). Studies on Enhanced Oxidation of Estrone and Its Voltammetric Determination at Carbon Paste Electrode in the Presence of Cetyltrimethylammonium Bromide. *B Korean Chem Soc*, 28, 1729-1734.
- [26] C. H. Hamann, A. Hamnett, W. Vielstich (1998) *Electrochemistry*. Weinheim-WILEY-VCH.
- [27] F. Scholz (2002). *Electroanalytical Methods-Guide to Experiments and Applications*. Greifswald- Springer.
- [28] V. S. Bagotsky (2006). *Fundamentals of Electrochemistry*. 2<sup>nd</sup> edn. New Jersey-John Wiley & Sons.
- [29] G. K. Nezhad, M. Hasanzadeh, L. Saghatforoush, N. Shadjou, B. Khalilzadeh, S. Ershad (2009). Electro-oxidation of Ascorbic Acid Catalyzed on Cobalt Hydroxide-modified Glassy Carbon Electrode. *J Serb Chem Soc*, 74(5), 581-593.

- [30] I. S. EL-Hallag (2009). Electrochemical and SEM properties of  $\text{Co}^{2+}$  ion in hexagonal mesophase of pluronic lyotropic liquid crystal template. *B Mater Sci*, 32, 555-560.
- [31] M. M. Ghoneim and I. S. EL-Hallag (2009). Electrochemical Behavior of Hexamethylbenzene Isocloso Ruthenium-Borane Complex at a Glassy Carbon Electrode in Non-Aqueous Medium. *J. Braz. Chem. Soc.*, 00, 1-9.
- [32] R. E. Sabzi (2005). Electrocatalytic Oxidation of Thiosulfate at Glassy Carbon Electrode Chemically Modified with Cobalt Pentacyanonitrosylferrate. *J. Braz. Chem. Soc.*, 16, 1262-1268.
- [33] R. N. Singh, T. Sharma, A. Singh, Anindita, D. Mishra (2007). Electrocatalytic Activities of Nano-Sized Spinel-Type  $\text{Cu}_x\text{Co}_{3-x}\text{O}_4$  ( $0 \leq X \leq 1$ ) for Methanol Oxidation in Alkaline Solutions. *Int J Electrochem Sc*, 2, 762 – 777.
- [34] M. R. Shishehbore, N. Nasirizadeh (2009). Simultaneous determination of ascorbic acid and uric acid at coumestan derivative modified carbon paste electrode. *J Iran Chem Soc*, 2, 47-56.
- [35] D. A. Skoog, F. J. Holler, S. R. Crouch (2007). *Principles of Instrumental Analysis*. 6<sup>th</sup> edn. Belmont- Thomson Books/ Cole.
- [36] P. Echlin (2009). *Handbook of Sample Preparation for Scanning Electron Microscopy and X-Ray Microanalysis*. Cambridge- Springer.
- [37] W. R. Knowles, N. Andover (1995). *Environmental Scanning Electron Microscope*, United States Patent, 5412211.
- [38] G. D. Danilatos (1991). *Multipurpose Gaseous Detector Device for Electron Microscope*, United States Patent, 4992662.
- [39] G. D. Danilatos (1986). *Method and Apparatus for an Atmospheric Scanning Electron Microscope*, United States Patent, 4596928.

- [40] F. Rouessac, A. Rouessac (2005). *Chemical Analysis-Modern Instrumentation Methods and Techniques*. John Wiley and Sons.
- [41] P. C. B. D. Ricci (2004). *Atomic Force Microscopy Biomedical Methods and Applications*. New Jersey – Humana Press.
- [42] G. D. Christian (2004). *Analytical Chemistry*. 6<sup>th</sup> edn. Washington-John Wiley and Sons.
- [43] J. A. DeVore (1989). Practical quantitative solderability testing. *IEEE*, 2027-2034.
- [44] C. L. Alger, D. E. Pope, P. M. Rehm, N. Sivasubramanian (1989). Solderability Test Requirements For Plastic Surface Mount Packages. *IEEE*, 30-37.
- [45] M. A. Kwoka, P. D. Mullenix (1990). The Association of Solderability Testing with Board Level Soldering Performance Automatic Optical Inspection (AOI). *IEEE*, 650-658.
- [46] C. Lea (1993). Solderability and Its Measurement. *Engineering, Science and Education Journal*. April, 1993.
- [47] J. L. Jellison, Johnson, F. M. Hosking (1976). Statistical Interpretation of Meniscograph Solderability Tests. *IEEE*, 126-133.
- [48] F. Steiner, P. Harant (2006). Solderability of the Lead Free Surface Finishes. *IEEE*, 365-369.
- [49] Resistancewire.com from URL: <http://www.resistancewire.com>. Retrieved March 13, 2008.
- [50] WireTronic Inc. from URL: <http://www.wiretron.com>. Retrieved March 15, 2008.
- [51] The General Atomics Sciences Education Foundation from URL: <http://www.sci-ed-ga.org/modules/materialscience>. Retrieved March 15, 2008.